RESEARCH & DEVELOPMENT

Determination of Vertical Resistance for Sheet Pile Abutments

Miguel A. Pando, Ph.D., P.Eng., Principal Investigator
Matthew Whelan, Ph.D., P.E., Key Researcher
Vincent Ogunro, Ph.D., Key Researcher
Corey Rice, Graduate Research Assistant
Matthew Sylvain, Graduate Research Assistant
Youngjin Park, Ph.D., Researcher

Department of Civil and Environmental Engineering
University of North Carolina at Charlotte
9201 University City Boulevard
Charlotte, NC 28223

NCDOT Project 2014-08

FHWA/NC/2014-08

July 2018

North Carolina Department of Transportation
Research Project No. FHWA/NC/2012-08

Determination of Vertical Resistance for Sheet Pile Abutments

Final Report

Miguel A. Pando
Principal Investigator

Matthew J. Whelan
Key Researcher

Vincent O. Ogunro
Key Researcher

Corey D. Rice
Graduate Research Assistant

Matthew B. Sylvain
Graduate Research Assistant

Youngjin Park
Researcher

Department of Civil and Environmental Engineering
University of North Carolina at Charlotte
9201 University City Boulevard
Charlotte, NC 28223

June 27, 2018

Technical Report Documentation Page

1. Report No. **FHWA/NC/2014-008**	2. Government Accession No.	3. Recipient's Catalog No.
4. Title and Subtitle Determination of Vertical Resistance for Sheet Pile Abutments		5. Report Date June 27, 2018 6. Performing Organization Code
7. Author(s) Miguel A. Pando, Matthew Whelan, Vincent Ogunro, Corey Rice, Matthew Sylvian, Youngjin Park		8. Performing Organization Report No.
9. Performing Organization Name and Address Department of Civil & Environmental Engineering The University of North Carolina at Charlotte 9201 University City Boulevard Charlotte, NC 28223 - 0001 Telephone: 704-687-1233 Fax: 704-687-0957		10. Work Unit No. (TRAIS) 11. Contract or Grant No.
12. Sponsoring Agency Name and Address North Carolina Department of Transportation Research and Development Unit 104 Fayetteville Street Raleigh, North Carolina 27601		13. Type of Report and Period Covered Final Report *August 16, 2013 – June 27, 2018* 14. Sponsoring Agency Code *NCDOT Project # 2014-008*
Supplementary Notes:		

16. Abstract

Short span bridges in the U.S. that are located near rivers and streams typically use sheet piles to protect the abutment against erosion and scour. In such bridges, the abutment axial load demands are usually carried by driven piles installed behind the scour protection sheet piles. An alternative bridge abutment design approach, successfully used for decades in Europe and in some projects in the U.S., involves installing sheet piles for the double function of scour protection and axial load bearing. This design paradigm shift has the potential to significantly reduce construction cost. However, widespread implementation and acceptance of this design approach requires full-scale axial load tests on instrumented sheet piles. This report describes and presents results of a research project funded by NCDOT to investigate the axial load capacity of sheet pile foundations. The project encompassed two test programs involving full-scale instrumented test piles. The first test program involved axial load tests under controlled conditions (e.g., controlled soil backfill, detailed geotechnical characterization, etc.) performed at a geotechnical test pit at UNC Charlotte. The second test program involved axial load tests at a field test site that allowed comparison of the axial stiffness and load capacity of a sheet pile wall and an H-pile. The second test program involved geotechnical conditions that are similar to those encountered in NCDOT bridge abutments in the Piedmont region. Additionally the project involved the assessment of the suitability of analysis and design procedures commonly used in practice for conventional deep foundations to the case of axially loaded sheet pile walls. The project also evaluated potential cost savings through a short parametric analysis that studied the axial load capacities of different abutment design configurations and the associated material costs for each design configuration.

Based on the research findings, the axial load capacity and axial stiffness of the sheet pile walls were found to be comparable to the values measured for H-piles installed under similar conditions and dimensions. Therefore, there is strong potential for incorporating the axial load bearing capacity of sheet piles for abutment bridge design that could result in substantial savings in terms of time and money.

17. Key Words *Sheet piles,*	18. Distribution Statement		
19. Security Classif. (of this report) Unclassified	20. Security Classif. (of this page) Unclassified	21. No. of Pages 150	22. Price

Form DOT F 1700.7 (8-72) **Reproduction of completed page authorized**

DISCLAIMER

The contents of this report reflect the views of the authors and not necessarily the views of the University. The authors are responsible for the facts and the accuracy of the data presented herein. The contents do not necessarily reflect the official views or policies of either the North Carolina Department of Transportation or the Federal Highway Administration at the time of publication. This report does not constitute a standard, specification, or regulation.

ACKNOWLEDGMENTS

The authors would like to thank the members of the project Steering and Implementation Committee, chaired by Thomas Koch, for their assistance and guidance throughout the project. In addition, many thanks to NCDOT geotechnical personnel that helped with preliminary geotechnical site investigation of several candidate field-test sites. The two graduate research assistants involved in this project greatly appreciate the financial support through this research grant that is also the basis for their doctoral dissertations.

The authors would also like to express their special gratitude to the following companies for their contributions to this project, as follows:

- Lee of the Carolinas for their assistance and support in several tasks of this project including assistance with installation of piles for the laboratory test and providing structural steel members for construction of the reaction frame for the field testing.
- Skyline Steel for donation of sheet pile test piles used in laboratory component, and for sheet piles and H piles (test pile and reaction piles) used in the field test program.
- ICE for donation of time and use of pile driving equipment used for the installation of the test piles and reaction piles used in both test programs. Additionally we thank ICE for allowing the use of their yard in Matthews, NC as the test site for the field test program.
- S&ME, Inc. for geotechnical drilling, CPT and DMT testing, and MASW at both test sites.
- In-Situ Soil Testing, L.C. for lending a CPT probe and assistance with CPT data graphical post-processing.
- GRL Inc. for PDA and CAPWAP services.

Executive Summary

Short span bridges in North Carolina and the U.S. that are located near rivers and streams typically use sheet pile walls to protect the bridge abutment and foundations against erosion and scour. In such bridges, the abutment axial load demands are usually carried by driven piles installed behind the scour protection sheet piles. An alternative bridge abutment design approach, successfully used for decades in Europe and in some projects in the U.S., involves installing sheet piles designed for the double function of scour protection and axial load bearing. This alternative design has the potential to significantly reduce construction cost and time. However, because of scarcity of full-scale axial load tests on instrumented sheet piles, this design alternative has not been implemented. The main purpose of this study was to assess the axial load bearing capacity of sheet piles through a full-scale, well-instrumented load-testing program. The project encompassed two test programs involving full-scale instrumented test piles. The first test program involved axial load tests under controlled conditions (e.g., controlled soil backfill, detailed geotechnical characterization, etc.) performed at a geotechnical test pit at UNC Charlotte. The second test program involved axial load tests at a field test site that allowed comparison of the axial stiffness and load capacity of a sheet pile wall and an H-pile. The second test program involved geotechnical conditions that are similar to those encountered in NCDOT bridge abutments in the Piedmont region. Additionally the project involved the assessment of the suitability of analysis and design procedures commonly used in practice for conventional deep foundations to the case of axially loaded sheet pile walls. The project also evaluated potential cost savings through a short parametric analysis that studied the axial load capacities of different abutment design configurations and the associated material costs for each design configuration.

Based on the research findings, the axial load capacity and axial stiffness of the sheet pile walls were found to be considerable and comparable to the values measured for H-piles installed under similar conditions and dimensions. Therefore, there is strong potential for incorporating the axial load bearing capacity of sheet piles for abutment bridge design that could result in substantial savings in terms of time and money.

Deep foundation methodologies for analysis and design of conventional driven piles were found to be applicable to assess axial load capacity of sheet piles. The methods evaluated included static methods based on geotechnical in-situ tests such as SPT and CPT, and methods based on dynamic measurements obtained during pile installation such as PDA and CAPWAP. The level of accuracy of the different methods evaluated showed comparable levels of uncertainty for the sheet pile capacity estimates as obtained for the H-pile used in the field test program. The applicability of load-transfer methods to predict load-settlement curves, and axial load transfer mechanisms, for sheet piles was also assessed using the results of the different axial load tests. Load-settlement curves predicted using load transfer analyses showed good agreement with the measured behavior during load tests.

An important design consideration for axial capacity determination of sheet pile walls is the formation or not of a plugged condition which can significantly increase the axial load capacity of a sheet pile wall. For preliminary design purposes it is recommended that the axial capacity of a sheet pile be estimated as the lowest value for the shaft and toe resistances computed using a plugged and unplugged condition. This conservative approach is consistent

with the design approach used for H piles and open pipe piles where the plugging phenomenon has also been reported as being a complex problem difficult to predict a priori.

The parametric analyses presented in Chapter 5 of this study show that significant cost and time savings are possible if alternative abutment configurations are used where even all H-piles can be eliminated and replaced with one or more sheet piles walls.

In order to incorporate sheet piles as primary load bearing elements as an alternative bridge abutment design approach there are important technical aspects that need to be addressed. The following recommendations for research needs are proposed:

- Structural design details for the connection of the sheet pile and bridge abutment.
- Design approach to deal with possible gap formation on the active side of the sheet pile wall (e.g., similar to Yandzio, 1998).
- Abutment longitudinal and flexural rigidity for bridge design.

Table of Content

List of Figures

List of Table

List of Acronyms and Abbreviations

Acronym	Definition
α	Coefficient used in the total stress alpha method to estimate side friction
β	Coefficient used in the beta method (effective stress based) for estimating side friction.
γ	Unit weight (F/L^3)
ϕ'	Effective friction angle (in degrees)
σ'_v	Vertical effective stress
ASTM	American Society of Testing and Materials
BDI	Bridge Diagnostic, Inc.
c	Cohesion
C	Celsius
CAPWAP	Case Pile Wave Analysis Program
CPT	Cone Penetration Test
D_r	Relative density
DMT	Dilatometer test
E	East
EPIC	Energy Production and Infrastructure Center
EOD	End of Driving
ft	Feet
in	inch
I_D	Dilatometer material index
ICE	International Construction Equipment, Inc.
K_a	Active lateral earth pressure coefficient
K_o	At-rest lateral earth pressure coefficient
K_p	Passive lateral earth pressure coefficient
K_s	Lateral earth pressure coefficient for use with the beta method in sheet piles
kip	1,000 lb
kN	Kilonewton
lb	Pound force
LCPC	Laboratoire Central des Ponts et Chausees
LL	Liquid limit
m	Meter
mm	Millimeter
MASW	Multichannel Analysis of Surface Waves
N	North
N_t	Bearing capacity equation for estimating unit toe resistance
NC	North Carolina
NCDOT	North Carolina Department of Transportation
pcf	Pounds per cubic foot
PDA	Pile Driving Analysis/Analyzer

Acronym	Definition
PI	Plasticity Index
PL	Plastic limit
S	South
SCPT	Seismic Cone Penetration Test
SPT	Standard Penetration Test
UNC	University of North Carolina
USGS	United States Geological Survey
Vs	Shear wave velocity
W	West

1 Introduction

This study was undertaken to investigate the axial load capacity of sheet piles currently used in bridge abutments for scour protection. The research need statement was generated by North Carolina Department of Transportation (NCDOT) motivated by the possibility of realizing significant construction cost savings through consideration of some or all of the axial load bearing capacity contribution from the scour protection sheet piles often installed in abutments of short to medium bridges in NC. In the U.S., axial load capacity from sheet pile facing is typically neglected, as the main function of these members is scour protection. However, as shown in the literature review section of this report, the axial load capacity from sheet piles has been considered in bridges in Europe and in some projects in North America. If the inclusion of this axial contribution can be safely confirmed for the appropriate design limit states, NCDOT could design alternative abutment designs featuring less bearing piles (e.g., H-piles) for potentially significant reduction in cost.

The funding for this study was for two-years. However, significant savings were possible thanks to time and material donations from several companies that contributed to this study. Due to contributions by many (see acknowledgments section of report for a complete list) and, in particular, the important donations of sheet piles and H piles from Skyline, the scope of the field test program was expanded to involve a load test on an H-pile to allow for direct comparison with the sheet piles. Unfortunately, the duration of the project was also greatly affected by delays associated with identifying a suitable NCDOT bridge project for the field component of the project. In addition, the original proposal called for field verification tests to be performed at an actual NCDOT bridge project. Unfortunately, after evaluating more than four candidate bridge sites where it was determined that this testing could not be accommodated, the option of performing field load tests at an NCDOT bridge site was abandoned to avoid further delays in the project schedule. The project then shifted focus to identifying a field test site in the greater Charlotte area. Preliminary drilling was performed at three candidate field test sites and, ultimately, the ICE facility in Matthews, NC was selected as the location for the field load tests.

1.1 Need for the Research

NCDOT is responsible for more than 17,000 highway bridges throughout the state. A large percentage of these bridges use sheet piles for scour protection of the abutments. Many U.S. DOTs, including NCDOT, assume that abutment sheet piles do not carry vertical loads. A typical design for short span bridges in NCDOT is shown in Figure 1 1. In these designs, the sheet piles are located along the abutment face for scour protection, and some distance behind them it is common to install conventional driven piles (in this figure one row of H piles is shown) to carry axial loads. In this current design approach, any axial load bearing contribution from the scour protection sheet piles is neglected. This design approach, although practical, is also usually considered conservative. In contrast, Yandzio (1998) has reported that sheet piles have been used in Europe for more than 50 years as the main load-bearing element for bridge abutments.

In the U.S., a few bridge projects have also been reported in the literature where steel sheet piles have been used as the sole axial load bearing element for bridge abutments (e.g., Carle and Whitaker, 1989; McShane, 1991; Evans, 2010). In addition to scour protection, these references pointed out several advantages when using sheet pile abutments including reduced cost and construction time. Figure 1 2 provides details of a steel sheet pile abutment built in Alaska (Carl and Whitaker, 1989). The motivation for this research is primarily related to the potential for cost savings and reduced construction time.

Most short to medium span bridges in NCDOT's jurisdiction use deep piles (e.g., driven H-piles) as the main vertical load bearing elements for each bridge abutment and protective continuous steel sheet pile only for scour protection of the H-piles. Based on the reported use of sheet pile abutments globally, there seems to be strong potential for safely considering the contribution from abutment sheet piles in the axial load bearing capacity.

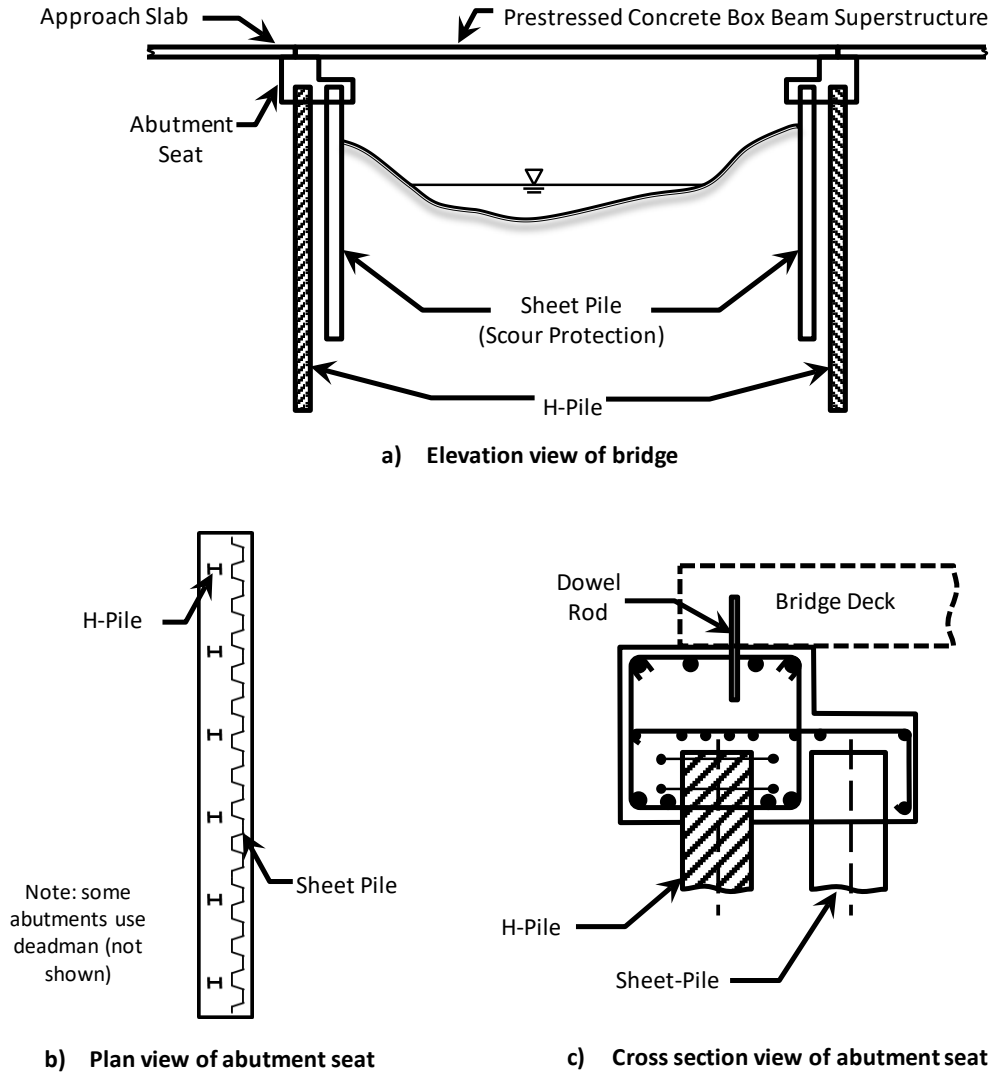

Figure 1-1: Schematic drawing showing typical NCDOT design for a short span bridge.

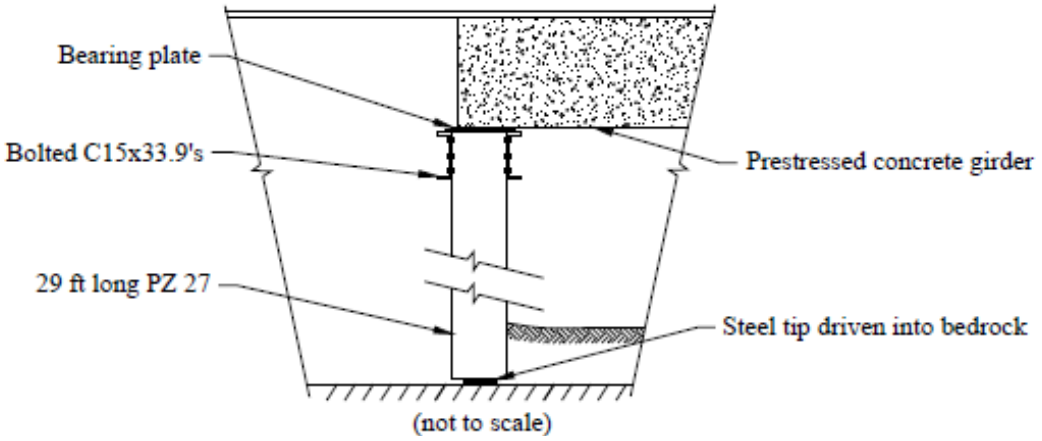

Figure 1-2: Sheet pile abutment at the Small Creek Bridge in Seward, Alaska (Carl and Whitaker, 1989).

1.2 Research Objectives

The main objective of this research project is to assess the axial load bearing capacity of sheet piles installed for scour protection in single short span NCDOT regional tier bridges through a full-scale, well-instrumented load-testing program. Specific objectives include:

1) assess axial capacity estimates of sheet piles from dynamic measurements obtained during installation using PDA and CAPWAP;
2) assess axial capacity and initial stiffness estimates from CAPWAP restrike;
3) carry out axial load tests on instrumented sheet piles to assess load transfer mechanisms under different geotechnical conditions;
4) assess accuracy of static methods to estimate side shear and end bearing of axially loaded sheet piles;
5) calibrate analytical procedures to be used in parametric analyses to assess feasibility and cost analyses for different abutment geometries involving vertical sheet pile elements.
6) Develop recommendations and preliminary guidelines for use of sheet piles in bridge abutments.

1.3 Scope of Work

The project was accomplished through a combined structural and geotechnical effort as the research involves a soil-structure interaction problem. The following tasks were pursued to accomplish the research objectives as follows:

Task 1: Review of current NCDOT design practices, and other state of the art approaches. This first task was essential, as a detailed understanding of the current design and analysis procedure is fundamental to providing NCDOT with a useful product. While the project team has an understanding of the assumptions made by both the NCDOT structural management and geotechnical engineering units, the methods and assumptions implemented by different

NCDOT units had to be reviewed. This success of this task was greatly assisted by regular meetings and conversations with NCDOT structural and geotechnical engineers. Coordination of these efforts were done through the chair of the project Steering and Implementation Committee, Mr. Thomas Koch. A summary of the findings from this review of the current NCDOT design practices, other US DOTs current practices, and international practices is included in Chapter 2 of this report. Additionally, a standalone report was issued in a standalone report submitted to NCDOT on June 9, 2014 (Rice et al., 2014).

Task 2: Detailed parametric study to investigate different alternative abutment configurations using select typical NCDOT sheet pile abutment designs as benchmarks. This task will analytically explore the technical feasibility of different design ideas developed by NCDOT technical personnel. For example, incrementally removing number of H piles; or removing dead man anchor and replacing with a second row of sheet pile; or replacing row of H piles with sheet piles installed perpendicular to scour protection sheet pile. Figure 1-3 shows schematically some of the what-if scenarios and ideas generated during the December 17th, 2012 meeting between NCDOT and the PI. The parametric analyses is presented in Chapter 5 of this report.

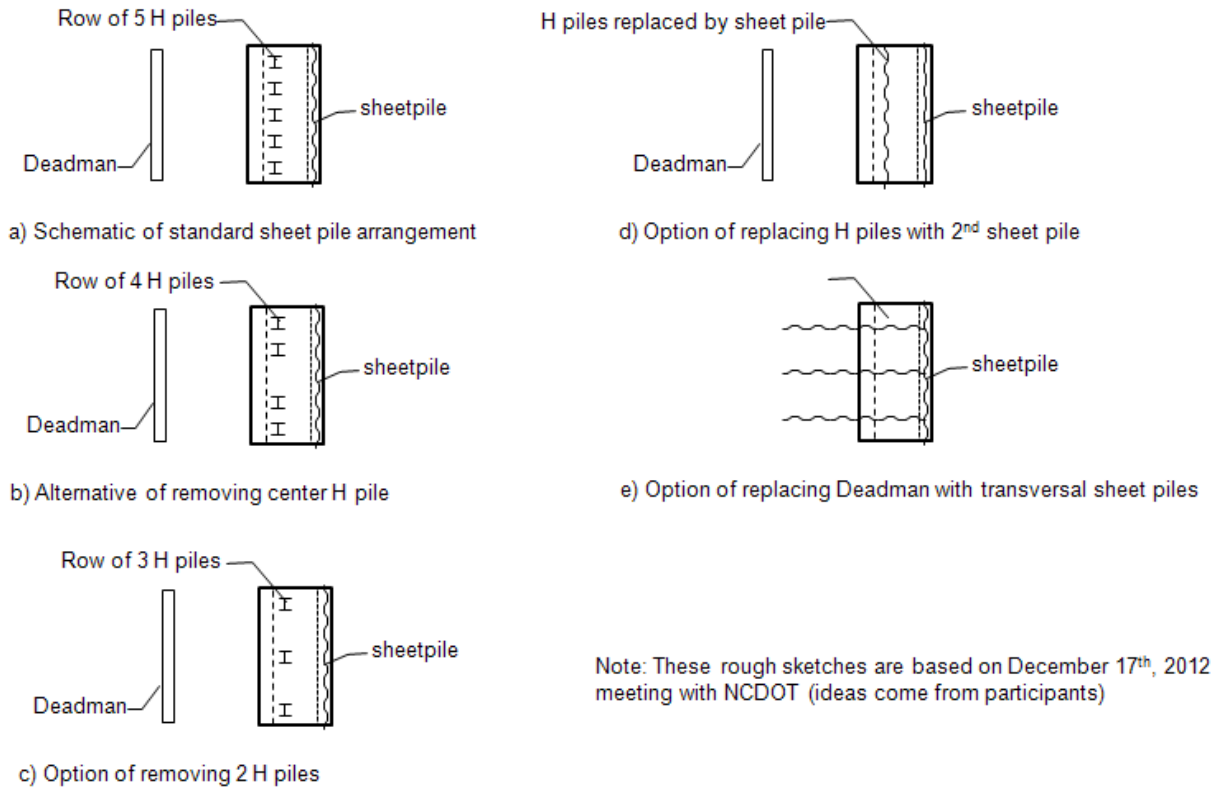

Figure 1-3: Potential alternative abutment investigated in parametric analyses of Chapter 5.

Task 3: Axial capacity and stiffness testing of sheet piles. Based on the literature review conducted for this research, very few well documented case histories involving static axial load tests on instrumented sheet piles have been reported in the literature. The research team also

contacted US sheet pile vendors and little to no information was available regarding well documented axial load tests on sheet piles. A few load tests were identified in the literature review efforts of Task 1 and are summarized in Chapter 2. This task was subdivided into two subtasks as follows:

Task 3.1: Axial load tests of sheet piles under controlled conditions. This task involved axial load tests of instrumented sheet pile walls at one of the geotechnical test pits at UNC Charlotte. This test program allowed for careful control of the soil conditions and a detailed characterization of soil backfill, installation, and testing procedures. This task facilitated collection of reliable experimental data to understand the axial load transfer mechanisms and vertical capacity of sheet piles such as the ones installed in many NCDOT bridge abutments for scour protection. The axial load tests for this component are described in detail in Chapter 3 and complementary information is presented in Appendix A.

Task 3.2: Axial load tests of sheet piles under field conditions. This task involved axial load tests of a pair of instrumented sheet piles at a field test site. As mentioned earlier, the scope of this task was expanded to include an axial load test on an instrumented H pile for comparison purposes. The instrumented H pile had the same length and was installed using the same procedures and with similar geotechnical conditions as it was located about 15 feet away from the sheet pile. This task facilitated collection of invaluable experimental data to further understand the axial load transfer mechanisms and vertical capacity of sheet piles under more realistic field conditions. Furthermore, the test site is located in the Piedmont physiographic region of NC and it is composed of fine grained residual soils that are encountered in many short span NCDOT bridges in the Piedmont region. The axial load tests for this component are described in detail in Chapter 4 and complementary information is presented in Appendix B.

Task 4: Development of design procedures and final report with results, conclusions, and recommendations. A preliminary design approach for estimating axial capacity of sheet pile foundations for possible use as load bearing elements in bridge abutments is presented in Chapter 6 of this report. The proposed procedure is based primarily on the findings of the axial load test programs presented in Chapters 3 and 4 and on the literature review effort in Chapter 2 that summarized experience with sheet pile abutments in other countries. The conclusions and recommendations for future work can be found in Chapter 7.

2 Result of Literature Review

2.1 Introduction

Steel sheet piles are one of the commonly used protection measures used to alleviate scouring of bridge foundations near streams and rivers. Scour of foundations has been reported by FHWA (2012) as one of the main causes of bridge failures in the U.S. Although it is well established that the practice of providing steel sheet piles for scour protection around bridge foundations has been very successful and has greatly reduced the occurrence of scour related bridge failures, the design approach of limiting the purpose of sheet piles to only scour protection is conservative and uneconomical. Contrary to this US practice, several European countries have been using sheet piles as the main vertical load-bearing element for bridge abutments for more than 50 years (Yandzio, 1998). In addition, a few recent bridge projects in the U.S. have demonstrated and reported successful use of the vertical load capacity contribution from abutment sheet piles (Evans, 2010). Despite these reported positive case histories, the axial load contribution from abutment sheet piles continues to be routinely neglected in design by most U.S. DOT's, including NCDOT.

As part of this research project, Task 1 involved a comprehensive literature review performed with the purpose of:

1) Summarizing the existing literature on the topic of axially loaded sheet pile abutments;
2) Reviewing the design guidance from existing literature in regards to axially loaded sheet pile abutments; and
3) Designing and administering an online survey soliciting information from all U.S. state transportation departments to find out which states incorporate sheet piles as axial load bearing structural elements for bridge abutments.

This chapter presents a summary of the main findings of the two volume literature review and state of practice report on sheet pile bridge abutments submitted to NCDOT on June 9, 2014 (Rice et al., 2014). The reader is referred to this literature review report (Rice et al., 2014) for a more detailed presentation than the summary presented in this chapter.

2.2 European bridges with sheet pile abutments

Several bridges in Europe have been reported in the literature where steel sheet piles act as the main load-bearing foundation element within their abutments. This section presents a summary of case studies reported in France, the United Kingdom, and Poland.

2.2.1 Case studies in France

Figure 2-1 shows the locations of the relevant case studies of steel sheet piles use as load bearing elements in bridges in France. This figure shows 13 case studies divided into: i) 7 case histories of bridges reported to have used steel sheet piles as bridge abutments (solid red dots), ii) 4 case histories where steel sheet piles were used in overpasses or tunnels (dots with red

diagonal hatching); and iii) 2 case histories where axial load testing was performed on steel sheet piles (red grid hatching).

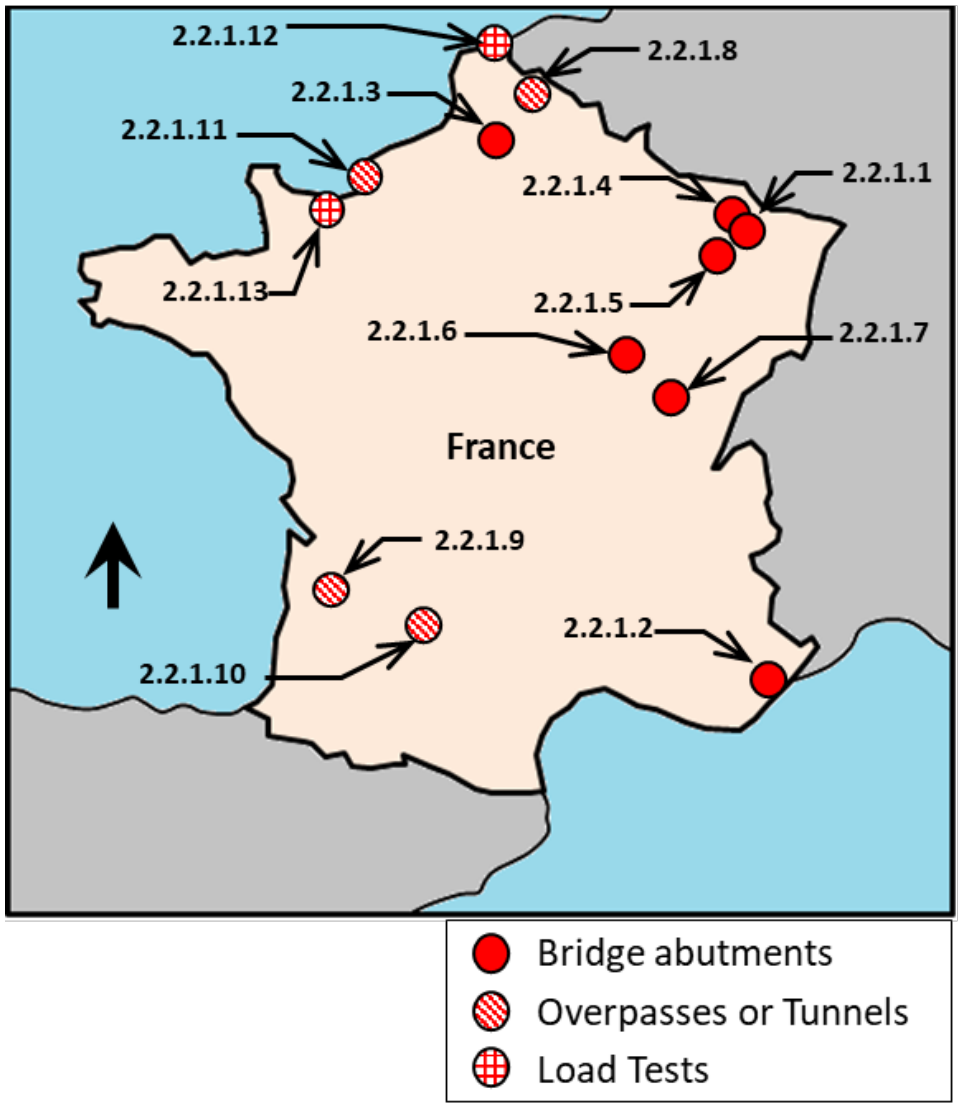

Figure 2-1: Locations of sheet pile case studies in France

The structures identified in this figure feature a variety of different design details, including both tie back and cantilever designs as well as open cross-section and box configurations of sheet piles. These bridges have been in service for over 25 years suggesting reasonably good long-term durability for these sheet pile supported abutments. Table 2-1 summarizes details of the design information for all the case studies found in France.

Table 2-1: Summary of sheet pile case studies in France (adapted from Rice et al., 2014)

ID in Figure 2-1	Structure Name	Location	No. of Spans	Span Length	Abutment Width	Sheet Pile Section (1)	Vertical Length of Sheet Piles	Additional Lateral Support[1]	General Soil Conditions	Flexural Rigidity of Wall, EI (2) [kip.in^2]	References
2.2.1.1	Pont de Chambiere	Chambiere Neighborhood, France	1	82'-0"	9'- 10"	LP IVs	46'-0"	Tie rod anchor	Sand/Gravel to Stiff Marl Clay	1.15E8	SACILOR (n.d.), Carle and Whitaker (1989)
2.2.1.2	A8	La Cagne River, Cagne-su-Mer, France	1	86'-7"	52'-6"	LP SL3 box column	31'-2"	Bridge deck	N/A	N/A	SACILOR (n.d.)
2.2.1.3	Somme River	Amiens, France	1	31'-6"	N/A	LP IIn LP IIIn Box	34'-2" 59'-0"	Bridge deck	N/A	N/A	SACILOR (n.d.), Carle and Whitaker (1989
2.2.1.4	A31	Metz, France	1	N/A	N/A	LP IIIs LP IIs box	N/A	Tie rods	N/A	N/A	Carle and Whitaker (1989)
2.2.1.5	Moselle Canal	Neuves-Maisons, France	1	146'-0"	40'-2"	LP IV LP IIIn box	40'-0" 42'-0" to 50'-0"	N/A	Gravel	N/A	SACILOR (n.d.)
2.2.1.6	Brenne River	Venarey-Les-Laumes, France	1	21'-11"	N/A	LP IIIs	19'-8"	N/A	Silt Clay	N/A	SACILOR (n.d.)
2.2.1.7	Saône River	Seurre-Ecuelles, France	3	138'-0"	23'-0"	LP IVs	N/A	N/A	N/A	3.834E7	SACILOR (n.d.)
2.2.1.8	Croisé Laroche overpass	Lille, France	1	40'-9"	NA	LP SL 5 LP SL 5 box	32'-9.7"	Overpass deck	Silty Sand	N/A	SACILOR (n.d.)
2.2.1.9	St. Genes tunnel	Barriere Saint-Genes road near Bordeaux, France	1	28'-2.6"	866'-1.7"	LP IIn LP IIn box	26'-3"	Overpass deck	N/A	1.879E8	SACILOR (n.d.)
2.2.1.10	Pont de Pierre overpass	La Garonne River, near Pont de Pierre, Agen, France	1	N/A	N/A	LP IIs LP IIs box	45'-11"	Prestressed tie rods	N/A	N/A	SACILOR (n.d.)
2.2.1.11	Winston Churchill overpass	Winston Churchill Boulevard near Le Havre, France	1	22'-9.6"	154'-2.4"	LP SL 4	22'-3.7"	Overpass deck	N/A	N/A	SACILOR (n.d.)
2.2.1.12	Dunkirk Load Test	Coastal Dunkirk area of Northern France				LP IIn	24'-3.3"[3]	Load Test	Sandy loose to very dense to soft clay		Bustamante and Gianeselli (1991)
2.2.1.13	Merville Load Test	Coastal Dunkirk area of Northern France				LP IIs	39'-5"[3]	Load Test	Loose to medium clay		Bustamante and Gianeselli (1991)

Notes: (1) Sheet pile sections as per local manufacturer.
(2) Refers to the flexural rigidity of the total abutment width.

2.2.2 Case studies in U.K. and Poland

Yandzio (1998) reports several bridges in the UK where steel sheet piles were successfully used as bridge abutments. In this section, we present information for the 5 case histories shown in Figure 2-2. As shown in this figure, four of these case histories are located in the U.K. and one in Poland.

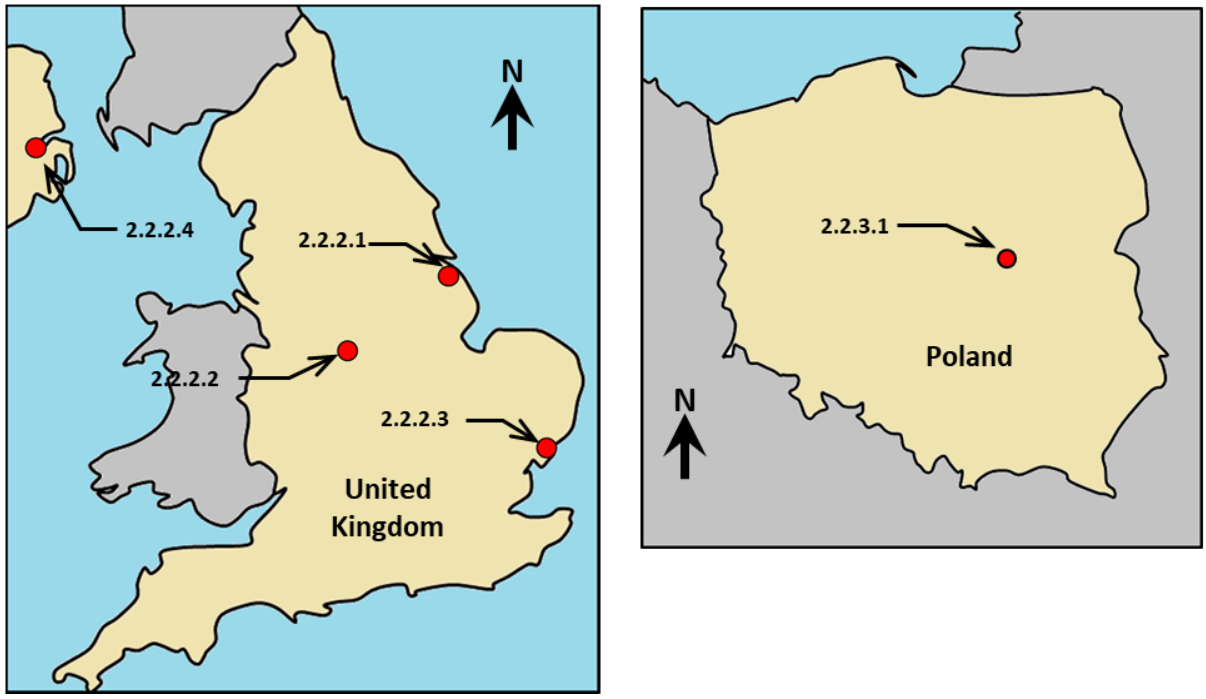

Figure 2-2: Locations of sheet pile case studies in the U.K. and Poland

The case histories presented in this section are summarized in Table 2-2. All case histories involved single span bridges with a wide range of sheet pile structural sections. Apart from the Capel St. Mary A12 Underpass bridge (Section ID 2.2.2.3) that involved use of high flexural rigidity Z-shaped sheet piles that were connected with H-piles for additional rigidity, most the bridges were constructed using U-shaped sheet piles. All case histories listed in Table 2-2 have been in service for at least 19 years, suggesting reasonably good long term durability. The case study in Poland involved a bridge with use of sheet piles as the sole abutment foundation element. The case history in Poland also involved an axial load test.

Table 2-2: Summary of sheet pile case studies in the U.K. and Poland (adapted from Rice et al., 2014)

ID in Figure 2-2	Structure Name	Location	No. of Spans	Span Length	Abutment Width	Sheet Pile Section (1)	Vertical Length of Sheet Piles	Lateral Support (2)	General Soil Condition	Flexural Rigidity of Wall, EI (3) [kip.in^2]	References
2.2.2.1	Humber Road	Immingham, England	1	118'-1"		LP 20W LP 30W	N/A	N/A	N/A	N/A	Yandzio (1998)
2.2.2.2	Canal	Stoke-on-Trent, England	1	N/A2	N/A	F 3N F 4N	N/A	N/A	N/A	N/A	Yandzio (1998)
2.2.2.3	Capel St. Mary A12 Underpass	Ipswish, England	1	32'-10"	N/A	N/A2	N/A	N/A	N/A	N/A	Yandzio (1998)
2.2.2.4	Stockman's Lane Bridge	Belfast, Ireland	1	N/A2	N/A	LP IV box	N/A	Concrete Anchor	N/A	N/A	Yandzio (1998)
2.2.3.1	S8 Express Road	Warsaw, Poland	1	49'-2.6"	N/A	AZ 37-700	46'-3"	Bridge Deck	Medium Dense Sand	N/A	Skyline Steel LLC (2009) Rybak and Zyrek, (2013)

Notes: (1) Sheet pile sections as per local manufacturer.
(2) Lateral support defined herein as the support provided to the pile in the abutment to resist horizontal loads along the longitudinal axis of the bridge.
(3) Refers to the flexural rigidity of the total abutment width.

2.2.3 Case studies in the United States

Five bridges case studies in the United States where sheet piles were reported as being the main axial load bearing elements are shown in Figure 2-3. All of these bridges are single span and in all abutments the steel sheet piles used were Z-shaped configurations. In contrast with European bridge case histories, no box pile configurations were used in these 5 case histories. The relevant information for each case history is summarized in Table 2-3. It is important to note that the sheet piles for most bridge abutments were driven to a competent bearing layer or to practical refusal.

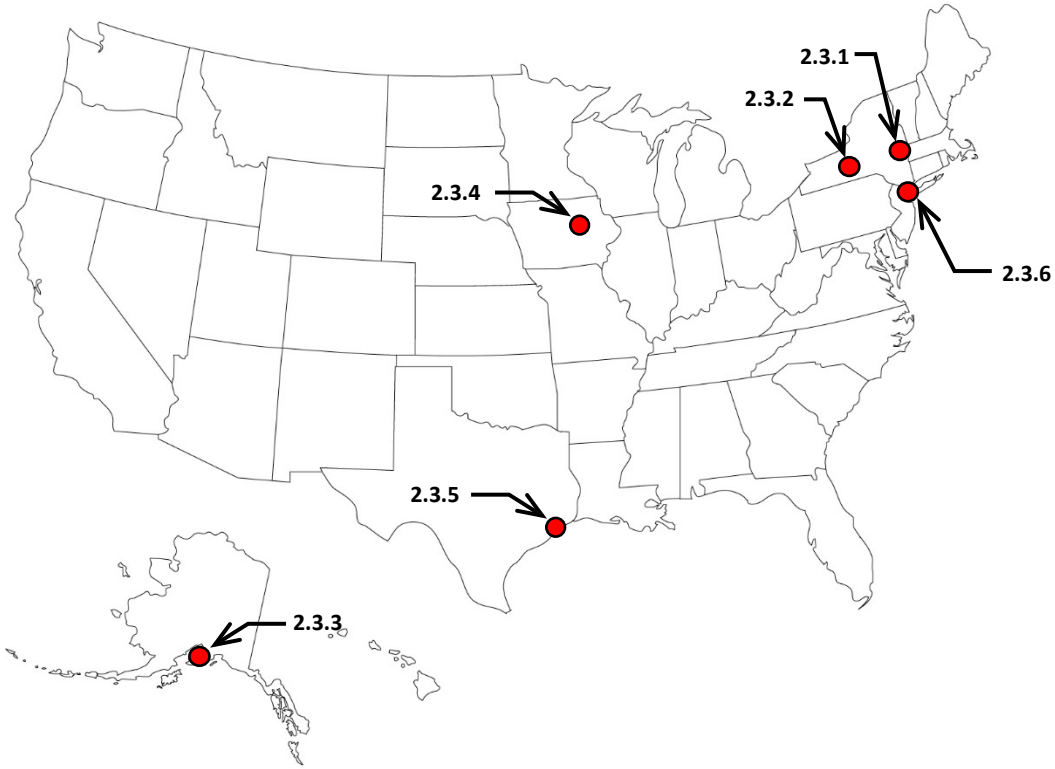

Figure 2-3: Locations of sheet pile case studies in the United States (adapted Rice et al., 2014)

Table 2-3: Summary of sheet pile case studies in the United States (adapted from Rice et al., 2014)

ID in Figure 2-3	Structure Name	Location	No. of Spans	Span Length	Abutment Width	Sheet Pile Section (1)	Vertical Length of Sheet Piles	Lateral Support (2)	General Soil Condition	Flexural Rigidity of Wall, EI (3) [kip.in^2]	References
2.3.1	Taghkanic Creek Bridge	Columbia County, New York	1	42'-0"	N/A2	PZ 22	16'-0"	N/A2	Compact Silty Gravely Sand	N/A	Carle and Whitaker (1989)
2.3.2	Banks Road Bridge	Tomkins County, New York	1	64'-11.25"	N/A2	PZ 22	45'-0"	Cabled Anchors	Clay	N/A	Carle and Whitaker (1989)
2.3.3	Small Creek Bridge	Seward, Alaska	1	79'-4"	N/A2	PZ 27	29'-0"	Bridge Deck	N/A2	N/A2	Carle and Whitaker (1989))
2.3.4	Bryan Road Bridge	Bryan Road over Spring Creek, Black Hawk County, IA	1	38'-4"	33'-0"	PZ 22	15'-0"	Concrete Deadman	Sand and Clay	8.076E7	Evans et al. (2012)
2.3.5	Lone Star Canal	Chamber County, Texas	1	80'-0"	42'-9"	AZ 14-770	44'-8.5"	N/A	Clay	2.136E8	LEAP Engineering, (2011)
2.3.6	Route 4 Bridge	over Sprout Brook, Paramus, Bergen County, NJ	1	48'-0"	209'-0"	AZ 36	N/A	Sheetpile Deadman	Sand, Silt, Clayey Silt, Gravel, Rock	3.674E9	Skyline Steel LLC (2001)

Notes: (1) Sheet pile sections as per local manufacturer.
(2) Lateral support defined herein as the support provided to the pile in the abutment to resist horizontal loads along the longitudinal axis of the bridge.
(3) Refers to the flexural rigidity of the total abutment width.

2.2.4 Literature review of axial load tests on sheet piles

The review of the open literature revealed only a few axial pile load tests on sheet piles as listed in Table 2-4. This table presents a summary of key information from the identified tests and a summary of the findings. The following subsections summarize the most relevant axial load tests available for sheet piles.

2.2.4.1 Axial Load Test Reported by Bustamante and Gianeselli (1991) – Sand Test Site

Bustamante and Gianeselli (1991) present results of a full-scale static axial load test of a sheet pile wall and box pile driven into a very dense sand soil at a site located in Dunkirk, France. The geotechnical conditions at this site and the embedment depth of the test sheet pile wall is shown in Figure 2-4. The test sheet pile wall consisted of four Larssen IIs sheet pile sections resulting in a wall width of 5' 3" (2 m) that were driven to a depth of approximately 24' 3.3" (7.4 m). The geotechnical conditions at the site were investigated using CPT soundings performed at the site. Figure 2-4 shows CPT tip resistance profiles and the geotechnical profile for the site that consisted of a sandy, clayey silt layer with loose to medium density extending to a depth of 8' 10" (2.7 m) and an average CPT tip resistance (q_c) value of approximately 290 psi (2 MPa). The silt layer was underlain by a dense to very dense sand that extended to a depth of about 16 meters that is beyond the final embedment depth of the tip of the test sheet pile. The CPT q_c values for the very dense sand layer increased with depth to approximately 5.07 ksi (35 MPa) at the pile tip depth of 24' 3.3" (7.4 m).

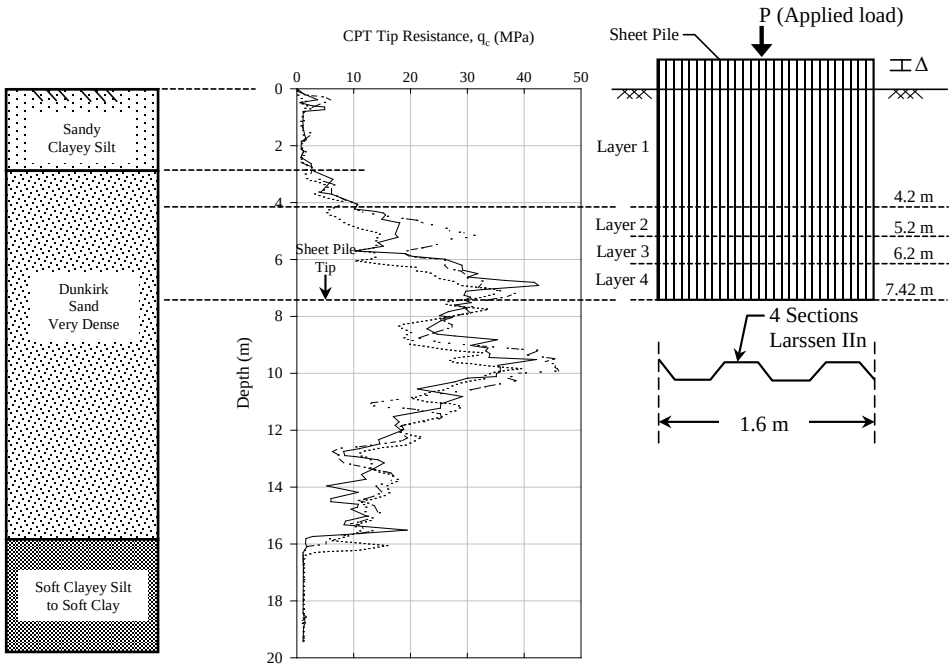

Figure 2-4: Geotechnical conditions at Dunkirk test site (adapted from Bustamante and Gianeselli 1991)

Table 2-4: Summary of axial load tests performed on sheet piles

Reference	Type of Load Test	Test Site Location	Type of Soil	Soil Characterization Tests	Sheet pile Length and Section	Description of Instrumentation installed on pile	Comparison Pile Used	Plugging Discussed	Summary of main findings
Bustamante and Gianeselli (1991)	Full Scale	Dunkirk, France	Sand	CPT, SPT		Strain gages along length of pile	Box pile	Yes	• Higher axial load bearing capacity observed in sheet pile as compared to box pile.
	Full Scale	Merville, France.	Clay	CPT, SPT		Strain gages along length of pile	Box pile	Yes	
Evans et al. (2012)	Proof test with live load	Black Hawk Co., Iowa, US	≈ 10 ft of sand, over 8 ft of clay, over bedrock.	SPT	15 ft, PZ-22	Vibrating wire strain gages.	N/A	No	• End bearing on bedrock. • Axial capacity adequate, controlled by structural capacity.
Taenaka et al. (2006)	Full Scale	Japan.	Sand, silt, and gravel	SPT		Strain gages along length of pile	Box pile	Yes	• Higher axial load bearing capacity observed in sheet pile as compared to box pile • Observations made regarding plugging behavior based on CT scans of model tests
	Model	Japan, University (controlled lab conditions)	Toyoura sand	Well characterized test sand		None	Box pile	Yes	
Rybak and Zyrek (2013)	Full Scale	Warsaw, Poland	Sand	Not reported		None	Box pile	Yes	• Successfully demonstrated ample axial load bearing capacity of sheet piles • Notes uncertainty regarding and importance of plugging

The results of the axial load test reported by Bustamante and Gianeselli (1991) are shown in Figure 2-5. The load test results indicate an axial load capacity of 539.5 kips (2,400 kN) for a corresponding pile head settlement of approximately 2.9 inches (73 mm). The sheet pile was instrumented which allowed determination of the axial load distribution and experimental load transfer curves (T-Z for side shear and Q-Z for end bearing). The shaft and tip resistances developed at the maximum axial load of 539.5 kips (2,400 kN) were measured to be 422.6 kips (1,880 kN) and 116.9 kips (520 kN), respectively. Using the CPT tip resistance values, the sheet pile geometry (assuming an unplugged condition) and the LCPC static method by Bustamante and Gianeselli (1982) for estimating axial capacity of single piles predicted shaft and tip resistance values of 467.6 kips (2,080 kN) and 67.4 kips (300 kN), respectively. Bustamante and Gianeselli (1991) attributed the higher measured tip resistance to partial soil plugging at the tip. The authors concluded that the axial bearing capacity of the sheet pile wall was high.

[Note:100 kN = 22.5 kips]

Figure 2-5: Axial load test results of sheet pile wall a sand site at Dunkirk, France (adapted from Bustamante and Gianeselli 1991)

2.2.4.2 Axial Load Test Reported by Bustamante and Gianeselli (1991) - Clay Test Site

Bustamante and Gianeselli (1991) present a second static load test of a sheet pile wall at a predominantly clayey site located in Merville, France. The site involved an upper clayey silt layer, about 6.6 to 9.8 feet (2 - 3 m) thick, underlain by Flanders clay. The Flanders clay is a high plastic clay with Atterberg liquid limit ranging between 72 to 92% and plasticity index from 38 to 58%. The natural water content of the Flanders clay was reported as varying between 30 to 41% with a total unit weight between 115.8 to 121.5 pcf (18.2 to 19.1 kN/m^3). Standard penetration tests (SPT) as well as CPT tip resistance values recorded at the test site are presented in Figure 2-6.

The test sheet pile wall consisted of four Larssen IIs sheet piles, which corresponds to a net wall width of 2 meters, a net cross section of steel of 54.87 in^2 (354 cm^2), and a total perimeter skin area per unit depth of embedment of 18.5 ft^2/ft (5.64 m^2/m). The load test results reported by Bustamante and Gianeselli (1991) for the axial load test at the Merville clay site are shown in

Figure 2-7. The ultimate load was 674.4 kips (3,000 kN) for a pile head settlement of about 0.6 inches (15 mm).

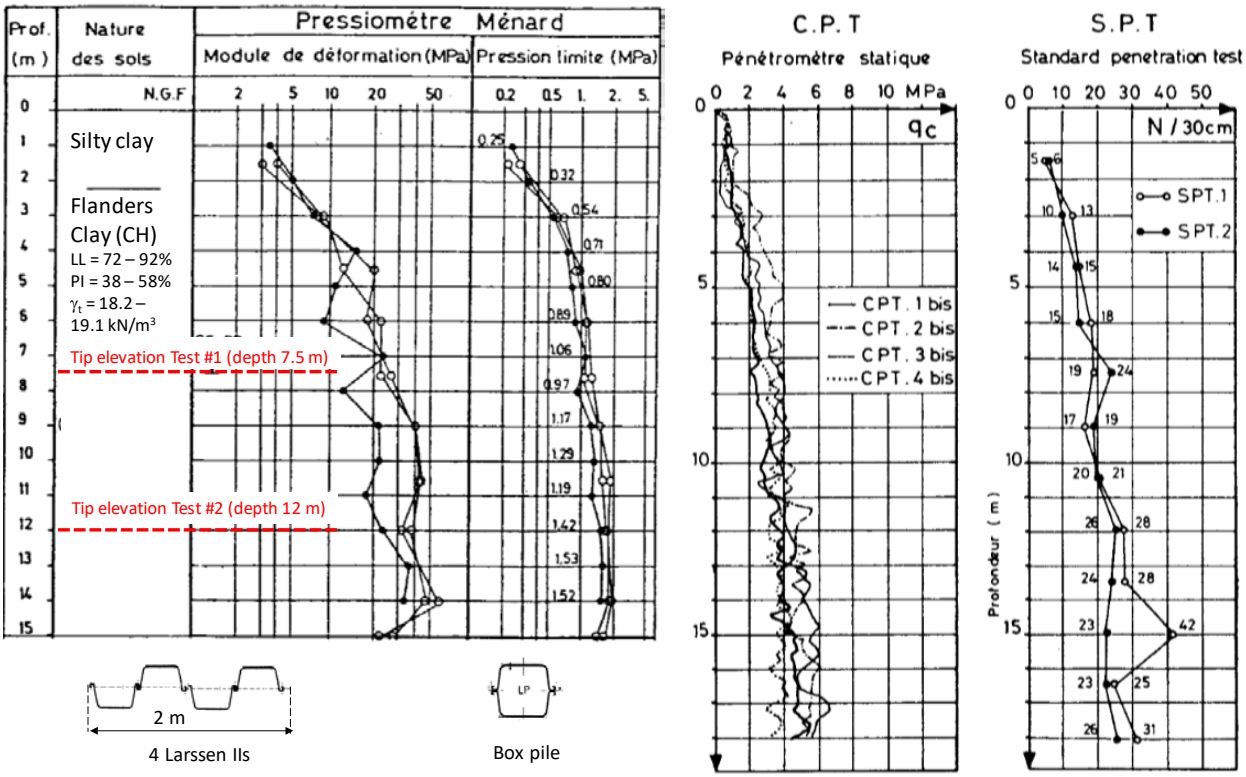

Figure 2-6: Summary of geotechnical information at Clay site at Merville, France (adapted from Bustamante and Gianeselli, 1991)

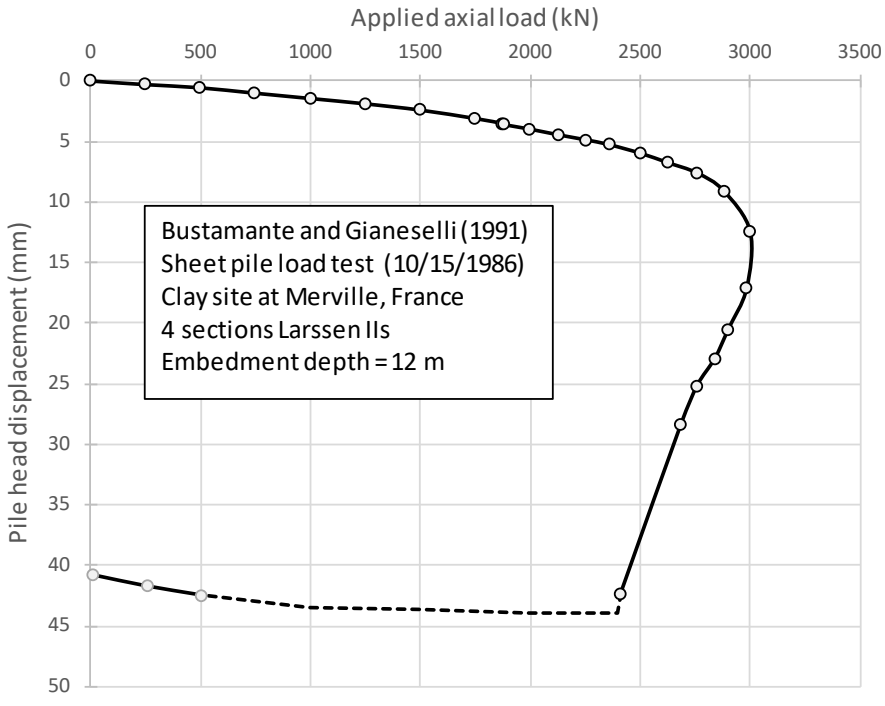

[Note: 100 kN = 22.5 kips]

Figure 2-7: Axial load versus settlement of sheet pile wall at clay site at Merville, France (adapted from Bustamante and Gianeselli, 1991)

Pile instrumentation was used to measure ultimate tip and shaft resistances of 114.4 and 560 kips (509 and 2491 kN), respectively. Using the CPT tip resistance values, the sheet pile geometry (assuming an unplugged condition) and the LCPC static method by Bustamante and Gianeselli (1982) predicted tip and shaft resistance values of 14.4 and 469.9 kips (64 and 2,090 kN), respectively. Similar to the load test at the sand site in Dunkirk, the tip resistance is underpredicted by the CPT based LCPC static method proposed by Bustamante and Gianeselli (1982). Bustamante and Gianeselli (1991) comment that the axial capacity of the sheet pile wall is extremely high compared to results carried out on a box pile with the same embedment depth (between 2.3 to 2.8 times higher). The relatively large tip resistance at the clay site in Merville is likely also associated with partial or total soil plugging at the tip, however the authors did not discuss this matter for the clay site load test.

2.2.4.3 Axial Load Test Reported by Taenaka et al. (2006) - Sand Site in Japan

Taenaka et al. (2006) reported a load test case history performed at a sand test site located at the Technical Development Bureau of the Nippon Steel Corporation in Japan. The test site consisted of layered stratigraphy, as shown in Figure 2-8 alongside SPT results from a geotechnical investigation. The field test program involved axial load tests on a sheet pile wall (two sections) and a box pile using the pile configurations shown in Figure 2-8. The test piles were driven using vibratory equipment to an embedment of about 11.6 m.

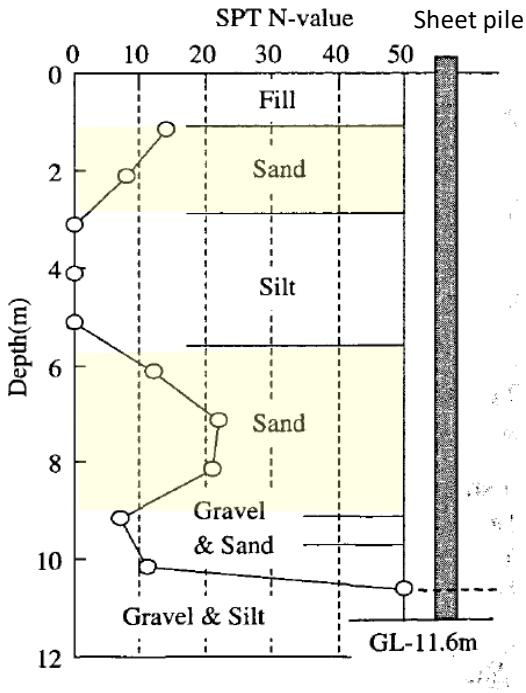

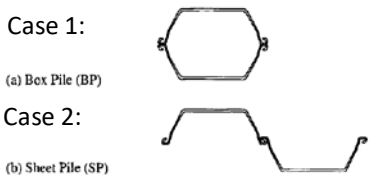

Case / Item	Case-1 Box pile	Case-2 Double sheet piles
Width of each pile (mm)	600.0	600.0
Embedment (m)	11.6	11.6
Total sectional area (cm^2)	207.8	207.8
Total perimeter (mm)	1895	3790
Plug area (cm^2)	1798.0	Unknown

Figure 2-8: Geotechnical profile and test pile information for axial load test at sand site in Japan (adapted from Taenaka et al. 2006)

The test piles were installed in close proximity to each other and it is reasonable to assume comparable soil conditions for each test pile. The axial load test results obtained for both test piles are shown in Figure 2-9(a). The load settlement curve for the sheet pile showed a stiffer response and a larger axial load capacity compared to the box pile. However, the sheet pile has twice the skin friction area due to the larger perimeter. A comparison of the development of shaft resistance (skin friction) is shown in Figure 2-9b. This figure shows an ultimate skin friction of about 1930 kN and 580 kN, for the sheet pile and box pile, respectively.

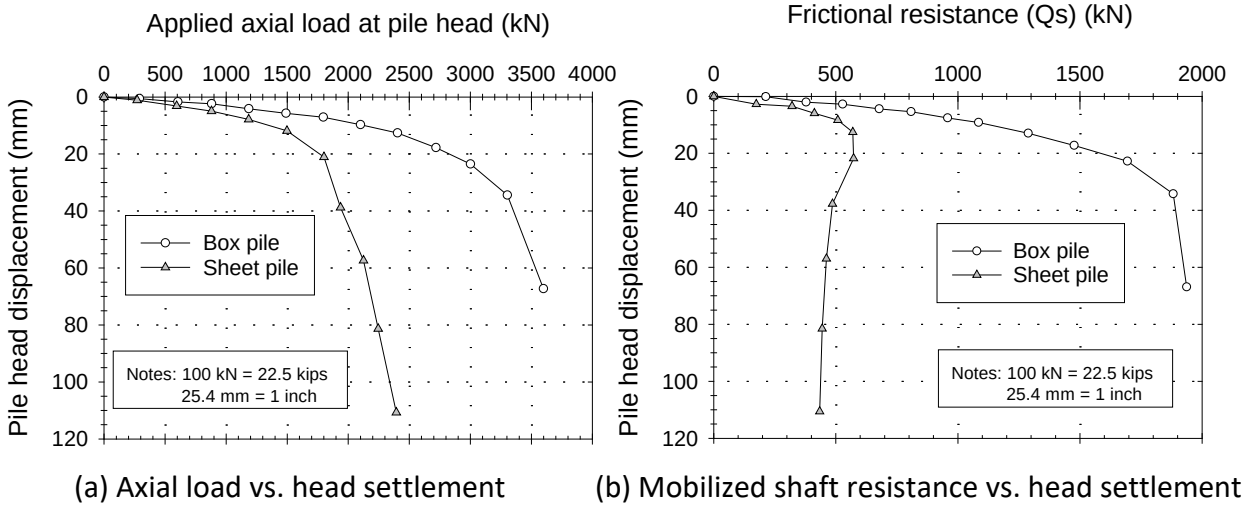

(a) Axial load vs. head settlement (b) Mobilized shaft resistance vs. head settlement

Figure 2-9: Axial load test results from Taenake et al. (2006)

The axial load distribution curves for the box pile and sheet pile, as reported by Taenaka et al. (2006), are shown in Figure 2-10. Taenake et al. (2006) present Q-Z load transfer curves for both piles as shown in Figure 2-11. This figure indicates that the development of the tip resistance as a function of the pile toe displacement was the same for both test piles. The authors conclude that a fully plugged condition developed for the box pile, and indicate an unknown plugging condition for the sheet pile test pile.

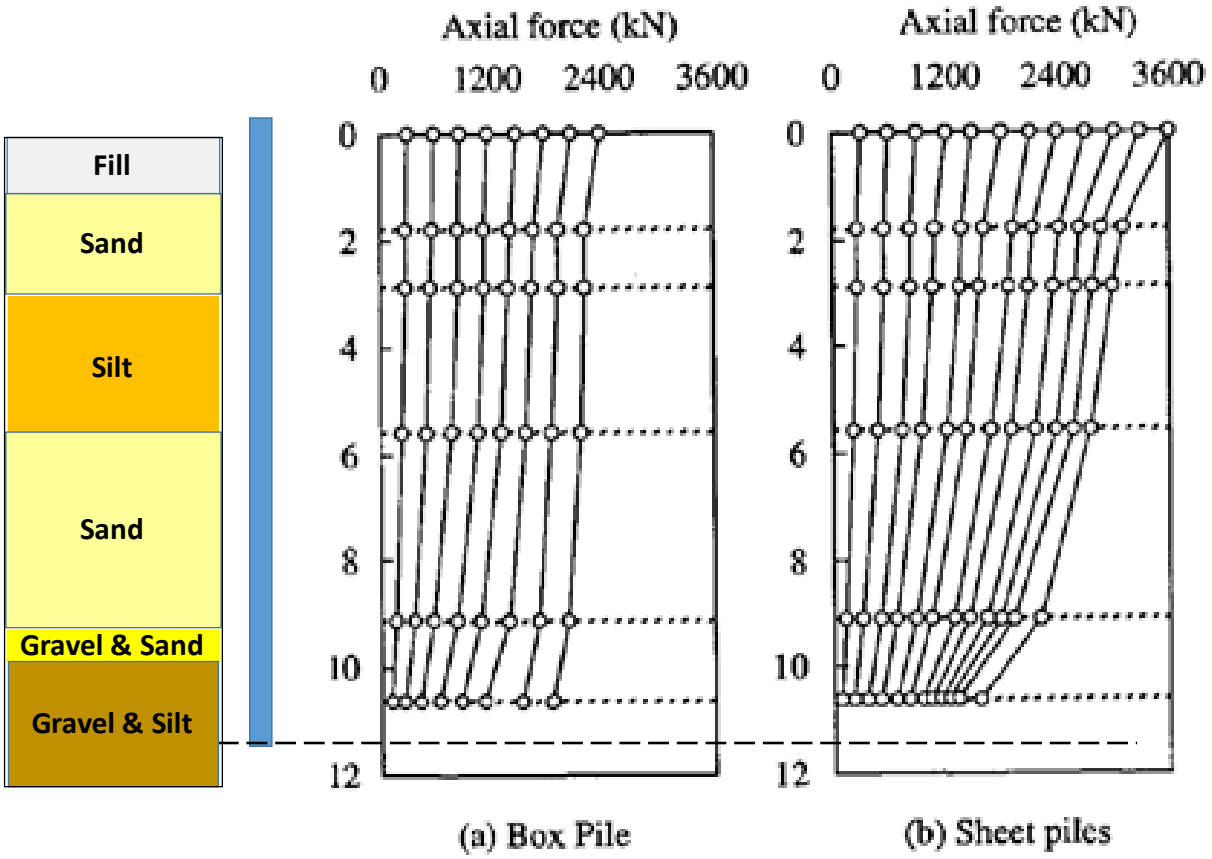

Figure 2-10: Comparison of axial load distribution curves (adapted from Taenaka et al., 2006).

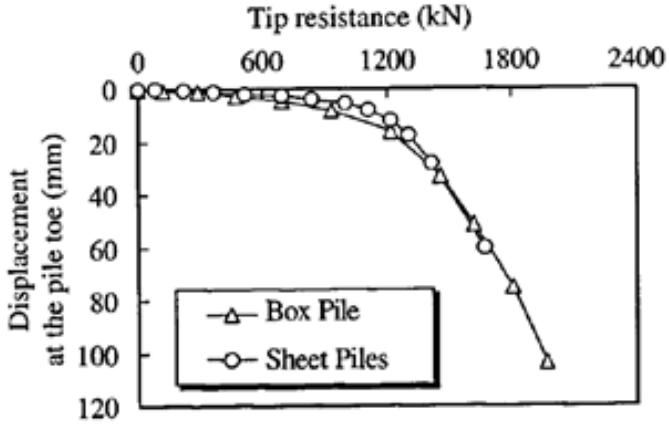

Figure 2-11: Q-Z curves for both test piles (adapted from Taenaka et al. 2006)

2.2.4.4 Model tests by Taenaka et al (2006) to investigate plugging potential of sheet piles

Taenaka et al. (2006) investigated plugging of sheet piles through a series of small-scale axial load tests performed on model tests installed in a rigid aluminum cylindrical container backfilled with dry, uniform sand. Recognizing possible limitations related to scale and boundary effects, this study is considered useful and relevant to our study because it included CT scan imaging results that provide evidence of occurrence of plugging for these types of piles and sheds some light on shape of the plug as well as the type of geometry and soil conditions needed to produce a plug. The aluminum cylinder container used in this study is shown in Figure 2-12(a). The container a diameter was 140 mm with a total height of 445 mm, and a net soil thickness of 275 mm. The test plan included three types of model pile cross sections as shown in the three series photographed in Figure 2-12(b). The apparatus was filled with Toyoura sand that is a uniform fine grained sand with a mean particle size (D_{50}) of 0.16 mm, and a specific gravity of 2.64. The sand was reported as compacted dry at a very dense state (relative densities between 85 to 90%). The maximum and minimum dry unit weights were reported as 16.28 and 13.15 kN/m^3, respectively. Based on the range of compacted relative densities, and the maximum and minimum dry unit weights for the sand, the placement dry unit weights are computed to range from 15.7 to 15.9 kN/m^3 (100 to 101 pcf). The axial load tests on the model piles involved application of a dead load to simulate a large surcharge pressure (see Figure 2-12(a), surcharge pressures of 2.88 and 6.03 MPa were reported). After surcharge loading the axial load was applied to the top of the model pile using a displacement controlled procedure. The failure patterns under the pile tips, as well as evidence of plugging, were acquired through CT-imaging at the location shown in Figure 2-12(a).

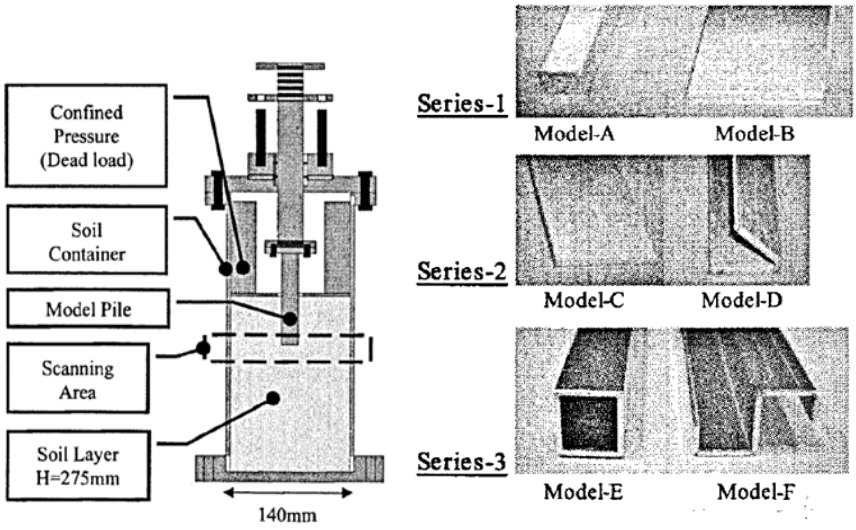

(a) Apparatus used in study (b) Cross sections of model tests

Figure 2-12: Information on model pile testing by Taenaka et al. (2006)

The tests for Series-3 involving model piles E and F were selected to approximately represent the box pile and double sheet piles field test piles, respectively. Series-3 model tests were performed with a surcharge of 6.03 MPa. Based on CT-imaging, the Taenaka et al. (2006) report the formation of a large area of increased soil density (i.e. soil plugging) near the pile tip of the model sheet pile. The CT scans reported for the box and sheet model piles are shown in

Figure 2-13. The lighter regions of the CT scans represent areas of higher soil density, and the darker regions correspond to regions of decreased soil density. The authors attribute these high density areas to the formation of a soil plug near the pile tip. Low density zones represent strain localization and the location of shear failure in the soil. The authors, based on CT-images, conclude that a partial to full plug was formed in the Model-E pile. Similarly, CT-scans for the Model-F pile indicate that a plug was formed for the model sheet pile. However, based on the images the authors consider the plug partial. Interpreted model images, in plan and elevation views, of the tip area for both model piles are shown in Figure 2-14. The applied load versus settlement curves measured for the two model test piles are shown in Figure 2-15. At a pile head settlement of 1 mm the total axial capacities were about 1.42 and 1.65 KN for the E and F model piles, respectively. The tip capacities for a pile head settlement of 1 mm were reported by the authors as 1.00 and 0.44 kN for the E and F model piles, respectively. The lower tip capacity for the sheet pile was attributed to the observed partial plug condition.

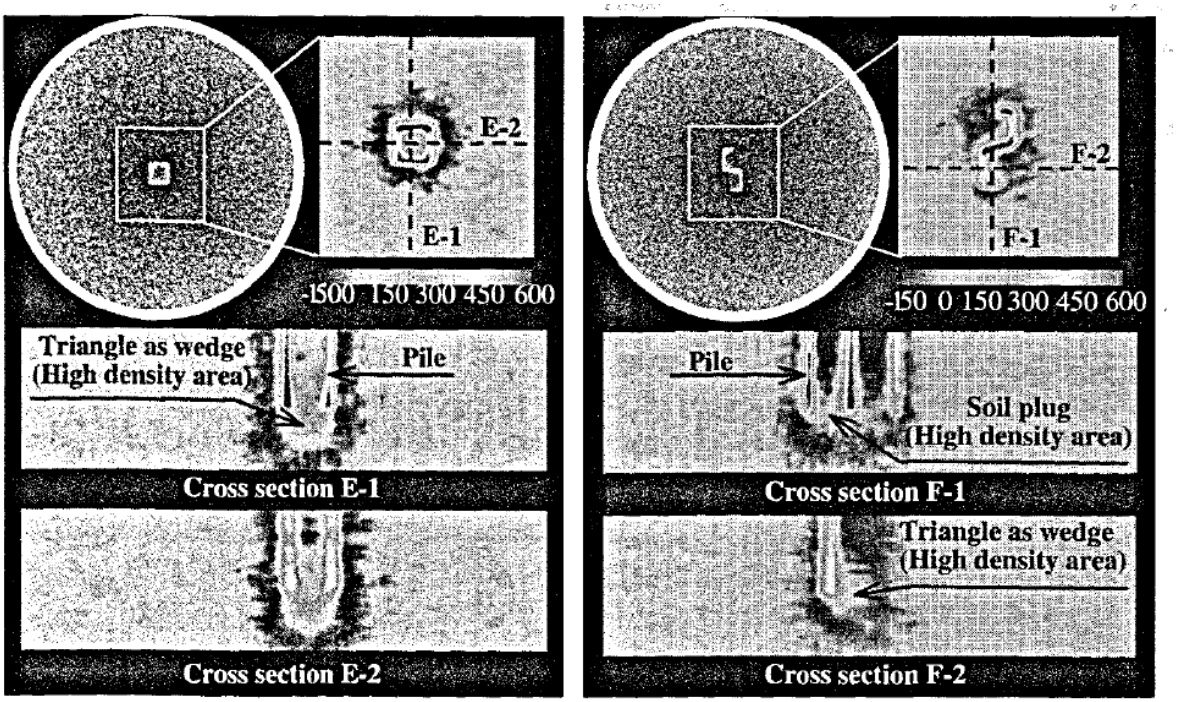

(a) Model-E: such as pipe pile (b) Model-F: such as double sheet piles

Figure 2-13: CT scans for Model piles E (box pile) and F (sheet pile) (adapted from Taenaka et al. 2006)

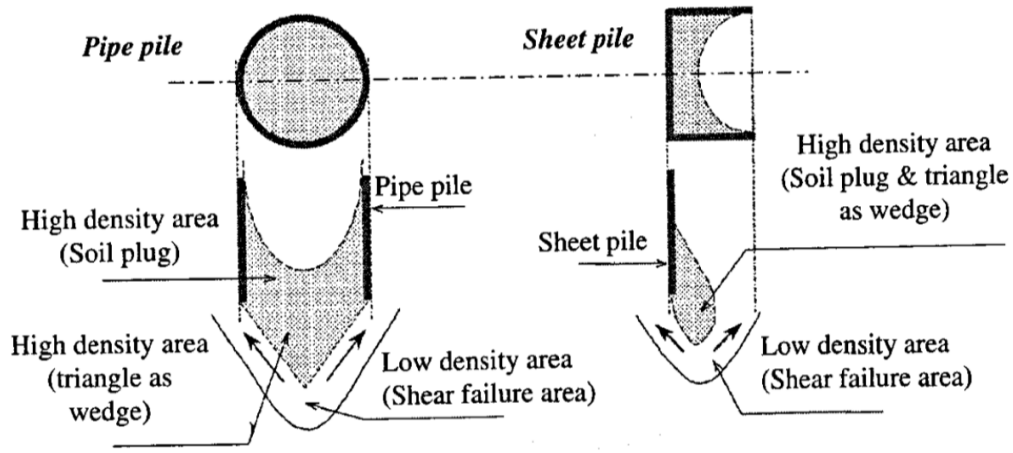

Figure 2-14: Model images of tip area of Model piles E (box pile) and F (sheet pile) (adapted from Taenaka et al. 2006)

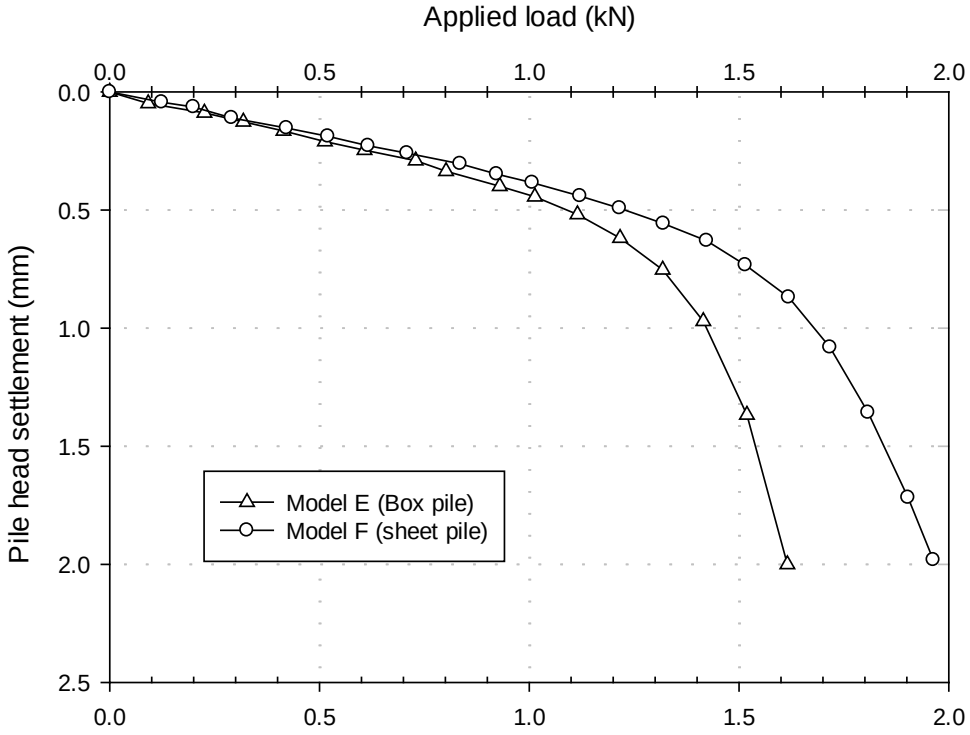

Figure 2-15: load-settlement curves for model piles E and F (after Taenaka et al. 2006)

2.2.4.5 Full scale load test of sheet pile used for bridge abutment in Poland

This case history involved a full-scale load tests on sheet piles to be used in the abutment of a bridge construction project located along the S8 Express Road in Warsaw, Poland (Skyline Steel LLC, 2009). The main purpose of the axial load tests was to demonstrate the axial load capacity of a double sheet pile wall proposed for the abutment of the bridge. The use of sheet piles was considered attractive due to their anticipated axial load capacity and time savings associated with rapid construction benefits, particularly considering the busy urban setting of this project. The bridge had a span of 15 meters (49 feet 3 inches). The final design of the bridge abutments

used double sheet pile walls constructed using Skyline AZ 37-700 sections of S355GP grade steel. The spacing between the two rows of sheet piles was 1.5 m (4 feet 11 inches). The axial load test was performed on a sheet pile pair driven into the free space between two parallel walls at a location considered to replicate similar soil conditions as the abutment piles. The setup used for the axial load test is shown in Figure 2-16. The axial load versus settlement recorded from the axial load test is shown in Figure 2-17 (Rybak and Zyrek, 2013). The maximum load applied during this test was 2,000 kN for a pile head displacement of about 25 mm. The specified design load for this project was reported as being 1,212 kN. This design load capacity was reached at a pile head settlement of about 3 mm.

Figure 2-16: Setup of pile load test at S8 Express road in Warsaw, Poland (Skyline Steel LLC, 2009).

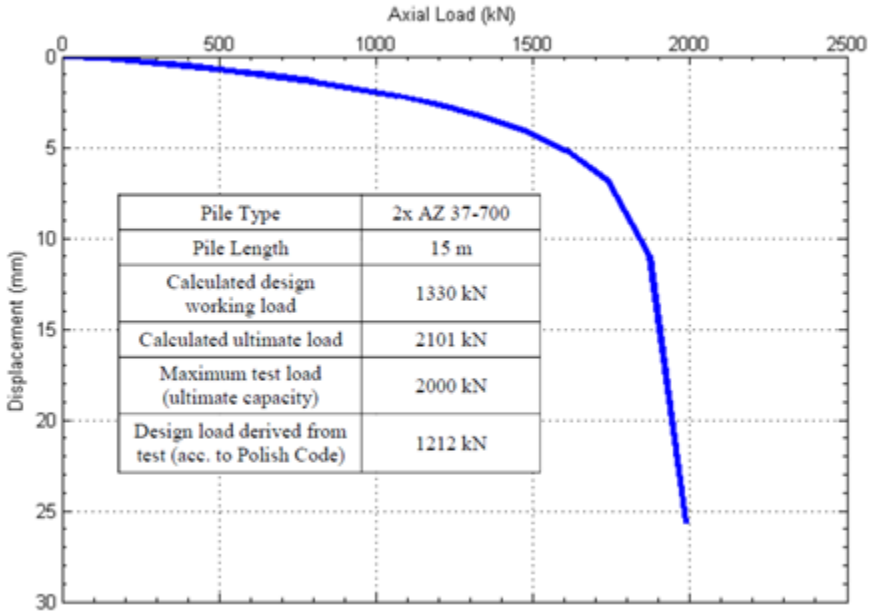

Figure 2-17: Axial load test results on double sheet pile wall in bridge in Poland (Rybak and Zyrek, 2013)

2.2.5 Summary of sheet pile case studies

A total of 24 case studies found in Europe and the U.S. were presented in sections 2.2 and 2.3 including a summary of relevant information for each case history presented in Table 2-1 through Table 2-3. Some important conclusions that can be made from these findings are that

all bridges identified are single span designs and abutments have been comprised of a wide range of sections, including both U-shaped and Z-shaped sections in opened, boxed, and mixed configurations. It was found during the literature review that there are more axially loaded sheet pile abutments in Europe than in the U.S. However, the European case studies typically present the use of a combination wall (e.g. regular sheet pile wall in combination with sheet box piles to carry axial loads) while the U.S. case studies typically present a single sheet pile wall of the Z-shaped configuration.

Abutment designs were found to differ slightly for cases where sheet piles are used as axial load bearing members. In some instances, these sheet pile abutments are laterally supported via tie rod anchors to a deadman. And in other cases, they are designed as a cantilever wall. Some abutment designs are integral or semi-integral, while others are conventional. In some rare cases in the US, a bearing plate was included to help distribute loads from the abutment to the sheet piles. In general, it was observed that axially loaded sheet piles had a greater embedment depth into the abutment cap than if the sheet piles were not loaded. The abutment cap may have many different configurations depending on the loading and design requirements. Axially loaded sheet piles are generally designed longer than piles that are designed only for scour protection, although when box piles are used in combination with sheet piles to carry axial loads, the design length of the sheet piles is typically reduced.

Overall, the wide range of design details and locations where sheet piles have been used as the primary bearing elements in bridge abutments, including in some cases for over 25 years (particularly in Europe), suggests the strong potential for incorporating the contribution of sheet piles to the axial capacity of abutment designs. Furthermore, these case studies suggest that the number of conventional bearing piles can be reduced or perhaps safely eliminated, from the abutment design altogether under appropriate conditions. It is consistently reported that these sheet pile abutments save a significant amount of construction time and cost where sheet piles would be normally installed only as facing or scour protection elements. Nevertheless, it should be noted that significant details are missing from the literature regarding geotechnical conditions, long-term performance, and other pertinent information. The literature review highlights the important need for additional well documented case histories and, in particular full-scale axial load tests.

2.3 Summary of existing design methods for axially loaded sheet piles

The literature review performed for this project identified only the publication by Yandzio (1998) as having structural and geotechnical recommendations for designing steel sheet piles as load bearing elements of bridge abutments.

Yandzio (1998) reports several bridge case histories where sheet piles were successfully used as main load bearing elements in the bridge abutment. Several of these case histories were presented earlier in this chapter. Below is a summary of the main design recommendations that apply to the scope of this project as presented by this author.

2.3.1 Structural design considerations and design codes from Yandzio (1998)

As mentioned before the use of sheet pile walls as the foundation element of a bridge abutment is a soil-structure-interaction problem. Yandzio (1998) recognized this and presented several structural design considerations as follows:

- Only steel sheet piles were considered and several configurations that included walls composed of several Z-type sections or box configurations.
- The bridge abutment design needs to consider interaction with the bridge involving lateral displacements due to thermal expansion and contraction of the bridge. It also involves moment, lateral loads, and associated deformations and rotations, from the interaction with the bridge superstructure and bridge abutment fill. The design of sheet piles under this more general loading conditions was not part of this the current study focused on axial load capacity.
- Design guidelines must comply with applicable bridge design standards. Yandzio (1998) refers to several British standards including BS 5400 (on design of structural elements of bridges), BS 8002 (on the design of earth retaining structures such as an abutment sheet pile wall), BS 8004 (for foundation design), etc. Based on the year of publication, Yandzio (1998) refers to Eurocode 7 for geotechnical design considerations.
- Yandzio (1998) refers to documents from the British Highway Agency BD 57 and BA 57 to address durability considerations. A design life of 120 years is mentioned as the target, but it is recognized that it is difficult to meet in most modern reinforced and prestressed concrete construction. Durability although very important was not part of the scope of the present study.
- Consistent with modern LRFD design, the main limit states considered are ultimate limit state (ULS) and serviceability limit state (SLL). The main ULS failure modes considered in standard sheet pile design used in canals and for retention projects. A summary of the predominant limit states is presented in Figure 2-18.
- Load considerations include: soil weight, soil lateral earth pressures, ground water and seepage forces, surcharge loads, interaction with bridge superstructure (dead loads, live loads, temperature, etc).

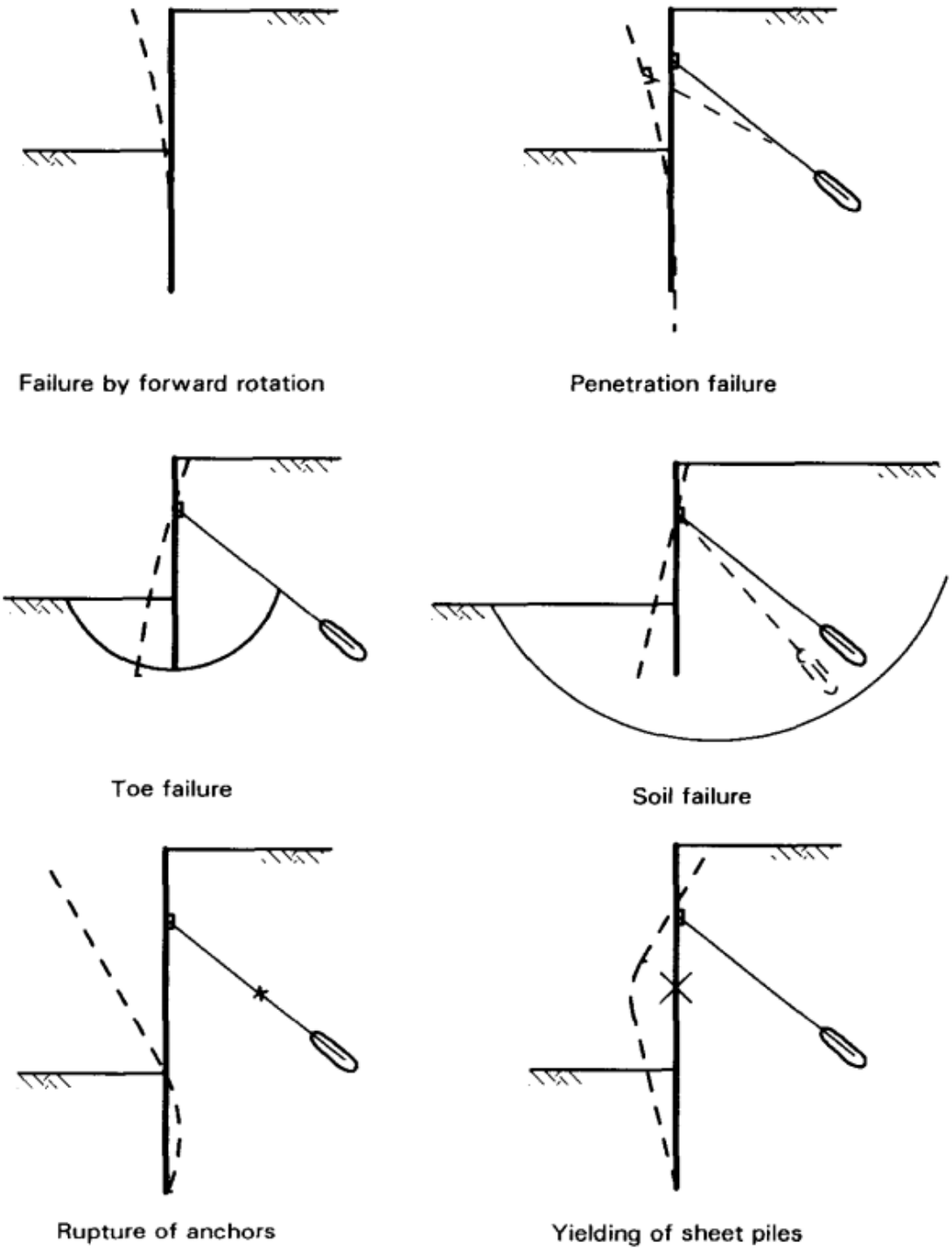

Figure 2-18: Main ultimate limit state modes of failure for sheet piles (adapted from Yandzio, 1998).

2.3.2 Geotechnical design considerations from Yandzio (1998)

Yandzio (1998) considers the axial load transfer mechanisms for a sheet pile wall the same as a conventional deep foundation with the two main components coming from skin friction resistance (shaft resistance) and from end bearing resistance (toe or tip resistance).

Yandzio (1998) refers to the alpha and beta methods as static methods suitable for estimating the unit side friction for cohesive and frictional soils, respectively. These methods are listed in Table 2-5. The two static methods mentioned by Yandzio (1998) are commonly used by USDOT and a detailed description of these, and other static methods, can be found in the FHWA driven pile manual (Hannigan et al., 2016).

Similarly, for estimating the unit toe resistance Yandzio (1998) described several static methods as listed in Table 2-5.

Table 2-5: Static methods described by Yandzio (1998) for axial load capacity sheet piles.

Component	Soil type	Details	Additional information
Side or shaft resistance (fs)	Sand with SPT data	$fs = 2N$ (1)	N = uncorrected SPT value at location of shaft (Meyerhof, 1956). Units = kPa.
	Sands and clays (drained behavior)	$fs = \beta \times \sigma'_v$ (2) $\beta = Ks \times \tan \delta$ (3) $\delta = 1/2\phi' - 2/3\phi'$ (4)	Beta method based on normal stress acting on pile wall and interface friction angle δ.
	Clays undrained	$fs = \alpha Cu$ (5)	Alpha method.
Toe or tip resistance (q_b)	Clay (undrained)	$q_b = 9\ Cu$ (5)	Cu = undrained shear strength of clay beneath toe. q_b in same units as Cu.
	Sand with SPT data	$q_b = 400N$ (1)	N = uncorrected SPT value at pile base (Meyerhof, 1956). Units = kPa.

Notes: (1): SPT based method proposed by Meyerhof (1956).
(2): Effective stress β-method (Details in Hunnigan et al. 2016).
(3): Yandzio (1998) reports use of K_s ranging from k_a (active wedge zone) and k_p (passive wedge zone).
(4): Yandzio (1998) reports this range for δ based on differences of mobilized interface friction for active and passive wedge zones.
(5) Total stress α-method (Details in Hunnigan et al. 2016).

An important design consideration reported by Yandzio (1998) is that the side friction (or skin friction) along the active side the sheet pile should be neglected above the so called point of stability. This point of stability can be determined from moment equilibrium and it corresponds to the first inflection point in the moment diagram along the length of the sheet piles where the moment is zero. This is shown schematically in Figure 2-19.

It should be noted that Yandzio (1998) reported a modified beta method for estimating the side resistance of sheet piles un bridge abutments to allow for consideration of the differences in the active and passive sides of the sheet pile. The beta coefficient is computed as:

$$\beta = k_s \cdot \tan(\delta) \quad \text{.....(2.1)}$$

Where k_s = the lateral earth pressure coefficient that can be taken equal to k_a if f_s is being evaluated in the active side, or k_p is it is being evaluated along the passive side of the sheet pile.

Regarding the possible presence of plugging, Yandzio (1998) indicates the toe capacity should be computed considering the unplugged toe area, i.e., the cross sectional area of steel assuming no plugging occurs. No comments were made regarding the consideration of plugging for the estimation of the shaft capacity.

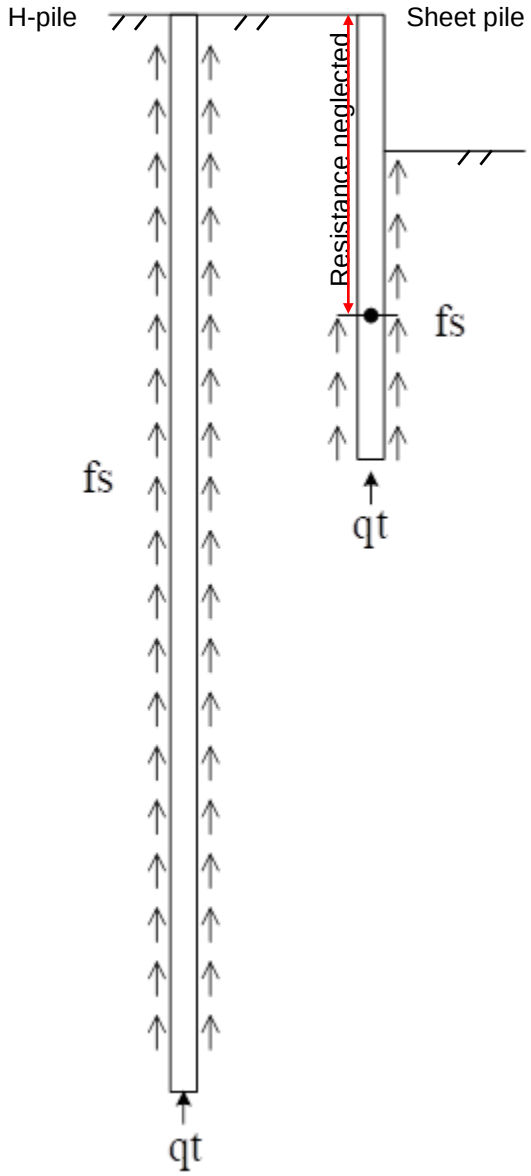

Figure 2-19: Locations along sheet pile where side friction is considered based on Yandzio (1998).

3 Load Test Program at EPIC High Bay Laboratory at UNC Charlotte

3.1 Introduction

This chapter describes the axial load test program performed on instrumented sheet piles installed at one of the geotechnical test pits of the EPIC High Bay Laboratory at UNC Charlotte. The axial load tests for this component of the research were performed in a concrete lined test pit with a 12 feet x 12 feet square footprint and a depth of 10 feet (Figure 3-1). The bottom of the geotechnical test pit was unlined and consisted of natural ground comprised of very stiff residual soils and highly weathered rock.

Figure 3-1: Geotechnical test pits at the EPIC Highbay Laboratory at UNC Charlotte.

3.2 Backfill soil and test pit compaction

The test pit was backfilled with compacted clayey to silty sand. The soil was characterized at UNC Charlotte and the main index properties of backfill soil are summarized in Table 3-1. Grain size distribution curves obtained from seven randomly selected samples are shown in Figure 3-2. Based on the laboratory characterization, the backfill soil was classified as SC to SC-SM under the Unified Soil Classification System. Compaction tests performed on this soil using Standard Proctor energy (ASTM D 698) yielded an average maximum dry unit weight of 118.8 lb/ft^3 (18.7 kN/m^3) and an optimum water content of about 12.25% (See Table 3-1 and results provided in Appendix A).

The sandy backfill was compacted in lifts of an average loose thickness of about 4 in (100 mm) (loose thickness refers to layer thickness before compaction). The soil was compacted by use of a vibratory plate and hand tampers. Compaction density and moisture were monitored during the backfilling operation using several tests, including nuclear density gage, sand cone, and drive cylinder tests. The average relative compaction achieved was approximately 92% with respect to the Standard Proctor maximum dry unit weight and the water content of the placed soil ranged between 11 to 13%, which was within one percentage point of the optimum moisture content. Photos of the test pit during backfilling are shown in Figure 3-3. The finished condition of the backfilled test pit is shown in Figure 3-4. The two rows of white PVC pipes were installed for seismic crosshole testing (described in the following section).

Table 3-1: Summary of index properties and compaction results of backfill soil.

Property	Value	ASTM Standard
Grain size distribution	**Figure 3-2 (N = 7)**	D422
D_{10} (mm)	0.0013 – 0.0088	
D_{50} (mm)	0.18 - 0.54	
D_{60} (mm)	0.38 – 0.82	
C_u	77.4 – 294	
C_c	0.86 – 4.86	
Specific gravity (Gs)	2.68 – 2.72 (N = 7)	D854
USCS	SC to SC-SM	D2487
Atterberg Limits		
Liquid limit (%)	26 – 34	D4318
Plastic Limit (%)	20 – 23	
Standard Proctor Compaction Tests (N = 2)		
Max. Dry Unit Weight $(\gamma_{dry})_{max}$ (kN/m^3)	18.66 – 18.86	D698
Optimum water content W_{opt} (%)	12.2 – 12.3	

Note: Ranges reported correspond to results of multiple tests. N = number of tests performed.

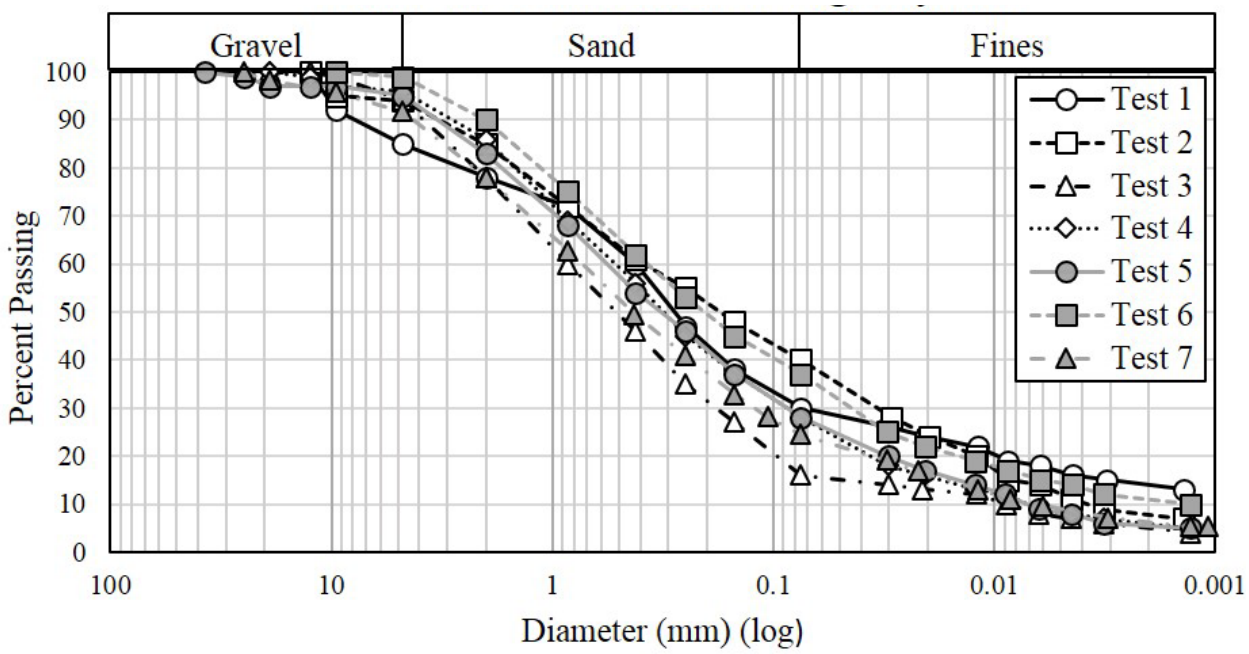

Figure 3-2: Grain size distribution curves for 7 samples of the backfill soil.

Figure 3-3: Photos of backfill compaction operation.

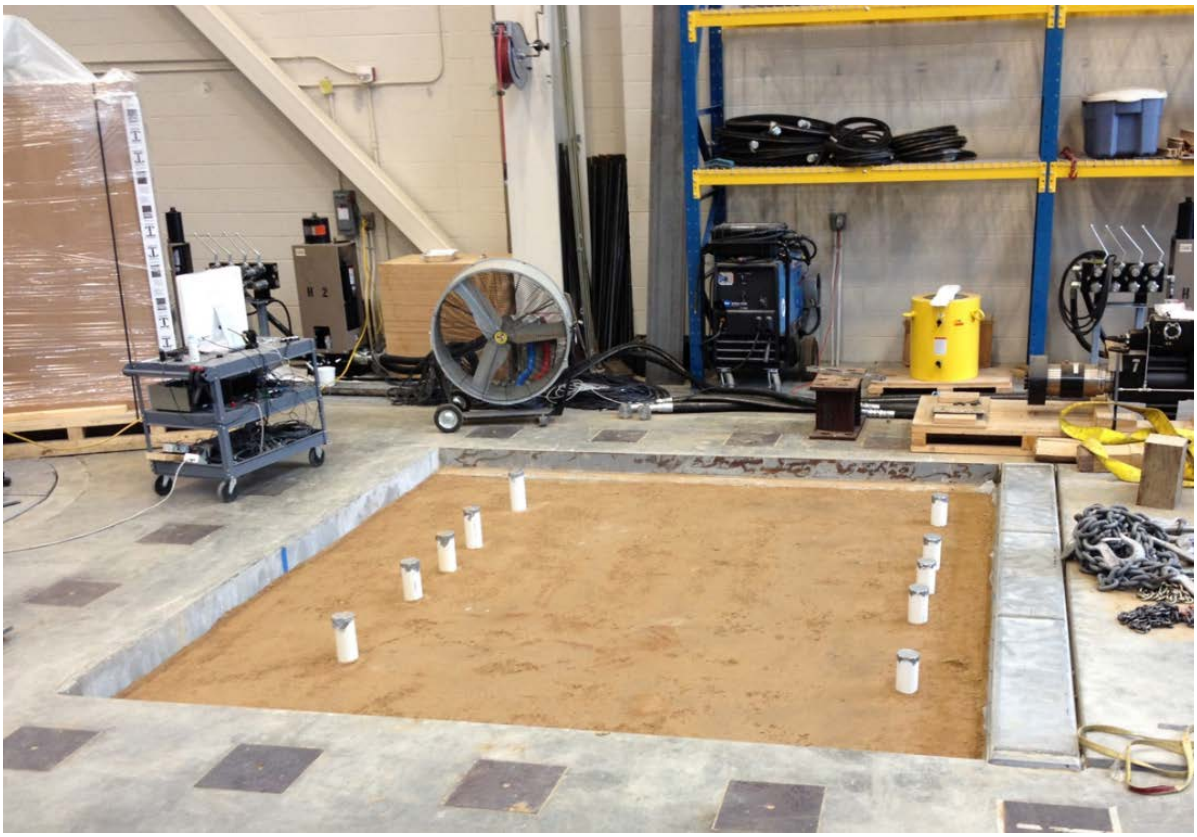

Figure 3-4: Photo of test pit at the end of backfill compaction.

3.3 Geotechnical and Geophysical Testing of the Test Pit

In-situ characterization of the compacted backfill soil was conducted by standard geotechnical field tests that included: geotechnical drilling with Standard Penetration Test (SPT), Seismic Cone Penetration Tests (SCPT), and dilatometer tests (DMT). Figure 3-5 indicates the locations of the different in-situ tests performed before and after pile installation.

A summary of the in-situ tests and the interpreted geotechnical profile in the test pit prior to pile installation is presented in Figure 3-6. As shown in this figure, the SC to SC-SM backfill soil had an average corrected SPT blow $(N_1)_{60}$ of 12 blows per 0.3 m (1 ft). The SPT blow count of the in-situ highly weathered bedrock/residual soil located at the base of the test pit was in excess of 50 blows per 0.3 m (1 ft). The pre-installation CPT tests yielded average tip resistance values of 4.1 MPa (42.7 tsf) and 6.8 MPa (70.8 tsf) for the clayey, silty sand backfill and the basal residual soil/weathered bedrock, respectively.

Figure 3-6 also shows dilatometer test results in the form of dilatometer material index (I_D) versus depth for the four DMT profiles performed. It can be seen that index values increased after pile installation as a result of densification. The effects of densification due to pile installation resulted in lower maximum depths for post-installation DMT soundings (DMT 3 and 4). The dilatometer material index (I_D) was used to estimate the dilatometer modulus (E_D) as

shown in Figure 3-7. Although the E_D modulus is not a material Young's modulus, it can be used to confirm backfill densification and increased lateral confinement due to installation of sheet piles.

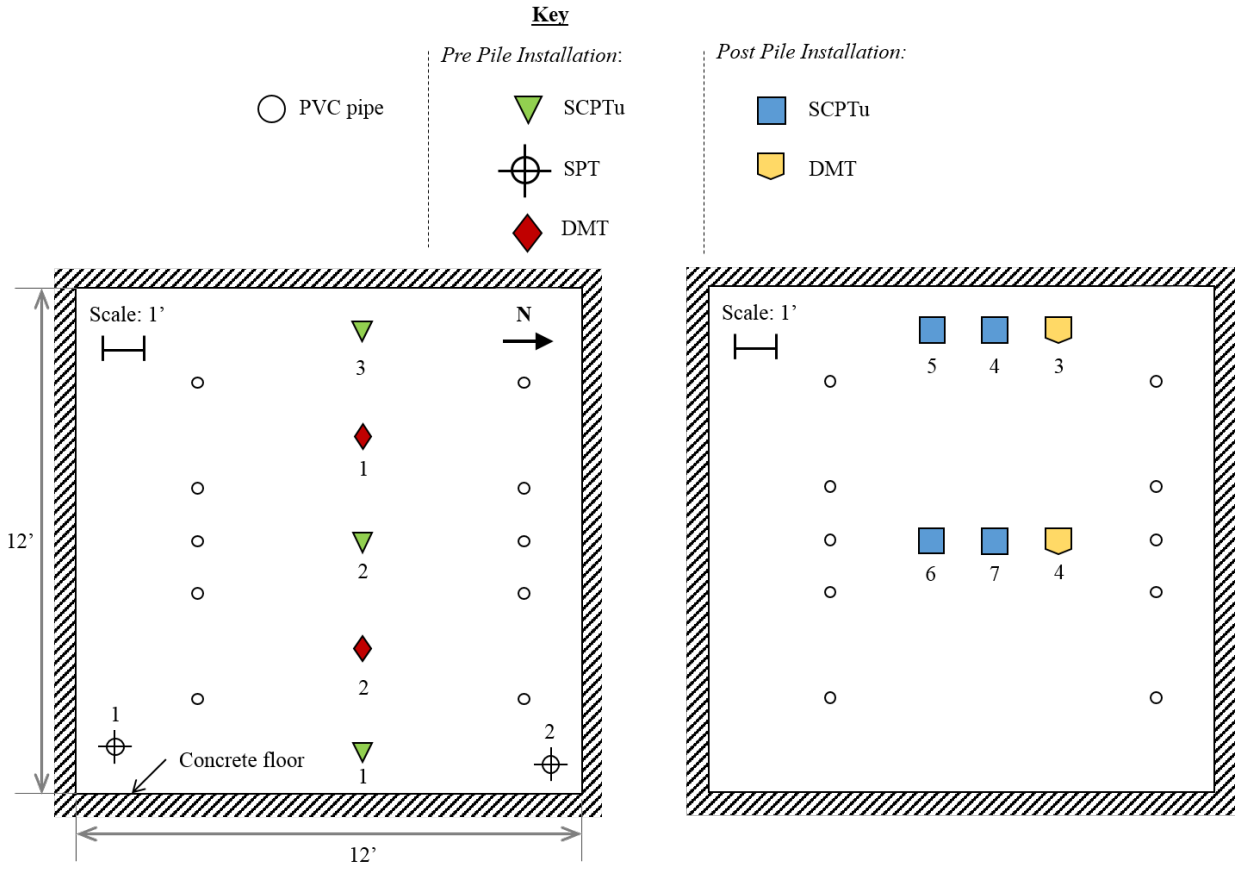

a) Tests performed prior to sheet pile installation. b) Tests performed after sheet pile installation.

Figure 3-5: Plan view showing locations of in-situ testing in test pit.

The effects of pile installation can also be assessed by comparison of the SCPTu tip and sleeve resistances measured in CPT soundings performed before (SCPTu 1, 2, and 3) and after (SCPTu 4 through 7) pile installation show in Figure 3-6. The CPT sleeve resistances increase after sheet pile installation, primarily due to densification of the soil along the pile length. It can be seen that post-installation sleeve resistance values did not increase as much below the depth of the pile toe. The post-installation CPT tip resistance values were observed to also increase with respect to pre-installation values, but to a lesser degree compared to the degree of increase observed for the CPT sleeve resistances.

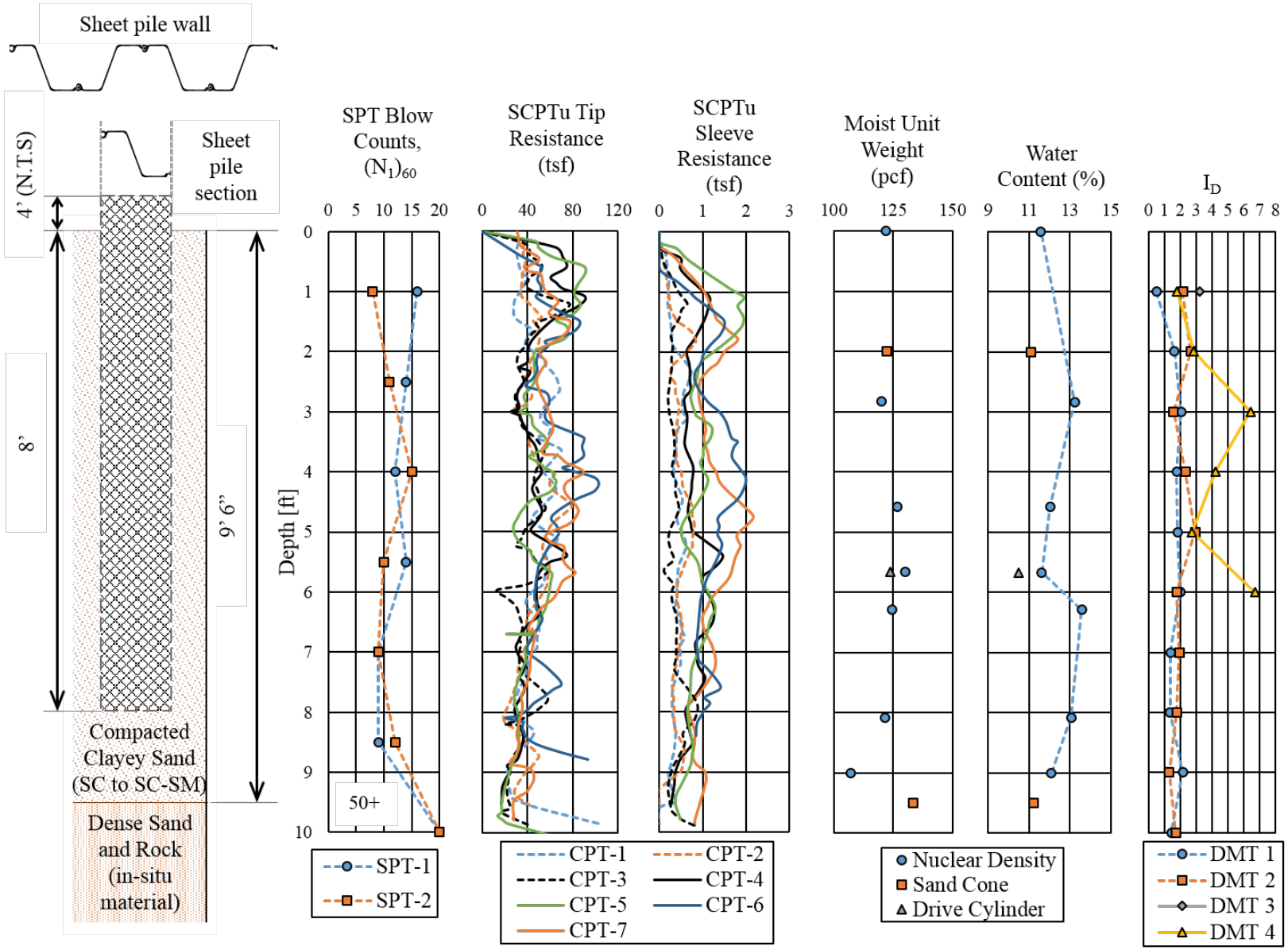

Figure 3-6: Simplified stratigraphy and select in-situ test results.

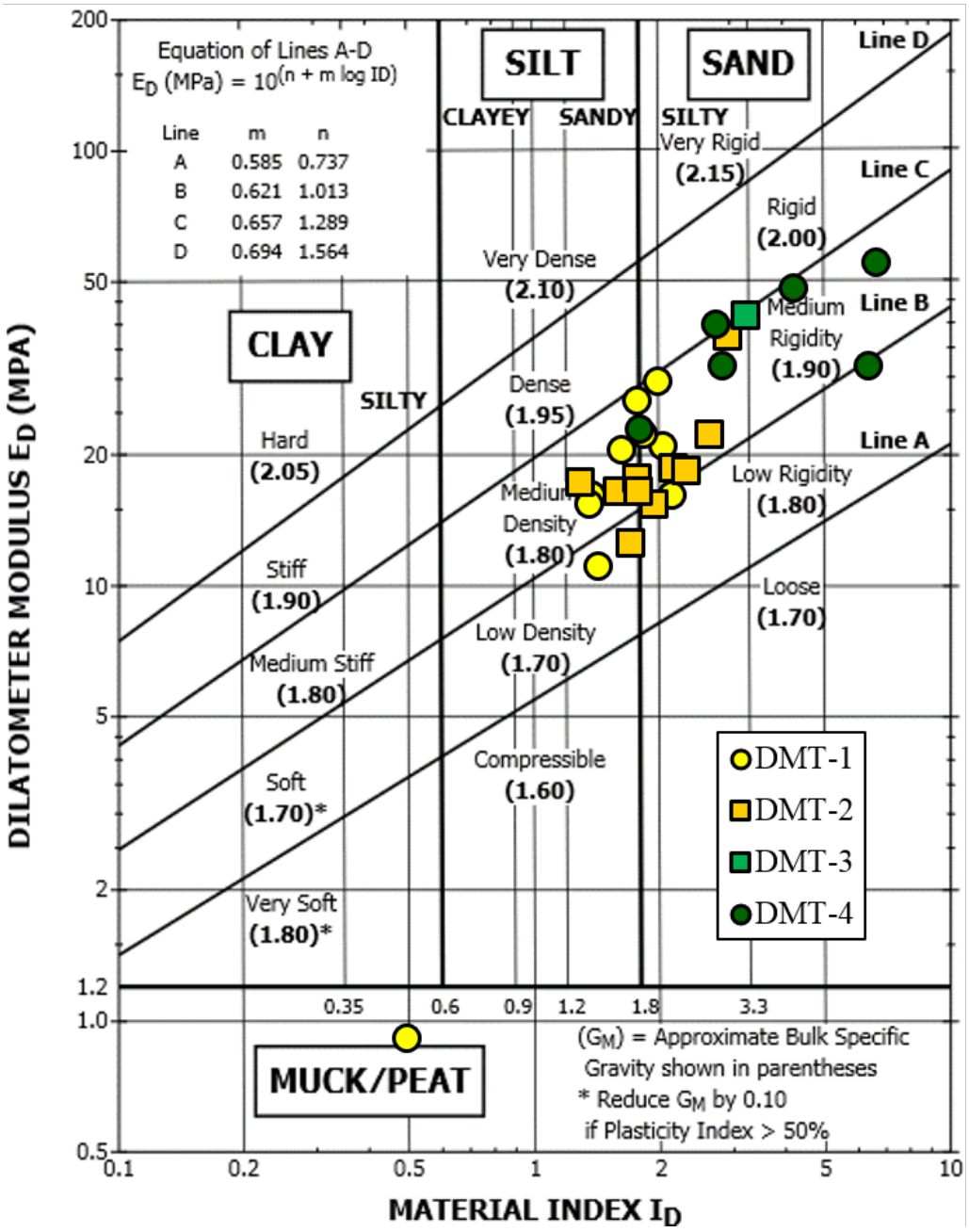

Figure 3-7: Summary of DMT test results.

3.4 Geotechnical tests on compacted backfill

The shear strength and stress-strain behavior of the compacted SC to SC-SM backfill soil were evaluated using direct shear testing (ASTM D3080) and UU triaxial testing (ASTM D2850). A summary of the main results from these tests is provided in Table 3-2. More details on geotechnical lab tests can be found in Appendix A.

Table 3-2: Summary of direct shear and UU triaxial testing of compacted backfill soil

Test	Value	ASTM Standard and notes

Direct shear test (compacted sample at target dry unit weight and moisture; not inundated)		
Peak ϕ' (deg)	39.3	ASTM D3080 Test rate = 0.0003 in/min. γ_{dry} = 17.18 kN/m^3 w = 13.1% (RC = 92% S.P.)
Peak c' (kPa)	8.4	
Residual ϕ' (deg)	n/a	
Residual c' (kPa)	n/a	
UU Triaxial compression tests		
Peak ϕ (deg)	32.2	ASTM D2850 Strain rate = 1% /min. γ_{dry} = 17.04 kN/m^3 w = 12.2% (RC = 91% S.P.)
Peak c (kPa)	22.9	
Residual ϕ (deg)	31.4	
Residual c (kPa)	22.4	
Tangential E_s (MPa)	7 - 9	

Notes: RC = relative compaction. S.P. = Standard Proctor.

The interface friction between a representative steel coupon from the sheet piles and the compacted backfill soil was assessed by means of interface shear tests performed using a modified setup of the direct shear device. A summary of the interface shear test results is provided in Figure 3-8. The measured peak interface friction angle was 28.8 degrees. Additional details in Appendix A.

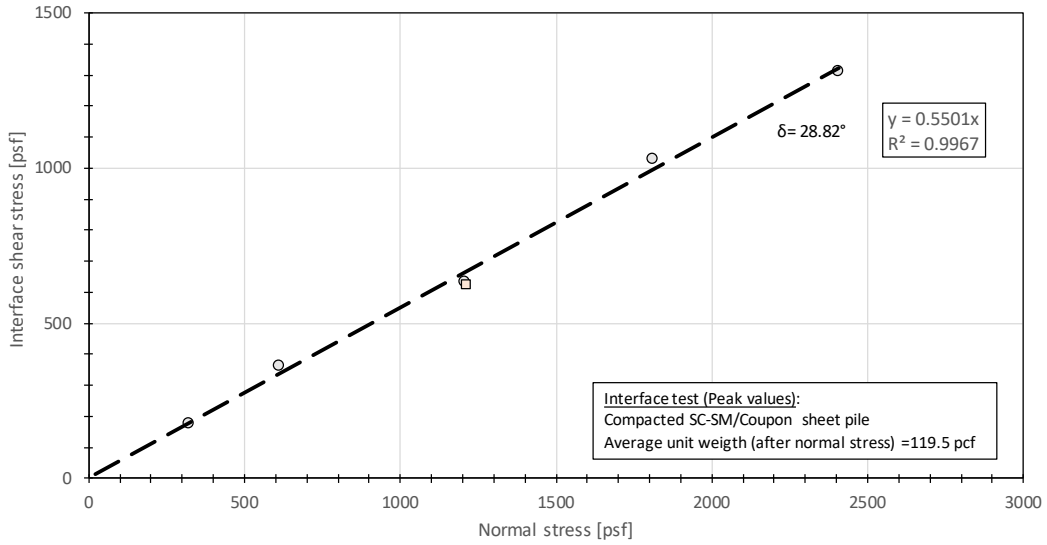

Figure 3-8: Interface friction test results (backfill soil against coupon of steel sheet pile).

3.5 Description of test sheet piles

The sheet piles used in this study were Skyline PZ-27 sections. These sheet piles are hot-rolled sections of Grade 50 steel (F_y = 50 ksi) with a nominal cross sectional area of about 11.91 in^2 per sheet (76.84 cm^2). One sheet section is 1.5 ft (0.46 m) wide and each test sheet pile wall consisted of 4 sections for a total width of 6 ft (1.89m). The total length of each test sheet pile wall was 12 ft (3.66 m) with an embedded depth of 8 ft (2.44m). The location of the two sheet pile test walls is shown in Figure 3-9. A photo of the test sheet piles prior to installation is shown

in Figure 3-10. The test sheet piles were instrumented with Bridge Diagnostics Inc. (BDI) strain transducers and Vishay Micro-Measurements constantan grid resistance strain gages. The layout of the instrumentation is shown in Figure 3-11. The dashed line shown in this figure corresponds to the ground line location after pile installation. Details on the strain gages including procedures used for installation can be found in Appendix A.

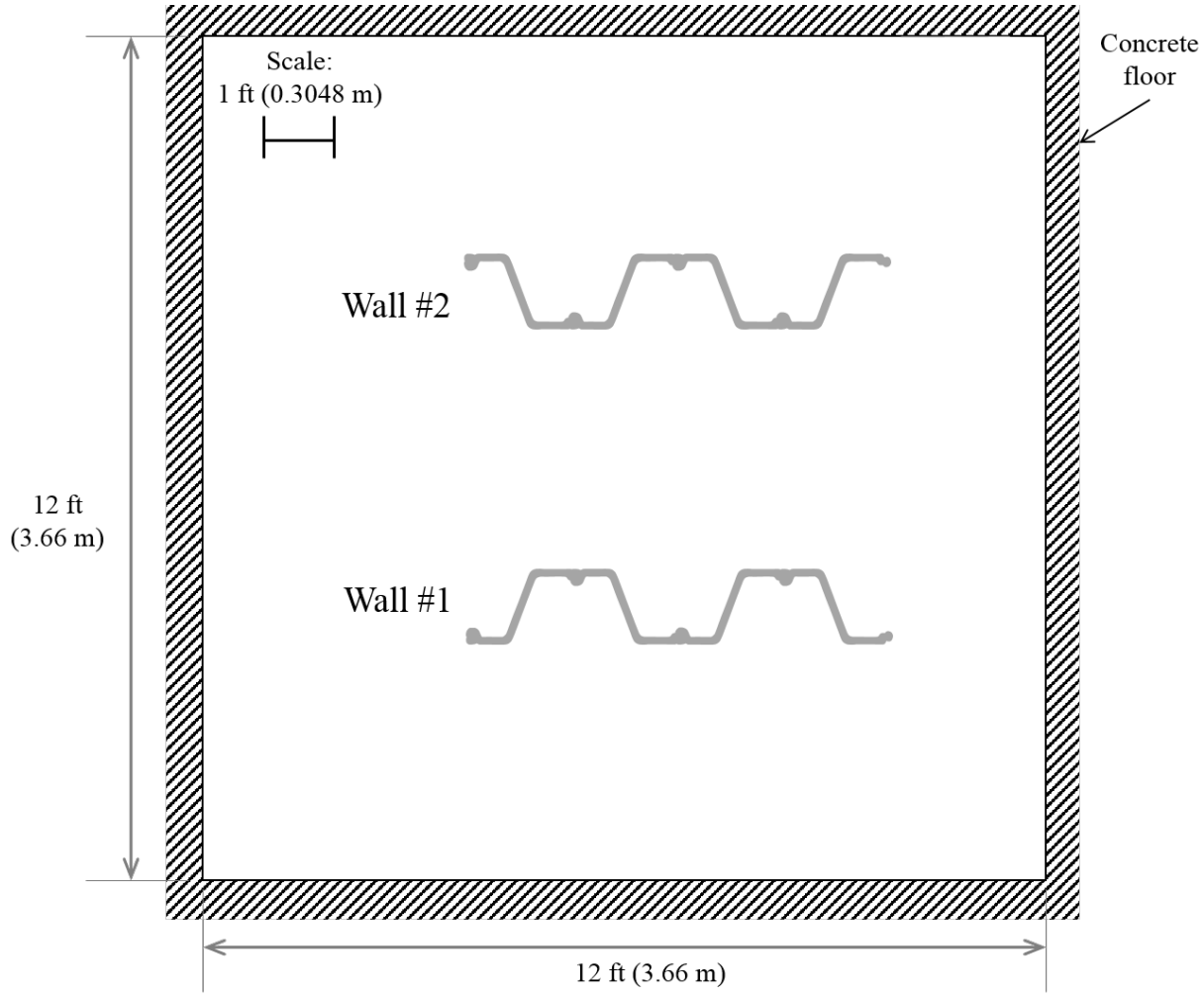

Figure 3-9: Plan view of geotechnical test pit showing locations of two sheet pile walls.

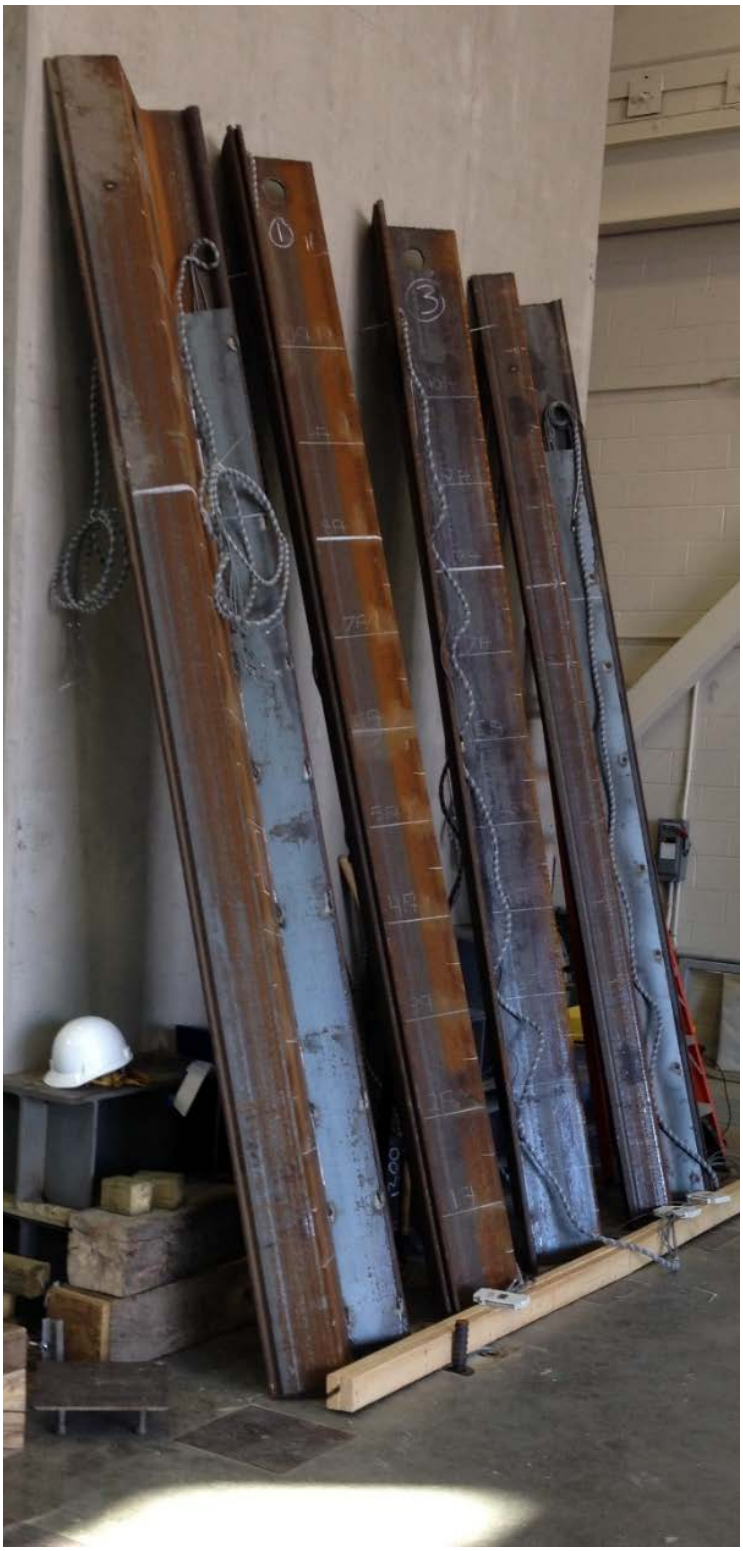

Figure 3-10: Photo of 12-ft length sheet pile sections used in laboratory load testing program.

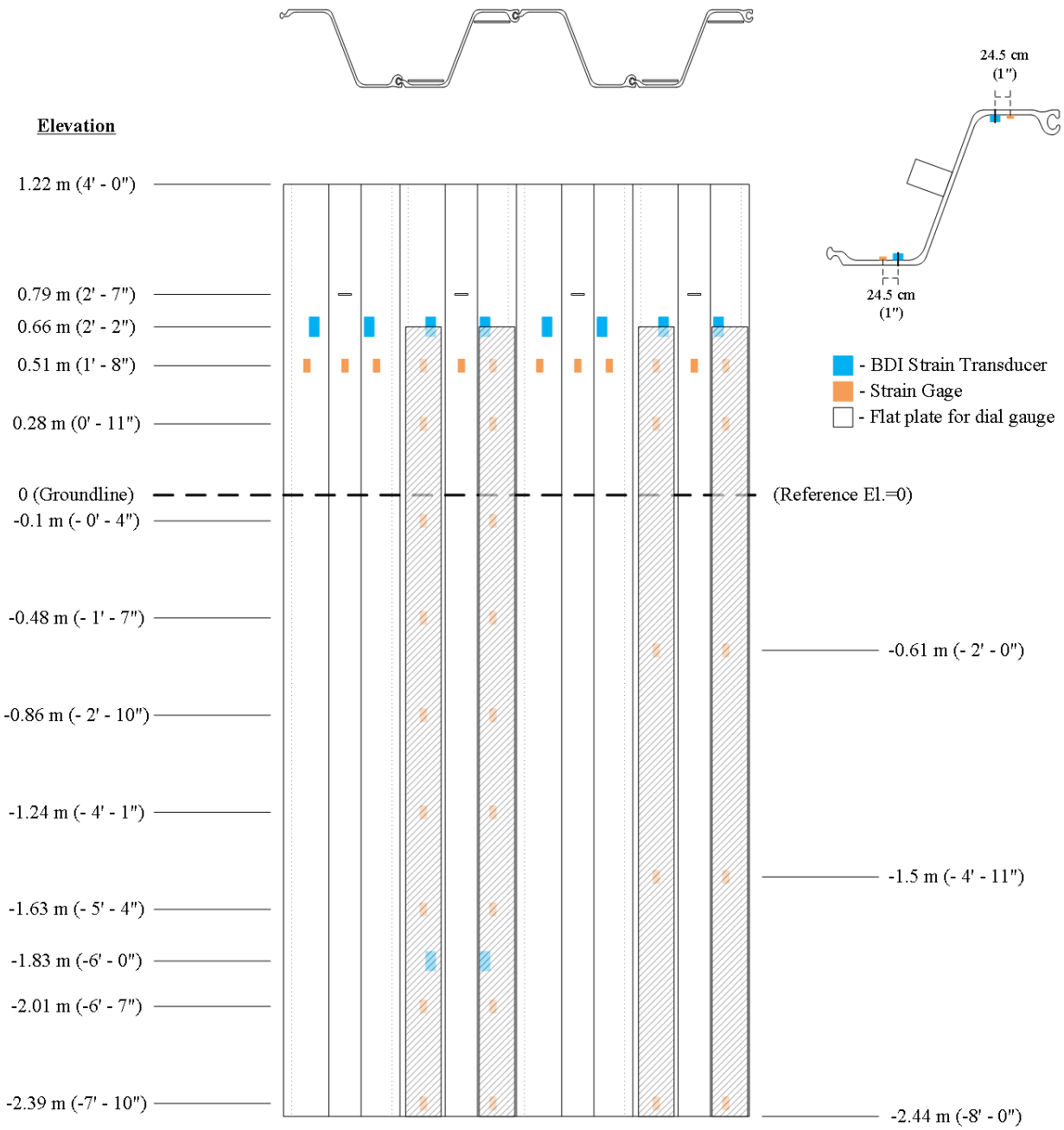

Figure 3-11: Layout of strain gages installed on the sheet pile walls (4 sections per wall).

3.6 Pile installation

The two sheet pile test walls were installed in different dates as each wall required installation of four sections of PZ-27 sheet piles. The installation dates of test walls No. 1 and No. 2 were July 29, 2014 and August 21, 2014, respectively. As shown in Figure 3-11, both test walls were installed to a final embedded length of 8 ft (2.44 m), which corresponds to an above ground length of 4 ft (1.22 m). The installation of the PZ-27 sections were performed primarily with a vibratory hammer Model ICE 6E. Figure 3-12 shows the installation records for test wall No. 2. In this figure the four PZ-27 sections are labeled Piles 1 through 4. The order of installation was first Pile #2 to a depth of about 4 feet, followed by installation of Pile #3 to the same depth of 4 feet. Then installation of Pile #2 was completed to the final depth of 8 feet, followed by Pile #3 also to 8 feet. Then installation of Pile #4 to full depth of 8 feet, followed by Pile #1.

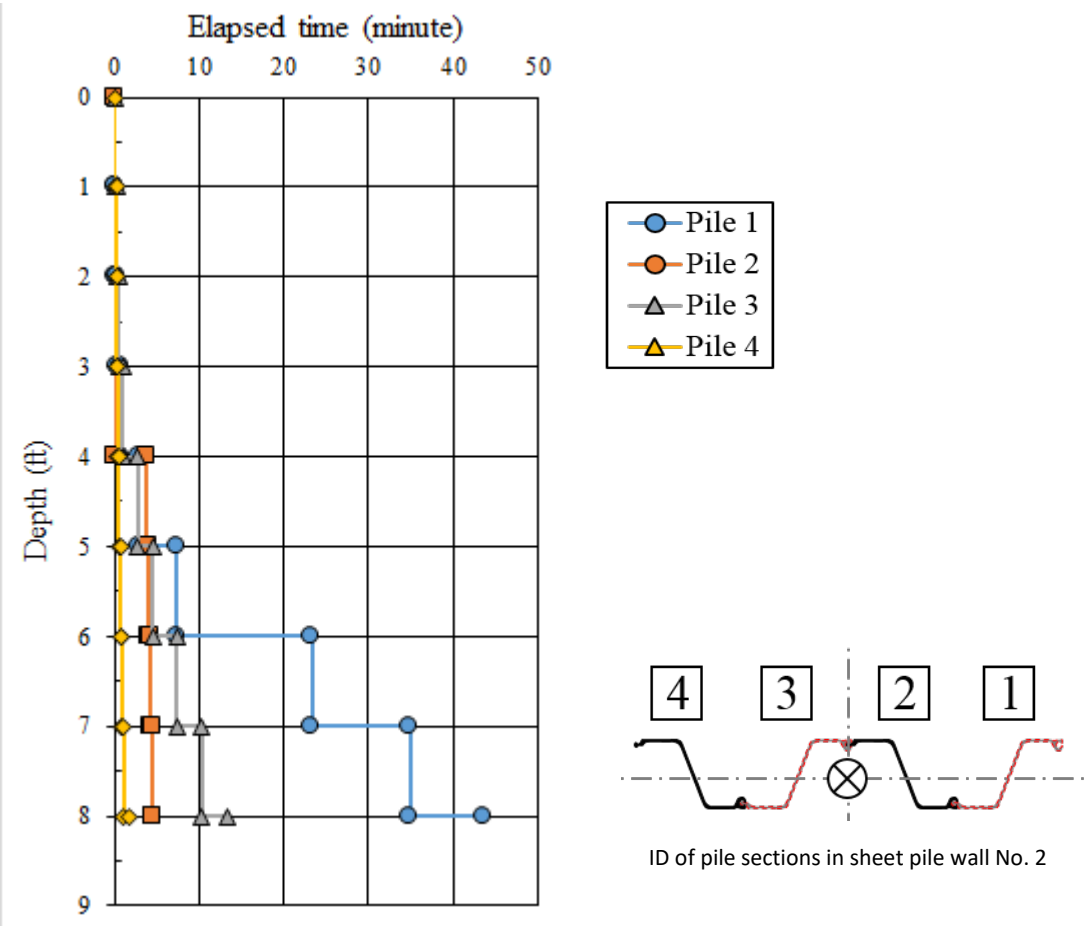

Figure 3-12: Installation record for four PZ-27 sections of test wall No. 2.

To allow for PDA and CAPWAP estimation of axial load capacity, a portion of sheet pile test wall No. 1 was installed with an impact hammer type MKT 9B3. PDA records from 15:55 to 16:02 on July 29, 2014 recorded a total of 178 blows for the installation of one sheet pile section. The PDA pile axial capacity estimate at End-Of-Driving (EOD), using the Maximum CASE Method Capacity with a JC = 0.7, was 57 kips for this single pile section. The CAPWAP analysis for hammer Blow 176, near EOD, yielded the results shown in Figure 3-13. The CAPWAP ultimate axial capacity for Blow 176 at EOD was estimated as 37 kips for this single pile section, with 16.8 kips (45.4 %) attributed to shaft resistance, and 20.2 kips (54.6 %) attributed to tip resistance.

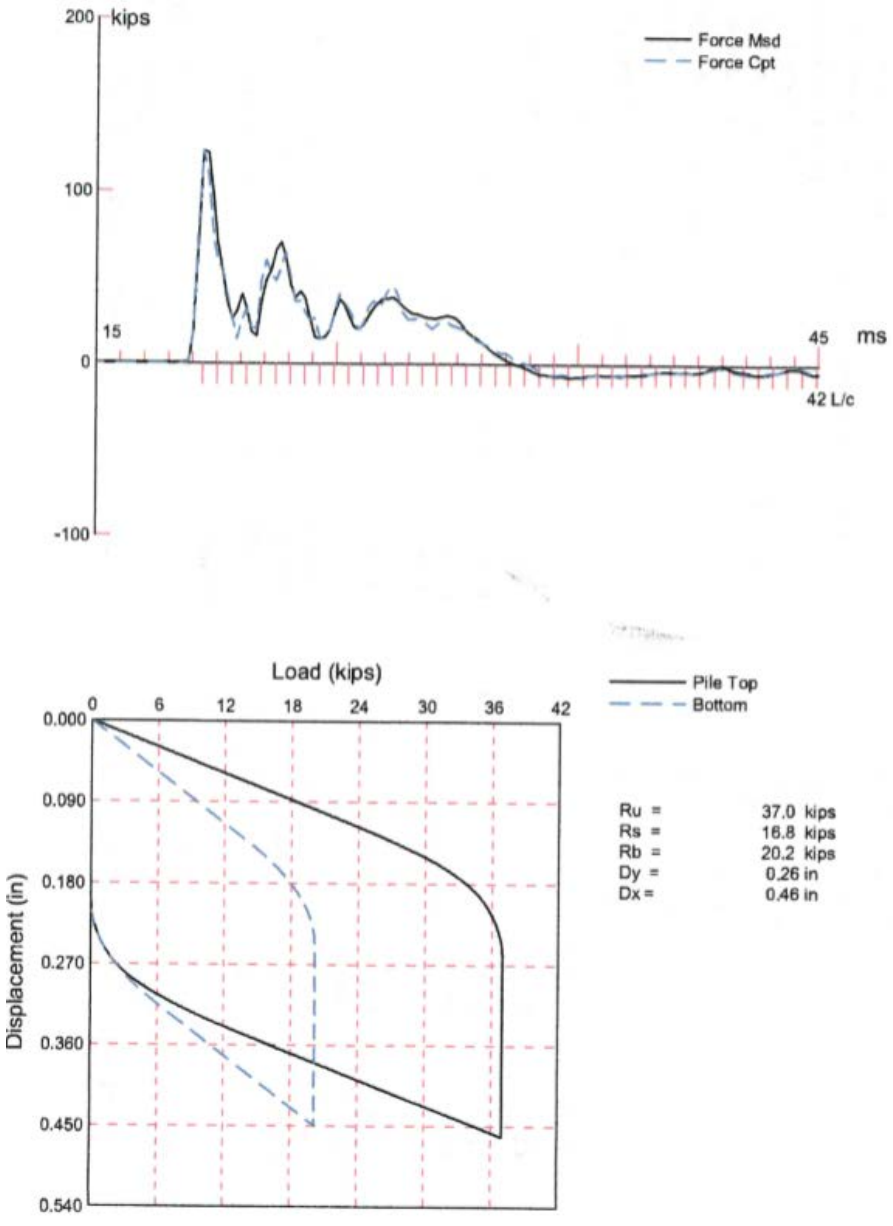

Note: Results reported by GRL Engineers, Inc (PDA Set 2: Blow 176, July 29, 2014 at 16:02)

Figure 3-13: CAPWAP results for PZ-27 section of test wall No. 1 – EOD (Blow 176).

Considering that each sheet pile wall consists of four PZ-27 sections, the estimated axial load capacity for the sheet pile walls based on the PDA and CAPWAP analyses for EOD conditions are 228 kip (1048.2 kN) and 148 kip (658.3 kN), respectively.

3.7 Axial load test program at UNC Charlotte EPIC High Bay Laboratory

3.7.1 General description

The axial load test program at the geotechnical test pits of UNC Charlotte used the general setup shown in Figure 3-14 through Figure 3-16. These figures show the reaction frame used, the load distribution assembly placed at the top of each sheet pile test wall, and the actuator, respectively.

Figure 3-14: Axial load test setup.

Figure 3-15: Load distribution beam assembly used for axial load tests.

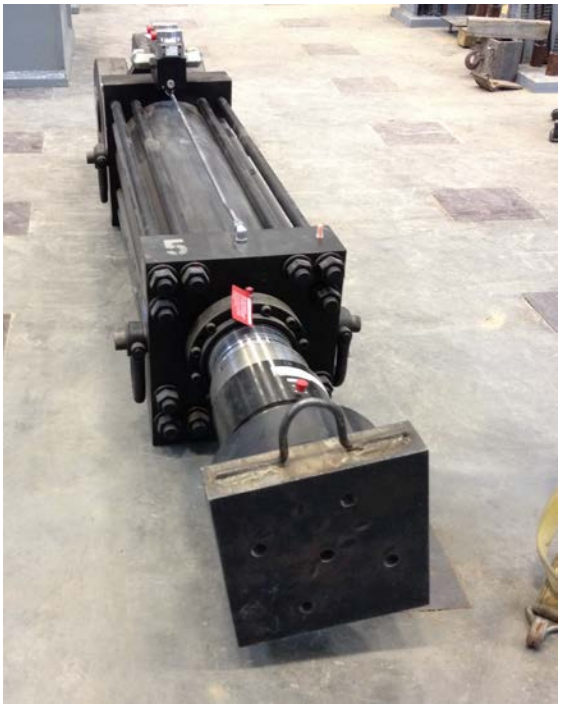

Figure 3-16: Photo of MTS actuator (328-kip capacity in compression).

3.7.2 Axial load test results

Several static load tests were performed on the two sheet pile test walls installed in the geotechnical pit at UNC Charlotte. Figure 3-17 shows a representative load-settlement curve obtained from a representative load test performed on test wall No. 2 on May 8, 2015.

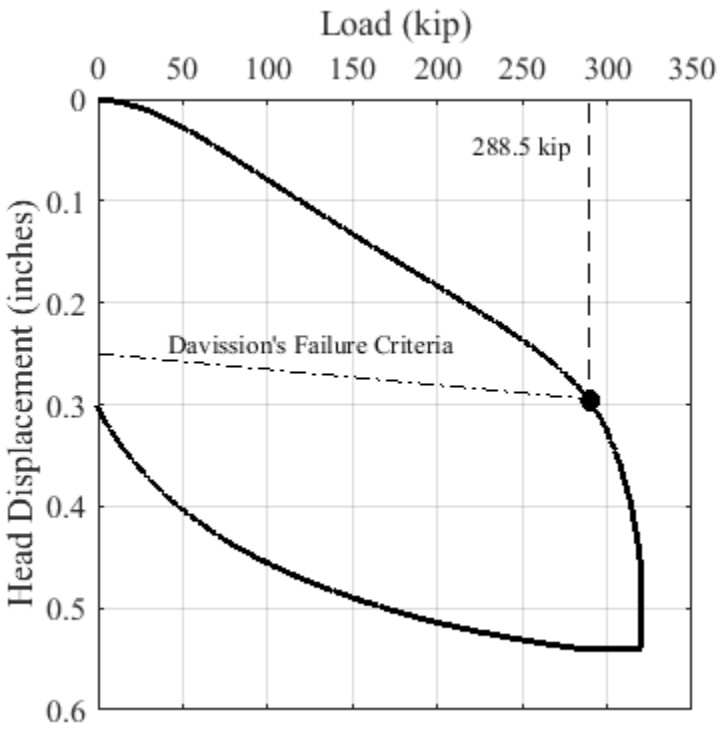

Figure 3-17: Representative load-settlement curve for sheet pile test wall No. 2.

The axial load capacity measured for test wall No. 2 was 288.5 kips (1283.3 kN) based on the Davisson failure load criterion. The corresponding pile head displacement for this failure load was measured as 0.2 in (5.1 mm). Using the measurement data from the strain gage instrumentation, plots of axial force versus depth along the sheet pile test wall were obtained for different levels of applied axial load (Figure 3-18). Based on measured load transfer, the contribution from shaft and toe resistances at the Davisson failure load of 288.5 kips (1283.3kN) are 265.6 kips (92%) and 22.9 kips (8%), respectively.

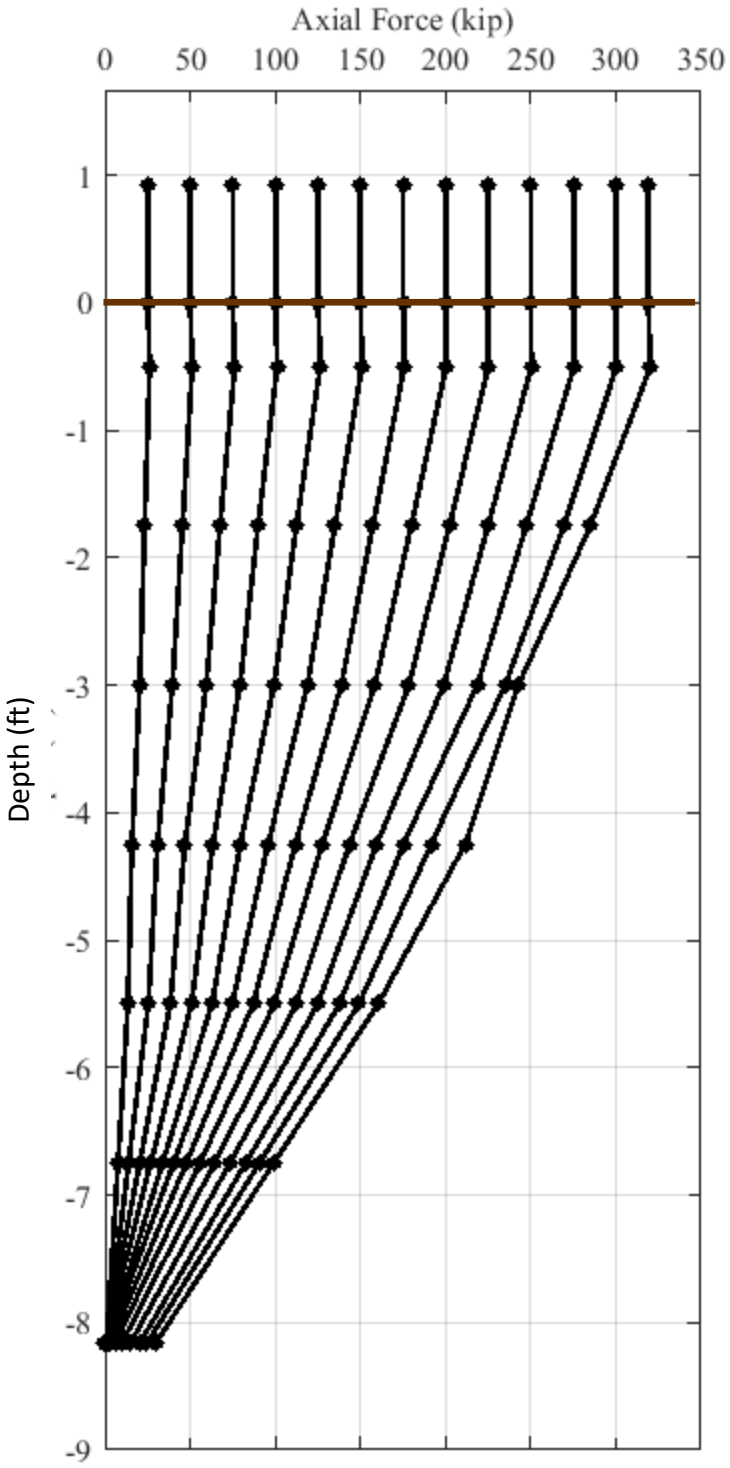

Note: Ground line located at depth 0.

Figure 3-18: Axial load distribution from representative load test.

3.7.3 Predicted axial capacities using static methods

Deep foundation design involves the prediction of axial load capacity through the use of static methods. Despite the extensive amount of research in this area, even for conventional deep foundations in relatively homogeneous soil deposits, this task is challenging as it involves great uncertainty (Randolph, et al., 1994, Olson 2002). Thus, in practice it is common to use factors of safety of two, three, or more, since measured pile capacities of driven piles have been found to differ from the calculated capacities by more than 300% (Olson 2002). It is expected that these uncertainties in predicted axial capacity by static methods will be applicable to the driven sheet pile walls. With this in mind, the axial capacity predictions presented in this section are at best expected to show a level of accuracy similar to predictions for conventional piles. In Chapter 4, a comparison of axial capacity predictions performed by static methods for a sheet pile and an H pile installed at the same field test site are presented to further support this analysis.

The static methods evaluated for prediction of the axial load capacity of the sheet pile wall were SPT-based (Meyerhof, Beta, and Brown) and CPT-based (LCPC and Nottingham and Schmertmann). The predictions of total axial capacity using these different static methods are summarized in Figure 3-19. This plot includes a horizontal dashed line indicating the result from the laboratory axial load test using Davisson's failure criterion. For each static method, two sets of predictions were performed to evaluate the two extreme pile conditions of plugged (square marker) and unplugged (horizontal line marker) behavior. The capacity estimates for the plugged condition assumed the plugged area shown in Figure 3-20. For all six static methods considered, the measured axial capacity was above the predicted capacity for the unplugged condition. The predictions using the unplugged condition assumption ranged from 44 to 114 kip. In contrast, the predictions of total axial capacity obtained using the plugged condition assumption were all above the axial load capacity measured in the load test, with the exception of the LCPC prediction. From the unplugged and plugged static capacity estimates, it is not possible to infer whether a full plugged condition developed within the laboratory tests at the UNC Charlotte geotechnical test pit as the degree of under- and over-prediction for both pile conditions is similar. However, given that nearly all methods place the measured capacity about halfway between the unplugged and plugged estimates thus suggesting that partial plugging likely developed.

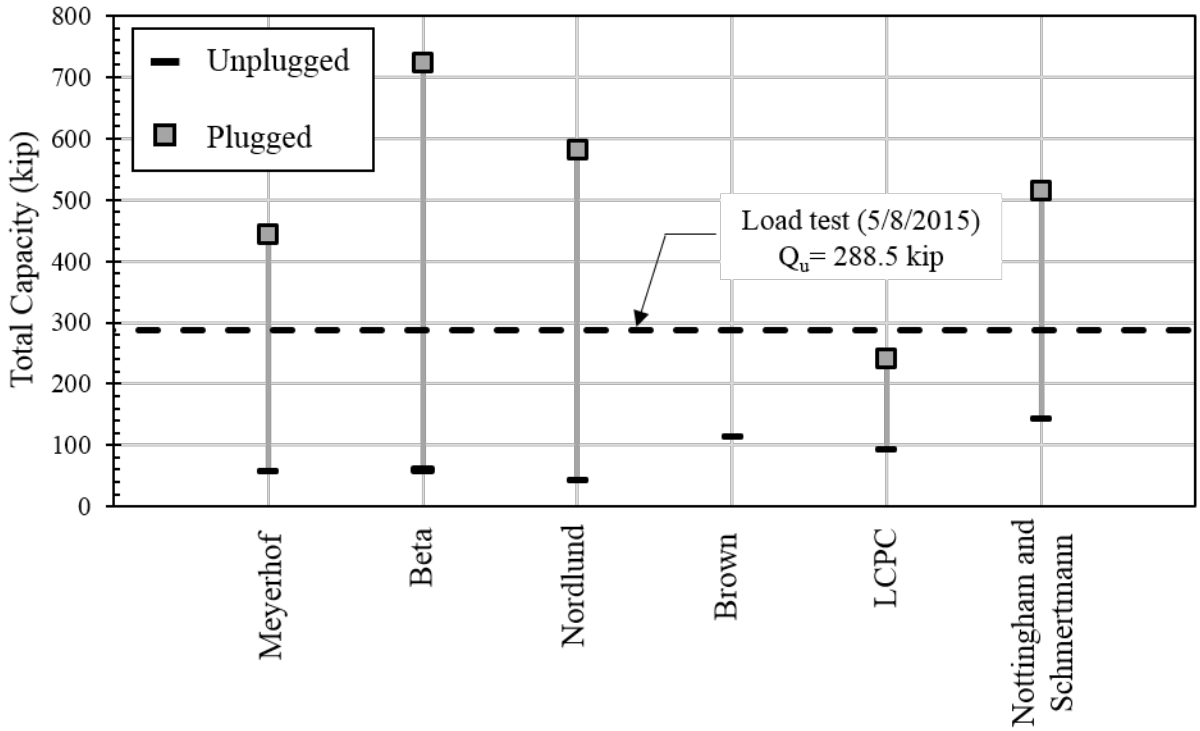

Figure 3-19: Comparison of static method predictions of total axial capacity to measured axial capacity.

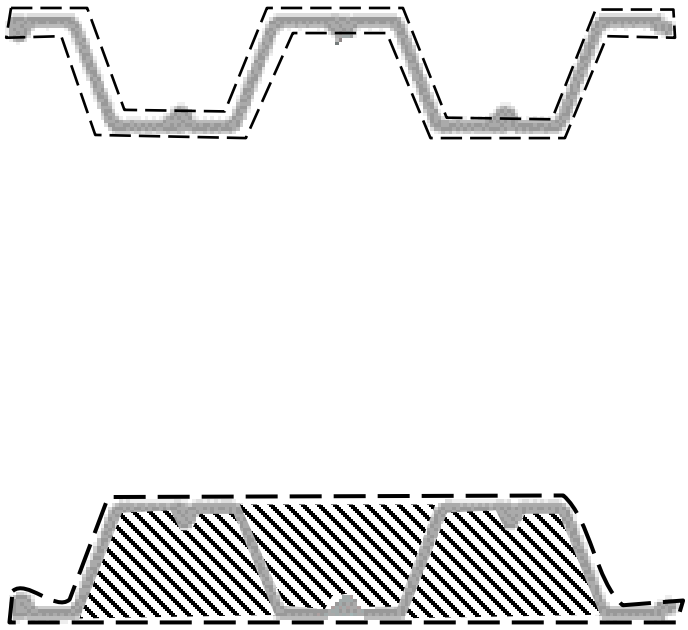

Figure 3-20: Comparison pile areas used for unplugged and plugged static method predictions.

A plot summarizing the shaft capacity estimates obtained using the six static methods is shown in Figure 3-21. This plot compares the static method predictions with the measured shaft capacity at the Davisson's failure load. In this plot, it can be seen that all shaft capacity predictions obtained by the static methods with either assumed plugged or unplugged pile condition were below the measured value of 265.6 kips.

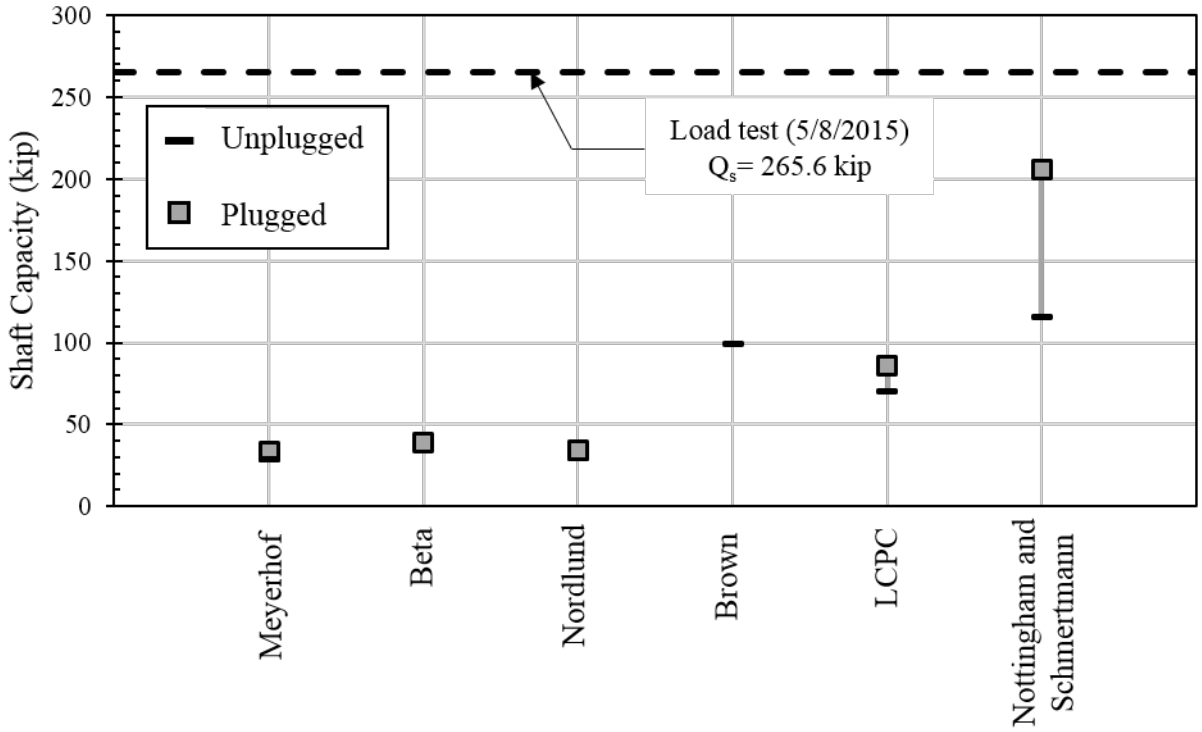

Figure 3-21: Comparison of static method predictions of shaft capacity to measured shaft capacity.

A plot summarizing toe capacity estimates obtained using the six static methods is shown in Figure 3-22. A comparison of the static prediction methods to the measured toe capacity indicates that the capacity predictions for the unplugged condition are most similar to the toe capacity observed experimentally.

The predicted axial pile capacity estimates presented above are summarized in Table 3-3.

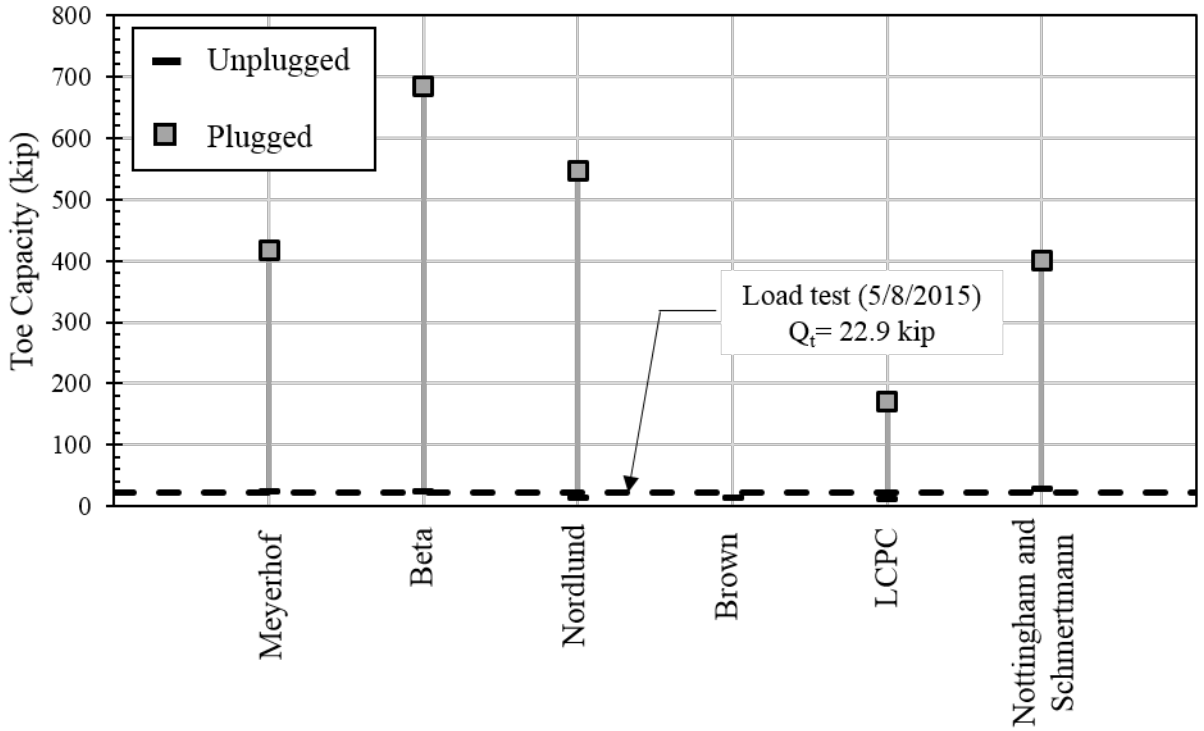

Figure 3-22: Comparison of static method predictions of toe capacity to measured toe capacity.

Table 3-3: Predicted axial capacities for laboratory sheet pile walls tested at the UNC Charlotte.

Prediction Method		Total Capacity		Shaft Capacity		Toe Capacity	
		Q_c (kip)	Q_c/Q_m	Q_c (kip)	Q_c/Q_m	Q_c (kip)	Q_c/Q_m
Meyerhof	Unplugged	58.4	0.20	33.6	0.13	24.8	1.08
	Plugged	445.0	1.54	28.7	0.11	416.3	18.15
Beta	Unplugged	60.1	0.21	36.0	0.14	24.1	1.05
	Plugged	723.5	2.51	39.3	0.15	684.1	29.84
Nordlund	Unplugged	44.1	0.15	29.4	0.11	14.6	0.64
	Plugged	581.9	2.02	34.6	0.13	547.3	23.87
Brown	Unplugged	114.2	0.40	99.6	0.38	14.6	0.64
LCPC	Unplugged	93.5	0.32	86.1	0.32	11.4	0.50
	Plugged	242.1	0.84	70.5	0.27	171.6	7.48
Nottingham & Schmertmann	Unplugged	144.6	0.50	115.6	0.44	28.9	1.26
	Plugged	515.8	1.79	205.8	0.77	400.2	17.45

Notes: Q_c = calculated value using static methods. Q_m = measured value corresponding to Davisson's failure criterion (total = 288.5 kip, shaft = 265.6 kip, toe = 22.9 kip). Q_c/Q_m = the ratio of calculated to measured. N&S = Nottingham and Schmertmann method.

The various static methods used to predict total axial pile capacity led to ratios of calculated-to-measured pile capacities (Q_c/Q_m) ranging from 0.15 to 0.50 for the unplugged condition assumption, and from 0.84 to 2.51 for the plugged condition assumption. In other words,

predictions obtained using the unplugged condition under-predicted the total axial capacity of the sheet pile wall pile by about 70 percent, while predictions obtained using the plugged condition over-predicted the total axial capacity by about 74 percent. This level of agreement between the static method predictions and actual capacity is comparable to that expected for conventional deep foundation design practice where factors of safety are typically 2.0 or higher.

In general, static analysis methods used for axial pile capacity predictions of conventional piles were found to be applicable to sheet pile walls. However a major challenge is to predict whether the formation of a soil plug will occur or not. Even if partial plugging develops along the sheet pile length, the plug formation appears to develop over a certain length of sheet pile above the toe. Thus the toe capacity mobilization, and the associated failure mechanism near the toe, appears to be localized to the steel cross section. At least for the soil conditions and sheet pile geometry at the high bay load tests.

Based on the high bay results, for design purposes we recommend selecting the toe and the shaft capacity as the lesser value obtained from considering the plugged and unplugged conditions.

The static method prediction made with the Nottingham & Schmertmann method with the unplugged assumption for the toe capacity (28.9 kip) and a plugged assumption for the shaft capacity (205.8 kip), results in a total capacity of 234.7 kip that is within 20% of the measured capacity. 288.5 kip).

3.7.4 Experimental load transfer curves and associated prediction

Using the different elevations of strain gage instrumentation on the piles (See Figure 3-11), load transfer curves were obtained. The T-Z curves experimentally developed for side friction are shown in Figure 3-23 for depth ranges of 0-51 inches (upper 4.25 ft) and for the range from 51 to 96 inches (lower 3.75 ft) of embedded depth. The T-Z curves show an increase in resistance with depth consistent with effective stress based methods. The amount of displacement required for mobilization of the peak side friction resistance was between 0.3 in (7.5 mm) and 0.5 in (12 mm). This level of relative shaft displacement required to mobilize peak side friction is higher than normally expected for steel deep foundations such as H-piles. For example, empirical load transfer curves proposed by API (1993) and Vijayvergija (1977) suggest relative displacements between 0.08 in (2 mm) and 0.3 in (8 mm), respectively.

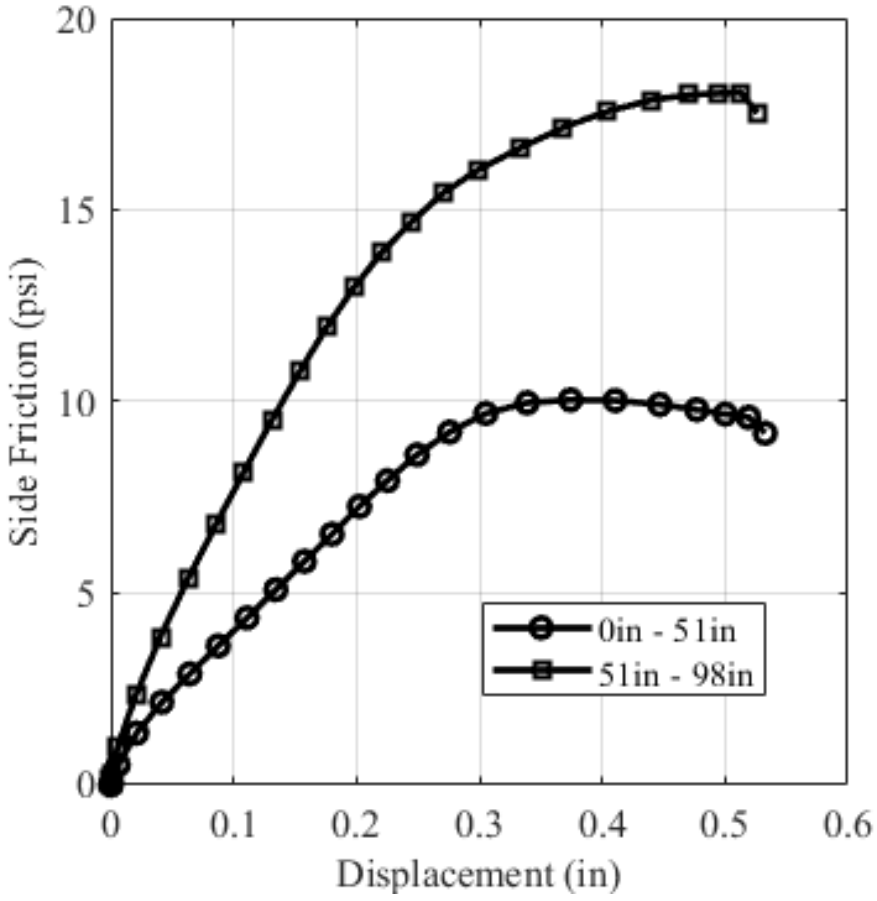

Figure 3-23: Experimental T-Z load transfer curves for representative axial load test.

The experimental load transfer curve obtained for the mobilization of the toe capacity is shown in Figure 3-24. This plot shows that the mobilization of the toe resistance was initially slow for small axial displacement, but started to mobilize rapidly beyond toe displacements of 0.1 in (2.5 mm) and reached a maximum value of about 31 kips at a toe displacement of about 0.5 in (12 mm).

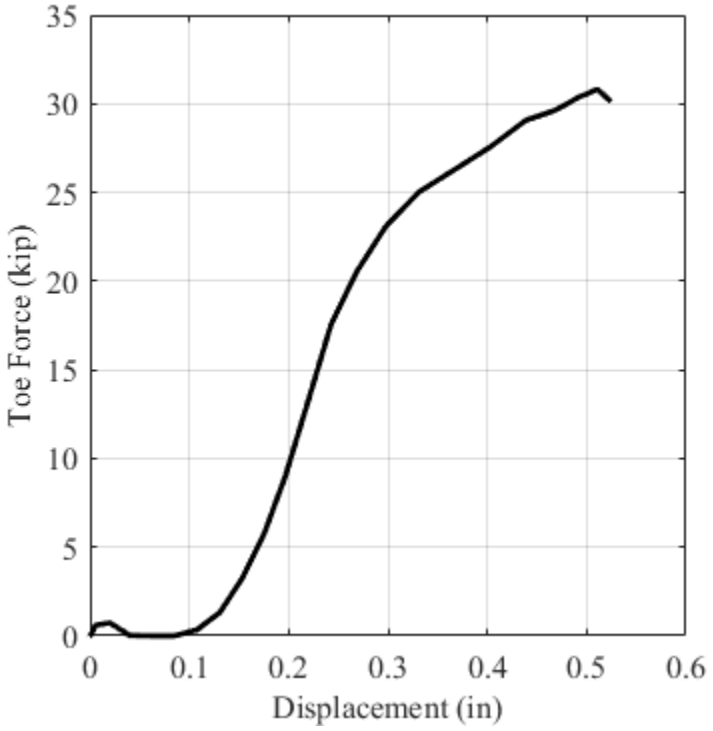

Figure 3-24: Experimental pile tip load-displacement (Q-Z) load transfer curves for representative axial load test.

The T-Z and Q-Z curves shown above can be used to predict the load-settlement response for the sheet pile test wall using the load transfer method. The load transfer method involves modeling the pile as a series of discrete nonlinear springs, which represent the resistance of the soil in skin friction (T-Z springs), and a nonlinear spring at the pile tip representing the end-bearing (Qb-Z) resistance. The numerical model used in the load-transfer method is shown schematically in in Figure 3-25. Using a load transfer model, the axial load-settlement response can be obtained with the aid of a computer program such as FB-Pier (BSI, 2016).

The predicted load-settlement curve obtained using the load transfer method with the experimental T-Z and Q-Z load transfer curves reported above, is shown in Figure 3-26. This curve shows the prediction is quite good given it is based on measured load transfer curves. However, the agreement is not perfect because a simplified 2 layer discretization was used to model the side friction thus resulting in a small over-prediction.

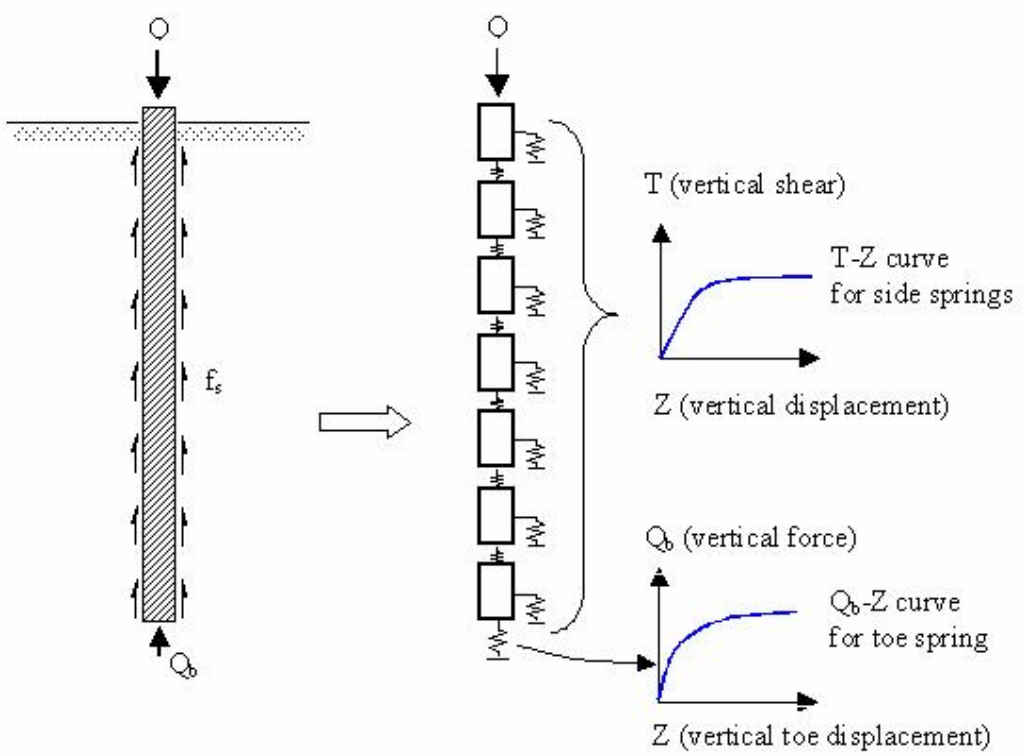

Figure 3-25: Idealized load-transfer model used to predict axial behavior of deep foundations (adapted from Pando et al. 2006).

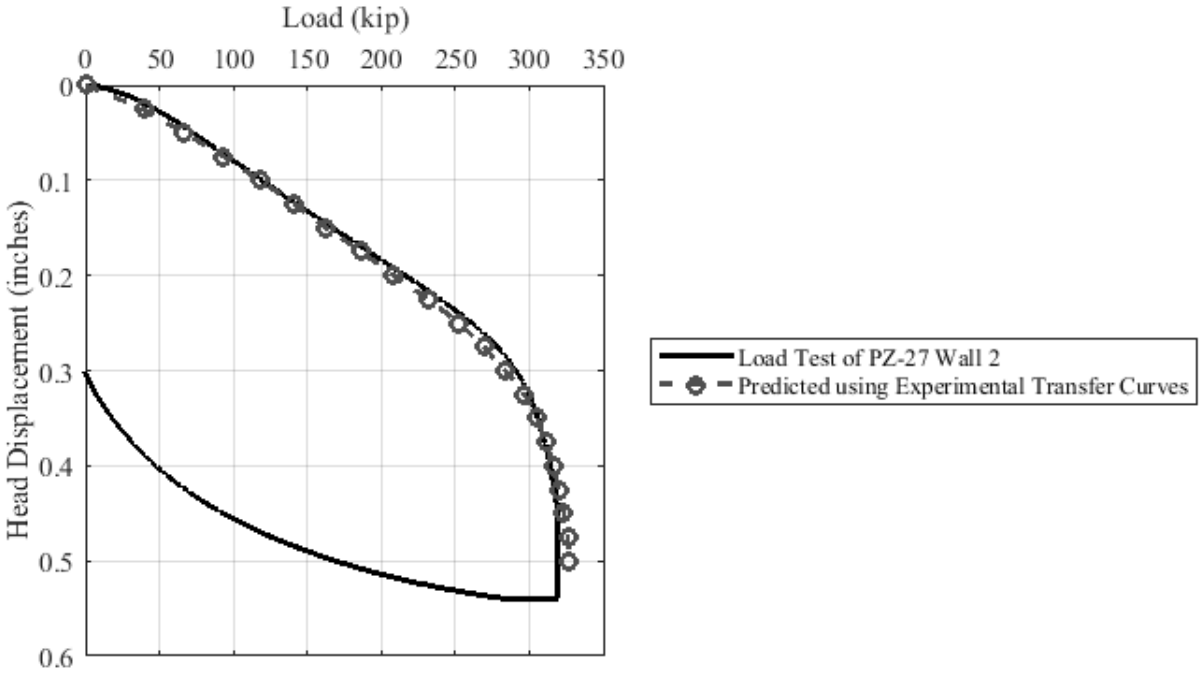

Figure 3-26: Settlement prediction for sheet pile wall using experimental load transfer curves.

3.8 Discussion of plugging

During axial load testing of the sheet pile walls, a pattern of cracking at the ground surface around the perimeter of the sheet pile was observed. A photo showing the nature of the surface cracking around the sheet is provided in Figure 3-27. The cracks were 8 to 12 inches from the outer edge of the sheet pile and suggest the possible formation of a soil plug along the embedded length of the test wall.

Figure 3-27: Photo showing surface cracks around the perimeter of the sheet pile wall.

The sheet piles were pulled out of the ground in a controlled fashion upon completion of the load test program. A photo showing the pile immediately after it was pulled out of the pit is shown in Figure 3-28. This photo reveals that soil plugging formed in the concave areas of the sheet pile. It should be noted that at the time of pullout, the geotechnical test pit had been inundated with water to decrease the pullout force requirement and that despite this inundated state a soil plugging condition was observed. The removal of the soil plugs was very difficult and required the use of a hydraulic jack hammer.

Figure 3-28: Photo showing soil plugging along the embedment depth of the sheet pile wall.

3.9 Summary

A full-scale axial load test program was conducted on instrumented sheet pile walls tested at one of the geotechnical test pits at UNC Charlotte. The tests allowed assessment of the axial load capacity of PZ-27 sheet pile walls installed in a homogenous geotechnical profile consisting compacted sandy backfill. The experimental program included detailed characterization of the soil backfill with SPT, CPT, DMT, and seismic testing. The axial load tests included dynamic measurements during installation that allowed for PDA and CAPWAP analyses. The static axial load tests permitted for evaluation of the mobilization of shaft and toe resistance under controlled conditions, in addition to the measurement of the total axial load capacity.

The following conclusions can be drawn from the test program.

- Results from static axial load testing of PZ-27 sheet piles indicate that these foundation elements have considerable axial load capacity (even for the relative short embedment length that was possible at the UNC Charlotte test pits.
- The axial capacity was obtained from the mobilized shaft friction.
- High axial load capacities and axial stiffness measured during testing suggest sheet pile walls have a strong potential to be used as axial load bearing foundation elements for bridge abutments.
- Due to the high level of instrumentation, rate of sampling during testing, and thorough characterization of the geotechnical properties of the backfill, these tests provide an excellent data set for improving our understanding of axially loaded sheet piles.
- It was found that static methods typically used to predict axial load capacity of driven piles are suitable for predicting axial capacity of sheet pile walls.
- Pile capacity estimates using PDA and CAPWAP from dynamic measurements of one pile section at the end of driving underestimated the measured axial load capacity of the total wall (4 sections) by 20% and 50%, respectively. This level of under prediction could be associated to friction between pile sections driven separately, and the possible need to include inertial effects if soil plugging phenomenon is present during sheet pile driving.
- The formation of pile plugging was confirmed at the end of the test program by carefully pulling out a sheet pile wall. The importance of soil plugging in the mobilized axial capacity was highlighted in this successful pile load test program under well controlled laboratory conditions.
- For design purposes it is recommended to use the lesser values for the shaft and tip capacities computed using the two extreme scenarios of i) unplugged, and ii) fully plugged.
- The need for detailed investigation of the plugging phenomenon in sheet piles in future studies is highlighted with the results of this laboratory test program.

4 Field Load Test Program at a Facility of ICE in Matthews, NC

4.1 Introduction

This chapter summarizes the results and findings of field load testing carried out at the facility of the International Construction Equipment (ICE) in Matthews, N.C. The original proposal called for field verification tests to be performed at an actual NCDOT bridge project. Unfortunately, after evaluating more than four candidate bridge sites where it was determined that this testing could not be accommodated, and to avoid further project schedule delays, the option of performing field load tests at an NCDOT bridge site was abandoned to avoid further delays in the project schedule. The project then shifted focus to identifying a field test site in the greater Charlotte area. Preliminary drilling was performed at three candidate field test sites and, ultimately, the ICE facility in Matthews, NC was selected as the location for the field load tests. Due to donations of H piles from Skyline, the scope of the field test program was expanded to involve a load test on an H-pile to allow for direct comparison with the sheet piles.

4.2 Description of field test site

The final site for the field load test program was located in the yard of the ICE facility in Matthews, NC. The general location of the site is shown in Figure 4-1. The test site was located in a relatively flat area of the equipment yard of the facility as shown in the photo in Figure 4-2.

Figure 4-1: General location map of field test site.

Note: flag tape demarks approximate rectangular area used for testing of piles.

Figure 4-2: Photo of field test site prior to installation of piles.

4.2.1 Geology

The test site is located in the Charlotte Belt of the Piedmont Physiographic Province of North Carolina. The geology map by Goldsmith et al. (1988) indicates the topography and relief of the Piedmont Province have developed from differential weathering of the underlying igneous and metamorphic rock. Due to continued chemical and physical weathering, the rocks in the Piedmont Province are now generally covered with a mantle of soil that has weathered in place from the parent bedrock. These soils have variable thicknesses and are referred to as residuum. The residuum is typically finer grained and has higher clay content near the surface because of the advanced weathering. Similarly, the soils typically become coarser grained with increasing depth because of decreased weathering. The boundary between soil and rock in the Piedmont is not sharply defined, and a transitional zone termed “Partially Weathered Rock” is normally found overlying the parent bedrock.

4.2.2 Geotechnical subsurface conditions

The test site was investigated with four hollow stem auger borings (two preliminary borings performed during field site evaluations, and two detailed borings performed after site selection), two cone penetrometer tests, and MASW geophysical testing. The locations of the borings and CPT probes are shown in relation to the test piles in Figure 4-3. The borings were advanced using hollow stem auger techniques and a CME 550 drill rig. Standard penetration tests (SPT) were performed in the borings using an automatic hammer. The SPT N-values corrected for energy and overburden are shown in Figure 4-4 together with descriptions of the soils encountered in the borings. Figure 4-4 also shows the tip resistance, the sleeve friction, and shear wave velocity profile measured from the two seismic cone penetrometer test (SCPTu) probes. Additional subsurface investigation information for the field load test area is provided in Appendix B.

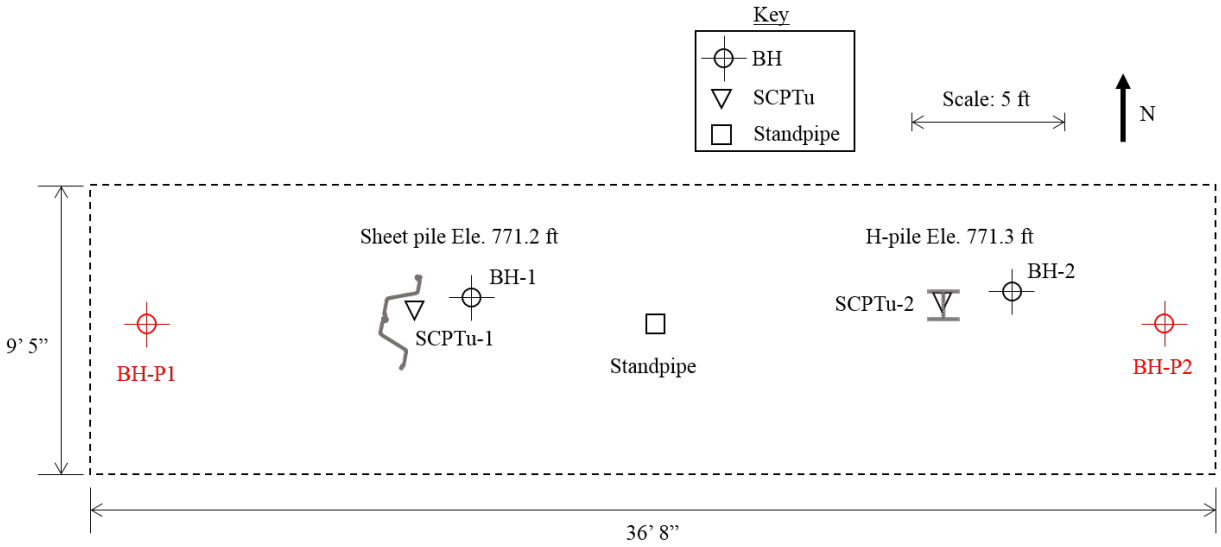

Figure 4-3: Pile load test layout and locations of select in-situ tests performed before test pile installation.

The soil stratigraphy at the test site is also shown in Figure 4-4. The upper layer of the test pile site is a gravel fill with sand, approximately 6 inch (0.15 m) thick. The gravel fill is underlain by medium stiff, low plastic, sandy clay (CL) to a depth of about 4 ft (1.2 m). The sandy lean clay becomes softer with depth and also includes sandy silts. USC classifications obtained for samples from this layer range from CL to ML. This CL/ML layer extends to a depth of 10 feet (3.05 m). Beneath the CL/ML layer, a soft to stiff, low plastic, sandy silt (ML) extends to a depth of about 20.5 ft (6.25 m). The sandy silt layer is underlain by a medium dense to very dense silty sand (SM) layer that was encountered to the bottom of the four borings that extended to depths ranging from 32.5 ft (9.91 m) to 47.5 ft (14.5 m). The ground water level was monitored with the standpipe shown in Figure 4-3 and was found to fluctuate from 4.7 to 12.4 ft (1.4 to 3.8 m) below the ground surface. Figure 4-4 shows that the final depth of the tip for both test piles was approximately 17 ft (5.2 m).

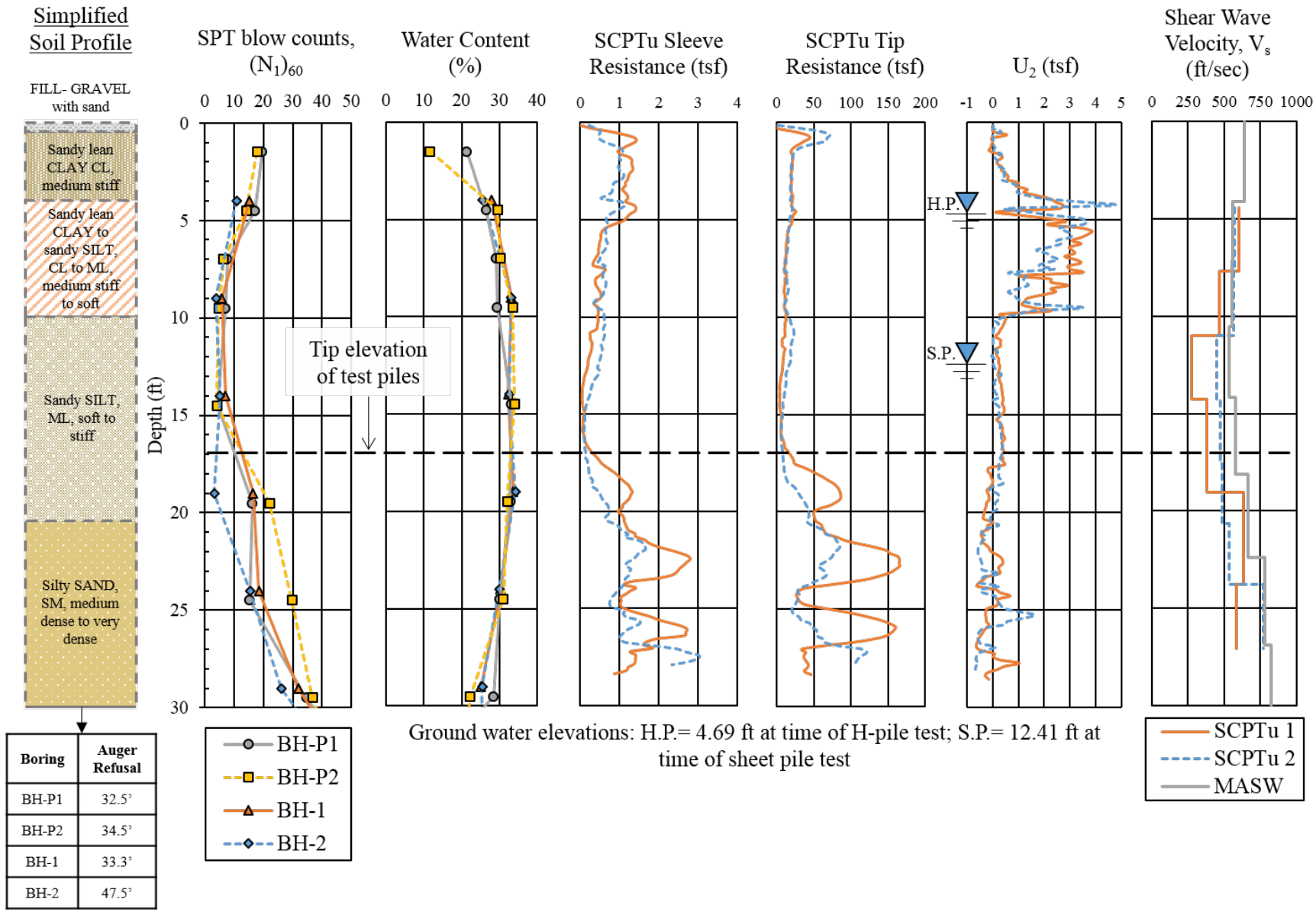

Boring	Auger Refusal
BH-P1	32.5'
BH-P2	34.5'
BH-1	33.3'
BH-2	47.5'

Figure 4-4: Simplified soil stratigraphy in the field test site.

4.3 Test piles

The field load test program involved sheet piling and an H-pile installed at the locations shown in Figure 4-3. The sheet piling consisted of a pair of PZ-27 sheet piles and the H-pile consisted of an HP 12x53. The cross sectional details for the test piles are shown in Figure 4-5, and summarized in Table 4-1. Both test piles had a total length of 20 ft (6.1 m).

Both test piles were instrumented with strain gages located at nine levels. The as-built instrumentation layouts for the sheet pile and H-pile are shown in Figure 4-6. A photo of both instrumented test piles is shown in Figure 4-7. Additional details on the pile instrumentation including procedures used for the installation of the strain gages can be found in Appendix B.

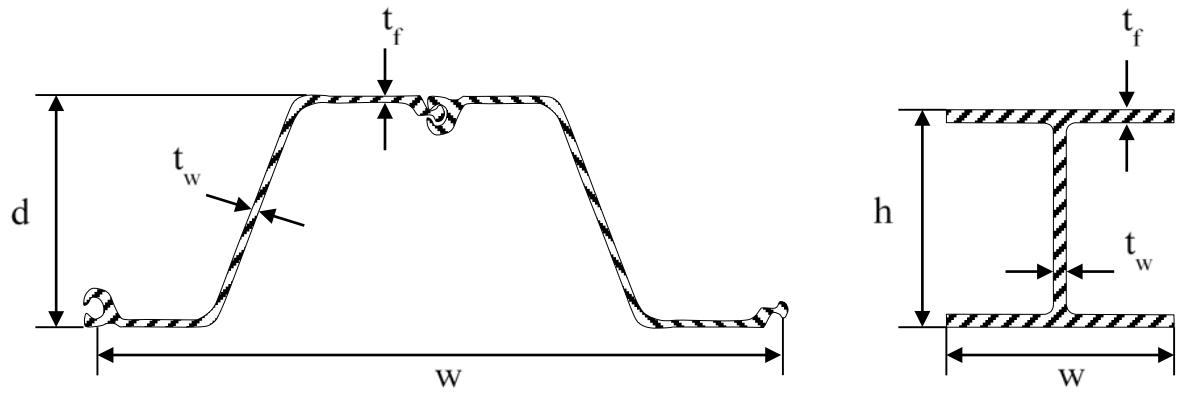

a) PZ-27 sheet pile b) HP 12x53 H-pile

Figure 4-5: Cross section of test piles installed at field test site.

Table 4-1: Summary of cross section details for test piles.

Test Pile Type	Pile Designation	Width, w (in)	Depth, d (in)	Thickness		Cross Sectional Area (in^2)	Perimeter Surface Area (ft^2/ft)
				Flange, t_f (in)	Wall, t_w (mm)		
Sheet pile	PZ-27	36	12	0.37	0.37	23.82(1)	8.99
H-pile	HP 12x53	12	11.8	0.43	0.43	15.5	5.81

Note: (1): Area reported corresponds to the total cross sectional area of the sheet pile wall that includes the pair of PZ-27.

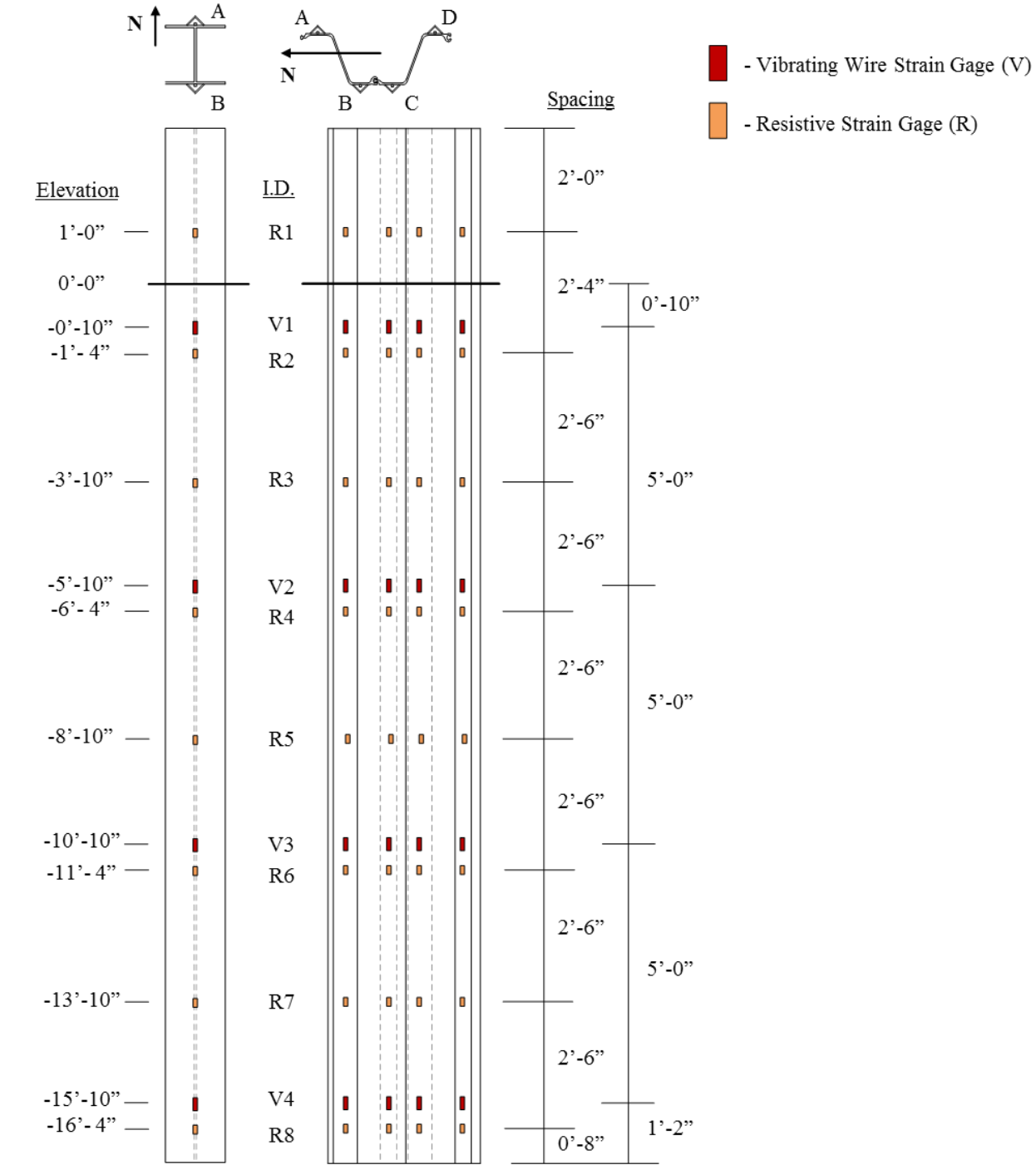

Figure 4-6: Layout of strain gages installed on field test piles.

Figure 4-7: Photo of instrumented test piles delivered at field site.

4.4 Pile installation and Dynamic Testing

4.4.1 Pile installation

The test piles were installed using both a vibratory and impact hammer. Vibratory driving to a depth of about 8 ft (2.4 m) was performed using an ICE Model 28C hammer (Figure 4-8). Below this depth, the test piles were installed using an ICE model I-12 single-acting diesel hammer (Figure 4-9). The maximum rated energy of the impact hammer is 33,173 ft-lbs (45 kN-m). The pile-driving records for both test piles are shown in Figure 4-10. At the end of initial driving (EOID) the test piles were driven to a final embedment depth of 17 ft (5.2 m). Pile installation photos for the sheet pile and H-pile are shown in Figure 4-11 and Figure 4-12, respectively.

Figure 4-8: Photo of test pile installation with vibratory hammer ICE 28C.

Figure 4-9: Photo of single-acting diesel hammer ICE I-12 used for final pile installation.

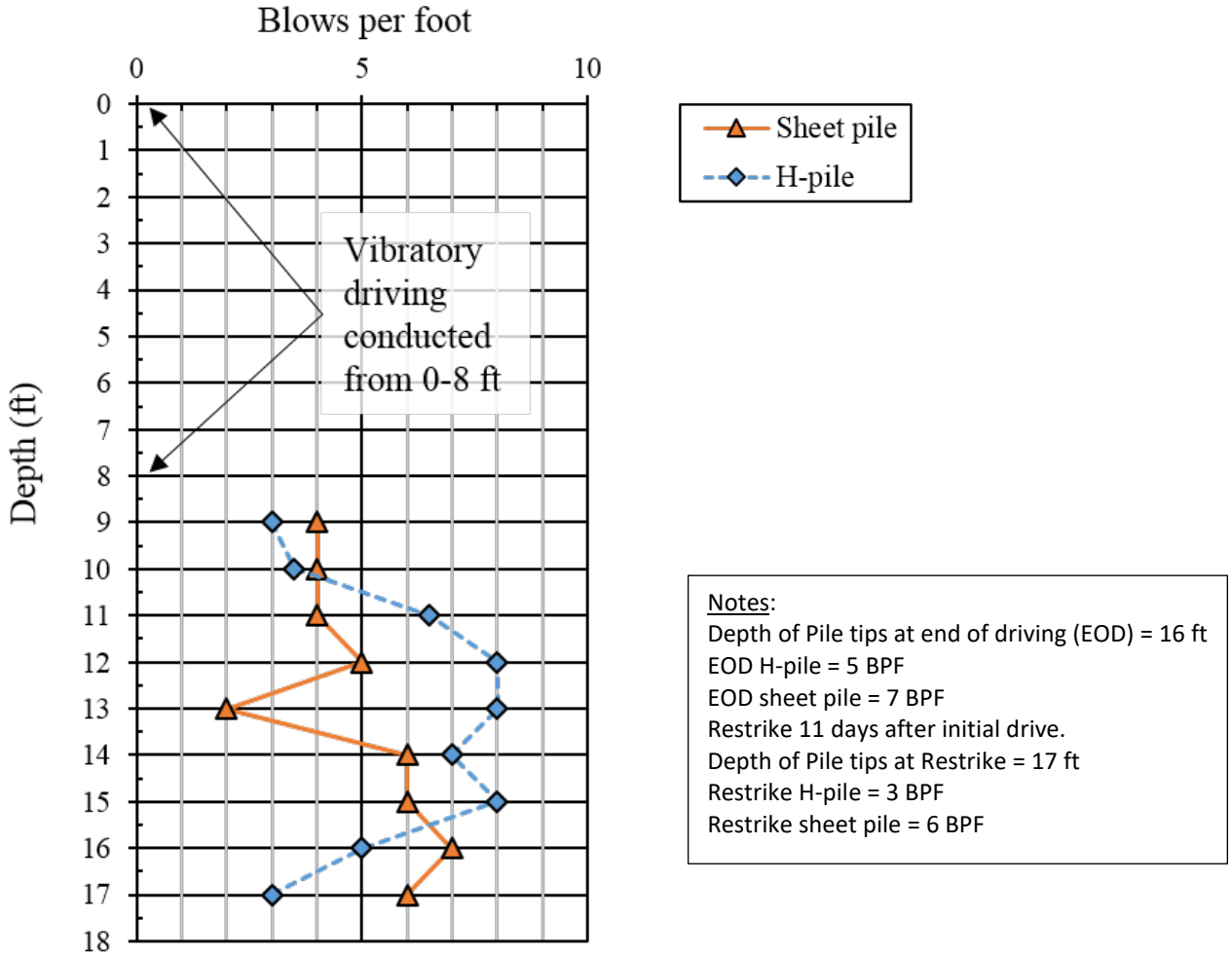

Figure 4-10: Driving records for field test piles.

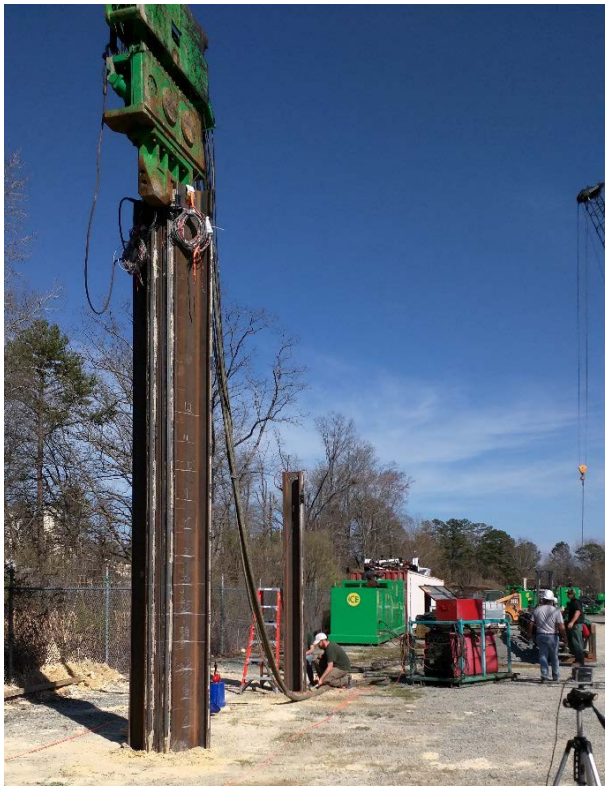

a) Vibratory driving

b) Impact driving

Figure 4-11: Installation of sheet pile.

Figure 4-12: Photo showing installation of H-pile.

4.4.2 Dynamic testing

Dynamic monitoring during pile installation was performed using a Pile Driving Analyzer (PDA). Monitoring was performed during initial driving and during restrike, which occurred 11 days after initial driving. Dynamic testing was accomplished by attaching strain transducers and accelerometers at about 2 diameters from the top of the piles in pairs spaced 180 degrees apart. PDA records for the two test piles at restrike are shown in Figure 4-13.

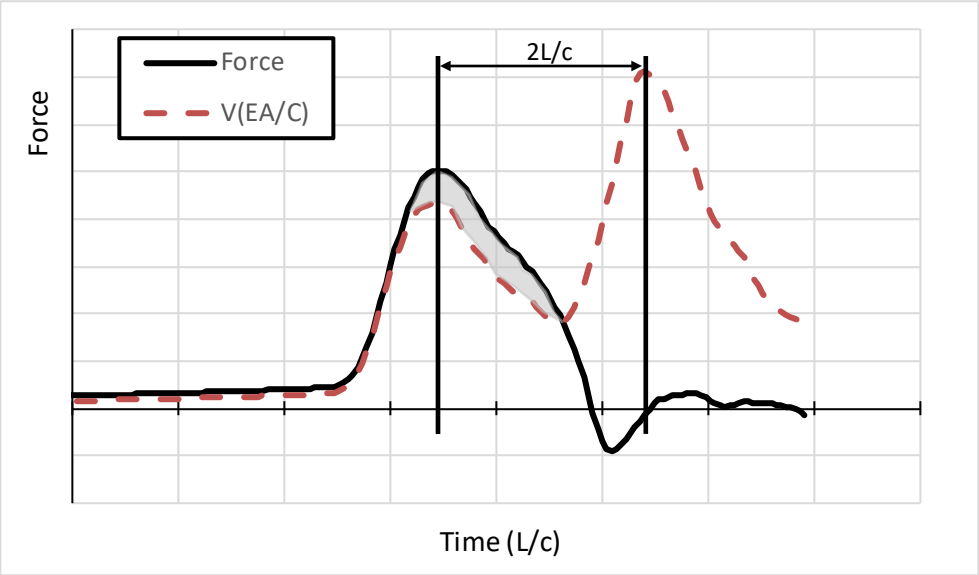

a) Sheet pile

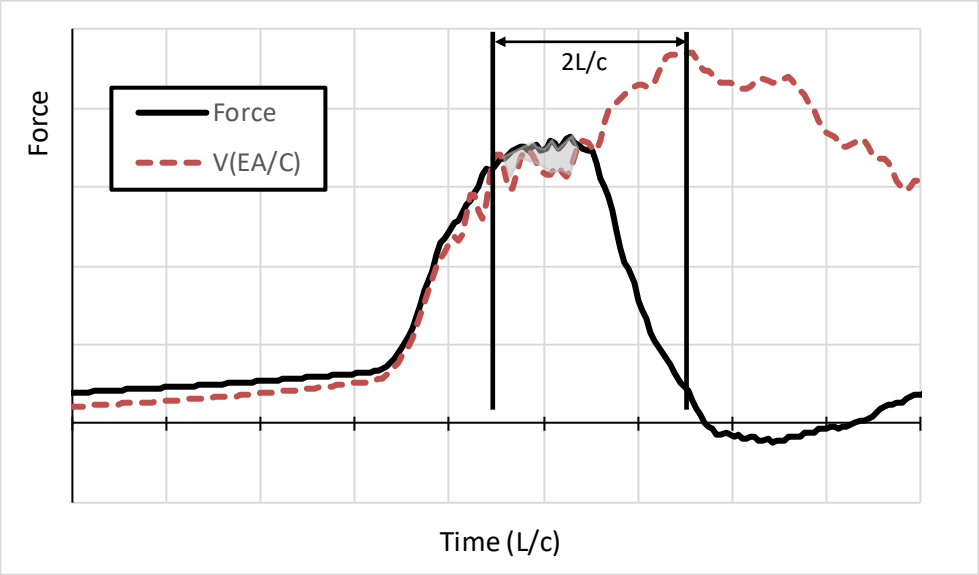

b) H-pile

Figure 4-13: PDA records during restrike.

The PDA records show development of peak force at the location of the first solid vertical line (time 0) as shown in Figure 4-13. The second solid vertical line in the PDA records indicates peak velocity and the time difference between these peaks corresponds to the travel time for the wave reach the toe of the pile and return back to the head of the pile (2L/c, where L is the pile length, and c the wave speed). At the first peak in the velocity trace for this driving record, the force trace exhibits a significant drop. This peak in the velocity trace is characteristic of a reflected tensile wave from the toe. Both the sheet pile and H-pile dynamic testing records

exhibited similar behavior. A small separation was observed between the force and velocity traces (denoted with shaded areas in grey) for both of these piles. This separation represents a small shaft resistance.

Estimates of pile capacity from the dynamic strain and acceleration measurements were obtained using the Case method (Goble et al. 1975). The strain and acceleration data from restrike were subjected to CAPWAP analyses (Goble et al. 1975). Both the Case method and CAPWAP capacities are listed in Table 4-2.

Table 4-2: Summary of pile capacities estimated from dynamic tests by GRL.

Method	Capacity Component	Sheet pile (Two PZ-27 sections)	H-pile
Case EOD(1)	Total	Not available	Not available
Case Restrike(2)	Total	44 kips	9 kips
CAPWAP Restrike(3)	Shaft	17.1 kips	12.3 kips
	Toe	22.1 kips	5.5 kips
	Total	39.2 kips	17.8 kips

Notes: (1) End of Driving PDA tests yielded poor data.
(2) Restrike of piles performed 11 days after initial driving.
(3) CAPWAP equivalent damping coefficient = 0.35.

According to the CAPWAP analyses, the sheet pile and H-pile have axial capacities of 39.2 kips (174.4 kN) and 17.8 kips (79.2 kN), respectively. The CAPWAP analyses also indicate that the shaft capacities, as percentages of the total capacities, are 43.6 percent and 69 percent for the sheet pile and H-pile, respectively.

4.5 Axial load test program at field test site

Static pile load testing for the sheet pile and H-pile were performed in general accordance with ASTM Standard D1143 (ASTM 2013). Drawings of the reaction frame used are shown in Figure 4-14. As shown in these drawings, the reaction piles were HP 14x73. The reaction beam was designed for a rated load capacity of 160 kip (712 kN). Photos of the reaction system at the location of the H pile shown in Figure 4-15.

The axial load was applied to each test pile using an Enerpac hollow plunger cylinder model RCH-603 with 120 kip (533.8 kN) capacity and a 3-inch (7.62 cm) stroke. The jack used to operate the piston was a model P-80 Enerpac hand pump. Vertical displacements were measured at no less than three locations of the test pile head using digital dial gauges with measurement resolution of 7.9×10^{-5} in (0.002 mm). A model TD175 Industrial Commercial Scales canister load cell with 100 kip (444.8 kN) full-scale range was used to measure the applied axial load at the pile head and was signal conditioned with a 24-bit PXI-4330 bridge input module. The displacement and load measurements were obtained concurrently by a digital data acquisition system. Additional details and photos of the field load test program are provided in Appendix B.

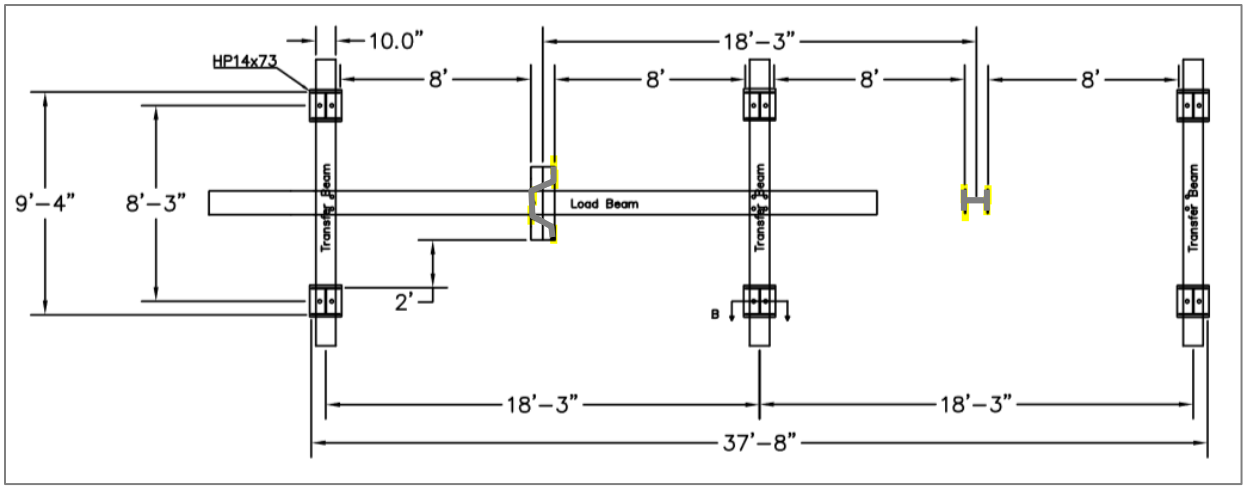

Plan view

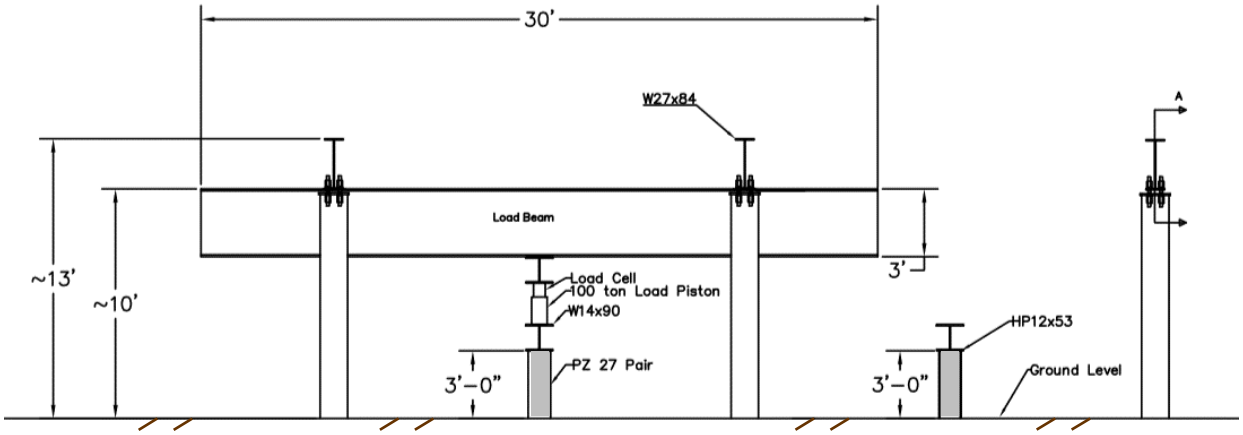

Elevation view

Figure 4-14: Drawings of reaction frame used for axial load tests at field site.

a.) Image of test pile and reaction frame

b.) Image of test H-pile prior to static load test

Figure 4-15: Axial load test setup.

Axial load test results, presented as pile head displacement versus applied axial load, for the sheet pile and H-pile, are shown in Figure 4-16. These results correspond to axial load tests performed at a constant rate of penetration of about 0.005 in/min (0.13 mm/min). The axial load capacity, based on Davisson's criterion, for the sheet pile and H-pile were 34.3 kips (152.6 kN) and 22.5 kips (100.1 kN), respectively. The corresponding pile head displacements for this failure load were measured as 0.27 in (6.9 mm) and 0.26 in (6.6 mm) for the sheet pile and H-pile, respectively.

The load-settlement curves in Figure 4-16 show that the sheet pile has a slightly higher initial slope or initial axial stiffness compared to the H-pile. For example, the axial load secant stiffness, computed as the slope of the line that connects the origin and the load-displacement responses at an arbitrary pile head displacement of 0.02 in (0.5 mm), were found to be 736 kip/in (128.9 kN/mm) and 664 kip/in (116.27 kN/mm) for the sheet pile and H-pile, respectively. The higher axial load secant stiffness values for the sheet pile is expected given its larger cross sectional area and skin friction surface area compared to the H pile (see Table 4-1).

Using the different levels of strain gages, plots of axial force versus depth along the sheet pile test wall were obtained, as shown in Figure 4-17. Based on measured load transfer, the contribution from shaft and toe resistances are 30.7 kip (89.5%) and 3.6 kip (10.5%), respectively, at the Davisson's failure load of 34.3 kip.

Unfortunately, the development of axial load distribution plots, and a full set of associated load transfer curves, for the H-pile were not possible because the instrumentation cables were sheared off during the installation of this test pile. Following efforts to repair cable of the H pile instrumentation it was possible to record data from a couple of strain gages located at the pile

toe. Using the strain gages near the toe of the H-pile the estimated contribution from shaft and toe resistances, at the Davisson's failure load of 22.5 kip, are 20.7 kip (92%) and 1.8 kip (8%), respectively.

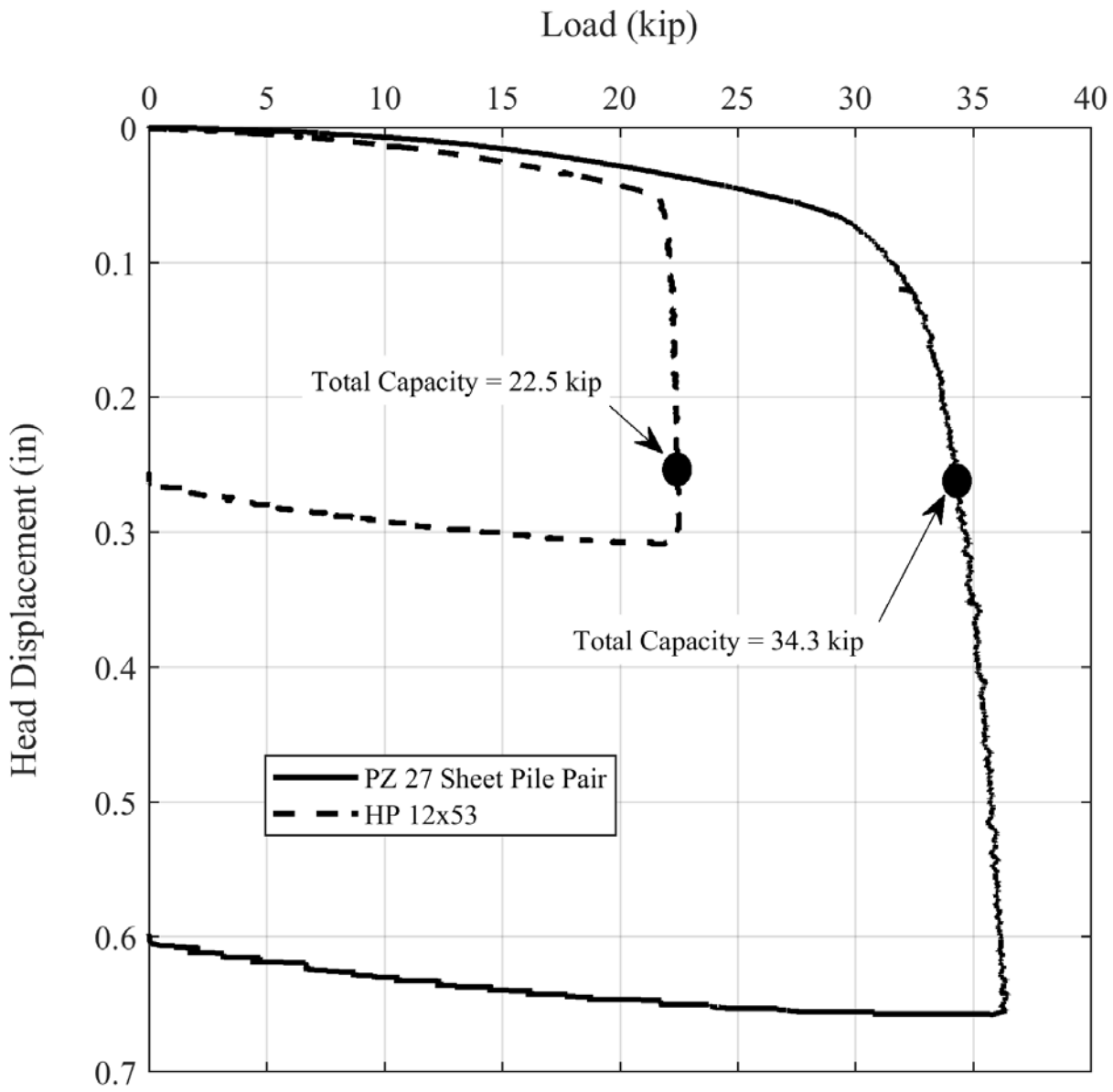

Figure 4-16: Axial load test results.

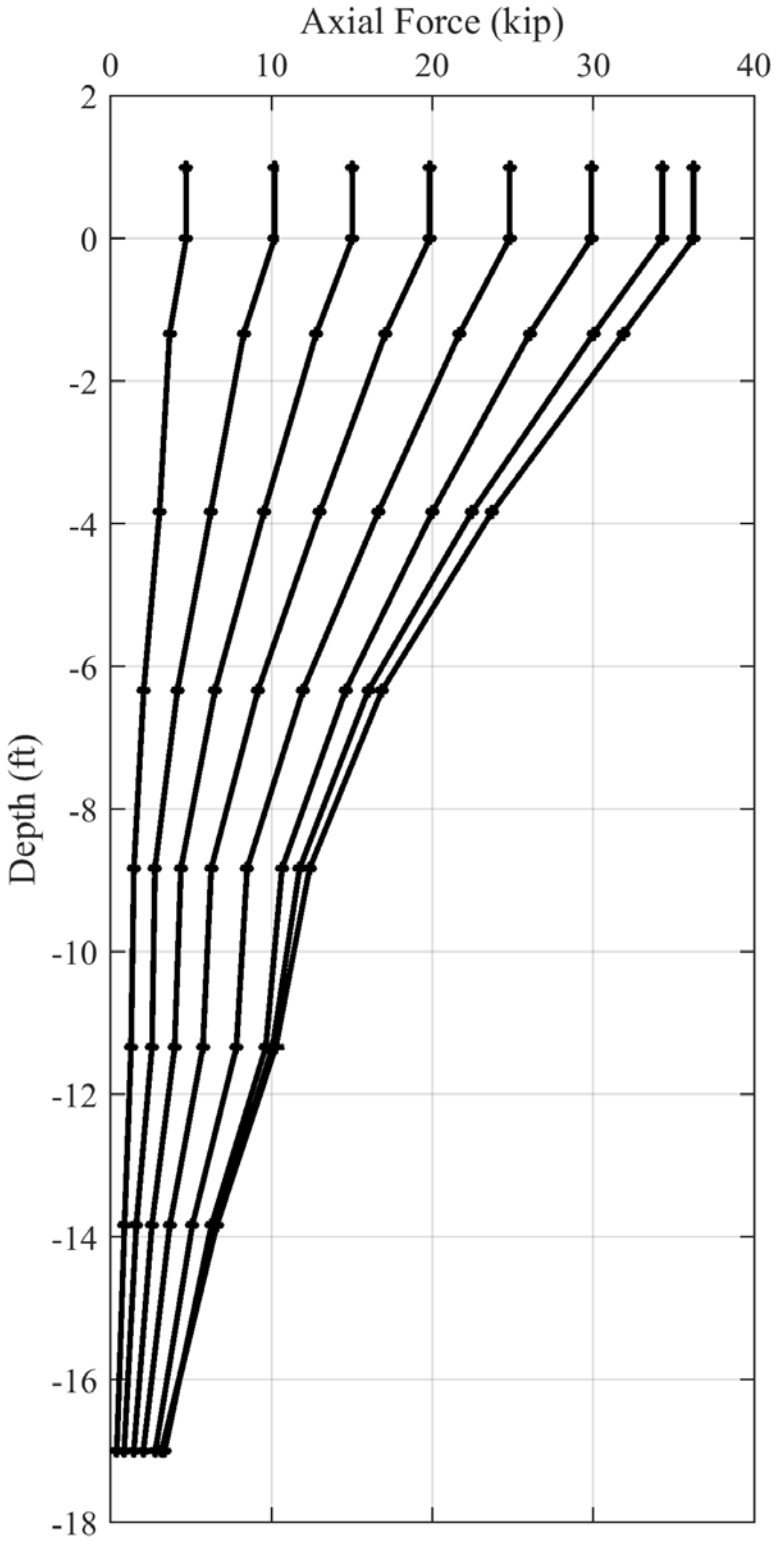

Figure 4-17: Axial load distribution for sheet pile during field load test.

4.6 Predicted axial capacities using static methods

This section presents axial capacity predictions for the sheet pile and H pile using the same static methods used in Chapter 3. Since this test program utilized the same field test site to experimentally determine the axial load capacity of two different pile types, the field data allows for a direct comparison of the prediction accuracies for both types of piles.

Predictions of the total axial load capacity using the different static methods are summarized in Figure 4-18 and Figure 4-19 for the sheet pile and H-pile, respectively. These figures indicate that a similar degree of accuracy was obtained for the prediction of the total axial capacity of both test piles when the same static methods were used. These plots provide a horizontal dashed line that indicates the load test result obtained using the Davisson's failure criterion and two set of predictions are presented for each static method to bound the estimates between the two extreme pile conditions of plugged (square symbols) and unplugged (horizontal dash line). For both test piles, and for the six static methods considered, the measured axial capacity was closer to the predicted capacity for the unplugged condition.

Comparisons of the estimated shaft capacities, using the six static methods, to the experimentally estimated shaft contribution are shown in Figure 4-20 and Figure 4-21 for the sheet pile and H-pile, respectively. For both test piles, and for the six static methods considered, the measured shaft capacity was closer to the predicted capacity for the unplugged condition. However considerable overprediction was observed in most of the CPT-based methods.

Predictions for the toe capacity using the different static methods are summarized in Figure 4-22 and Figure 4-23 for the sheet pile and H-pile, respectively. These figures show that the predictions assuming the unplugged condition for the toe generated the closest estimates of the measured toe capacities for both test piles.

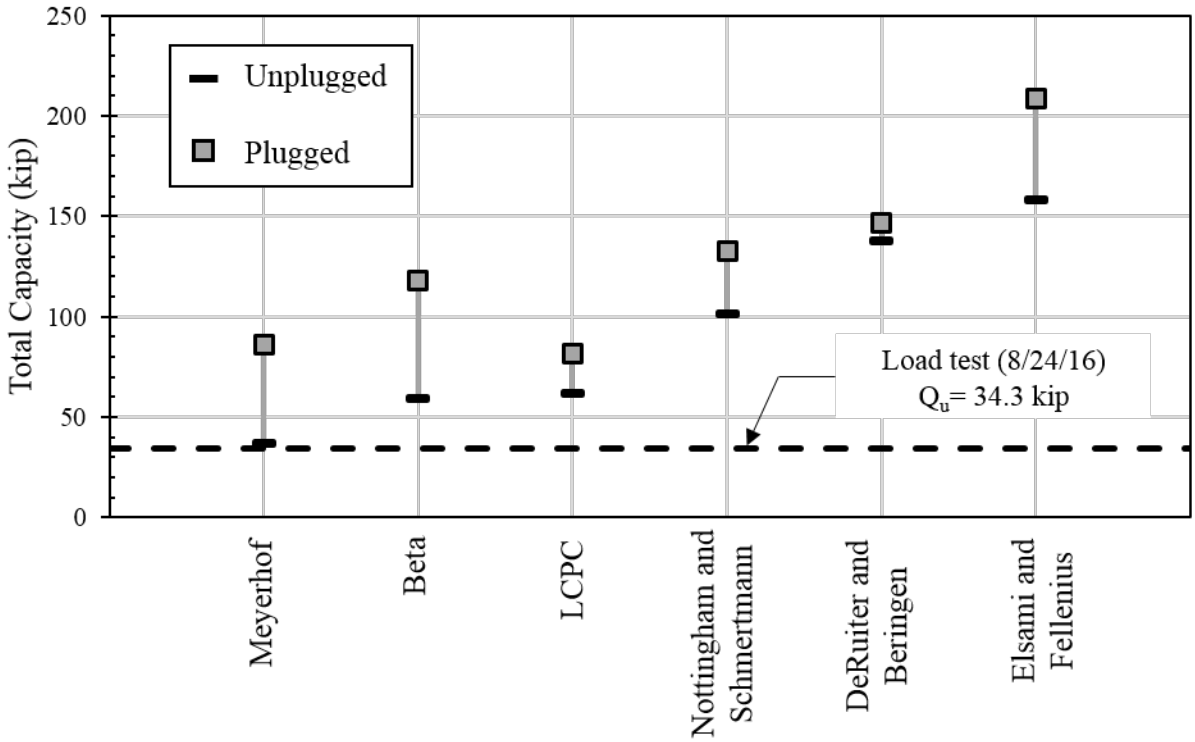

Figure 4-18: Comparison of static method predictions of total axial capacity of sheet pile wall to measured axial capacity.

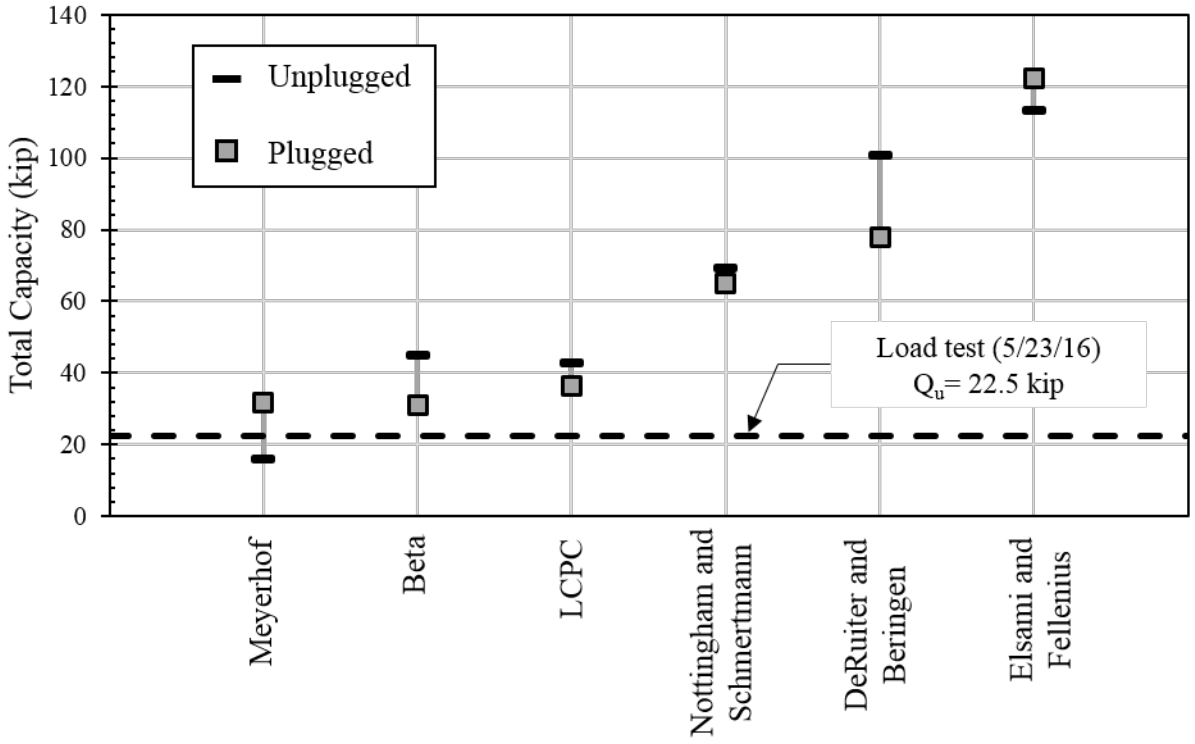

Figure 4-19: Comparison of static method predictions of total axial capacity of H-pile to measured axial capacity.

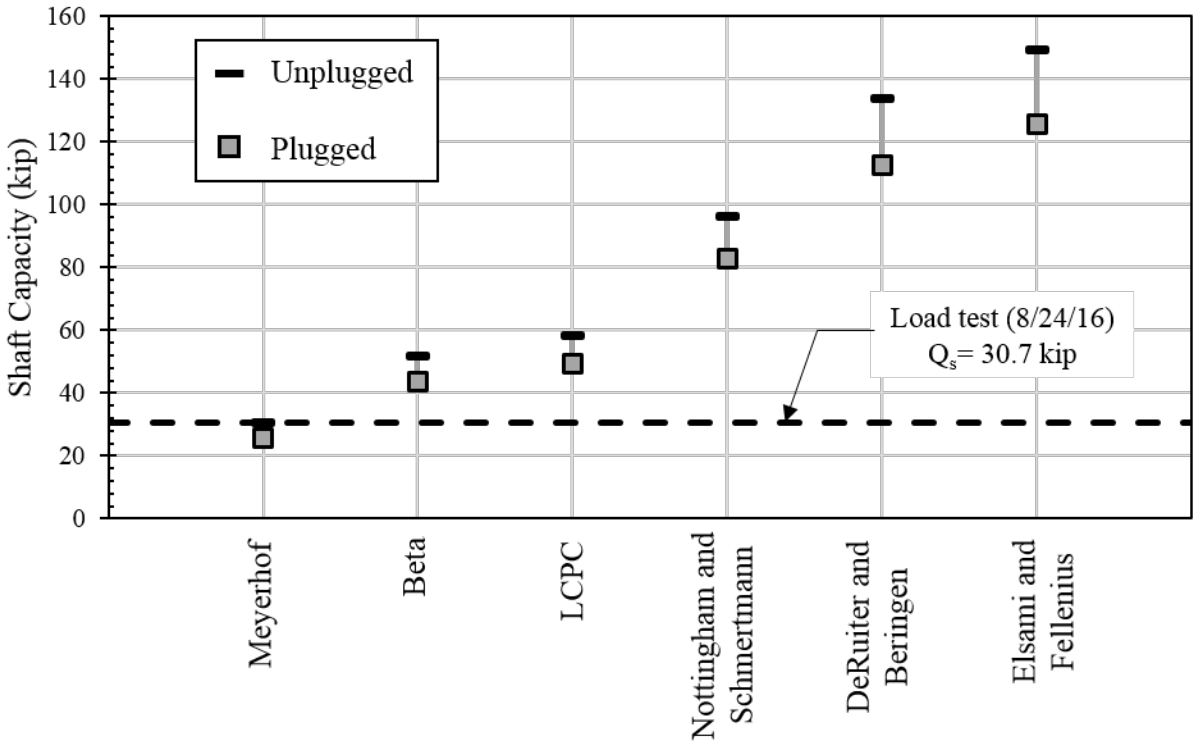

Figure 4-20: Comparison of static method predictions of shaft capacity of sheet pile wall to measured shaft capacity.

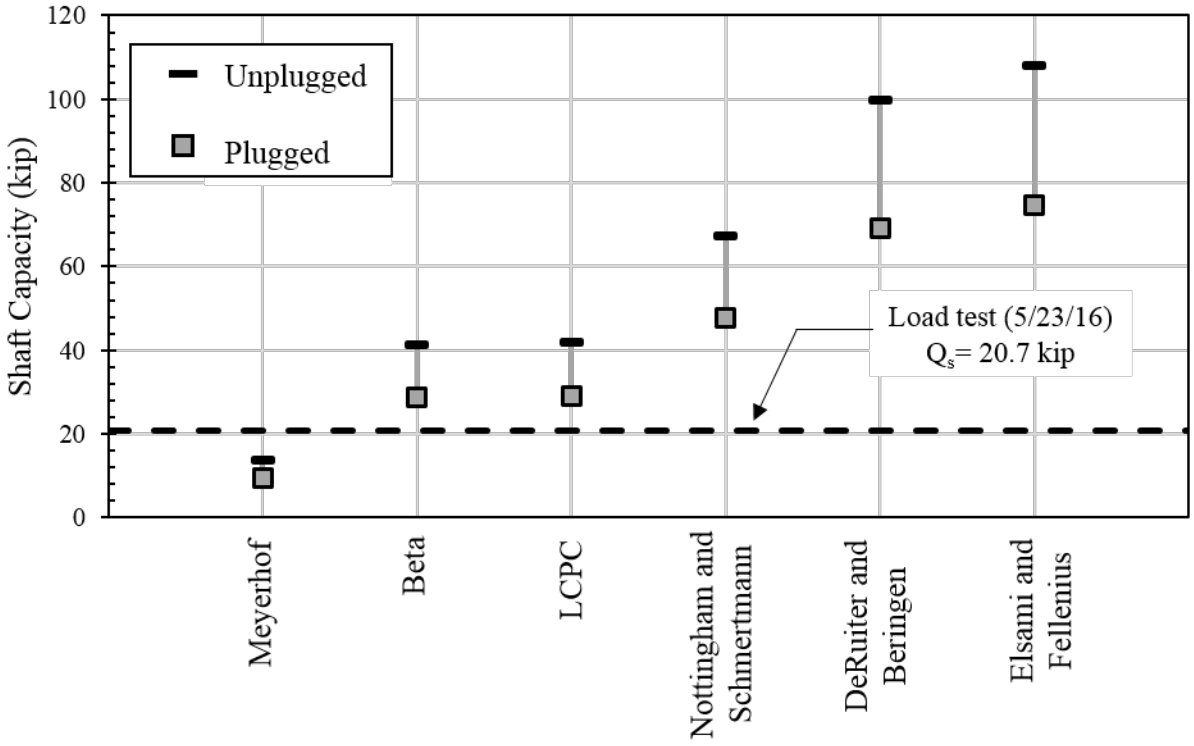

Figure 4-21: Comparison of static method predictions of shaft capacity of H-pile to measured shaft capacity.

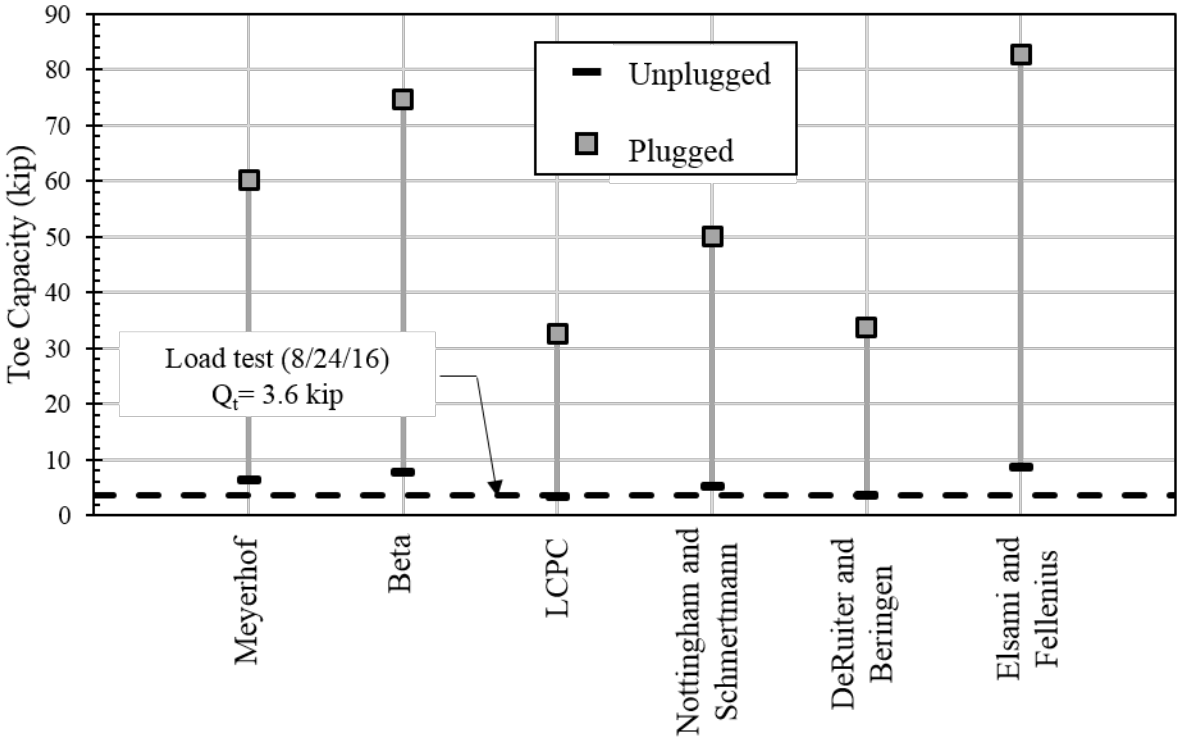

Figure 4-22: Comparison of static method predictions of toe capacity of sheet pile wall to measured toe capacity.

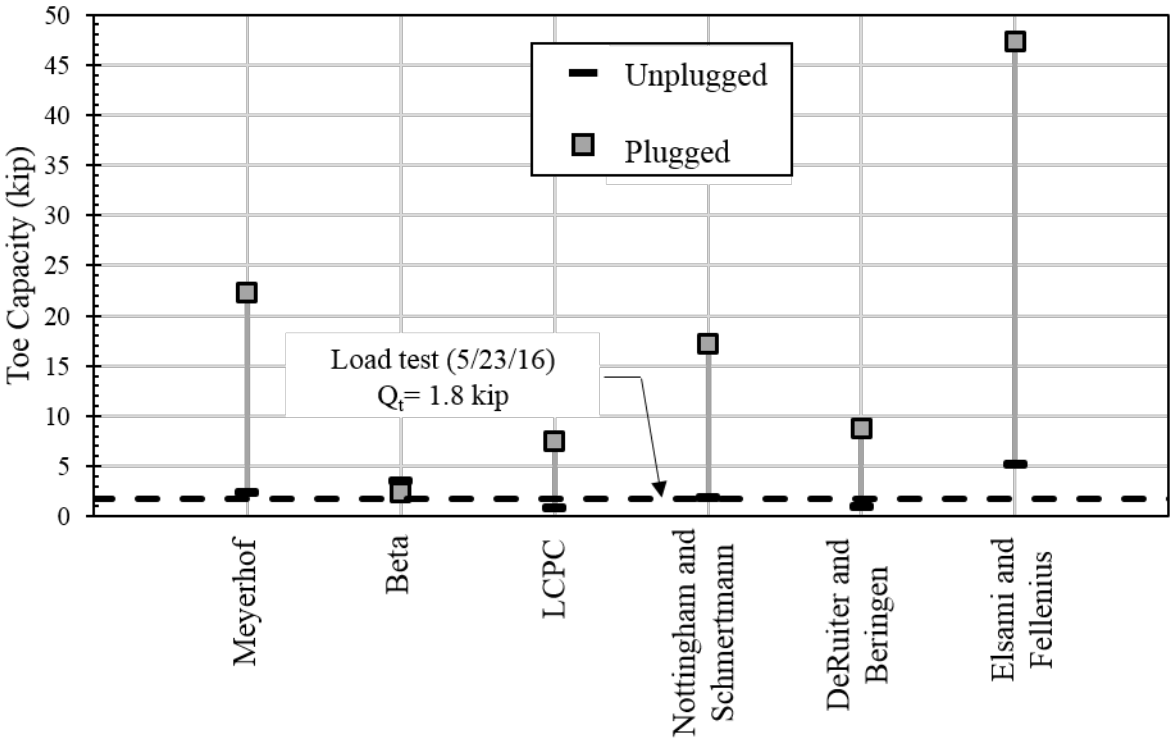

Figure 4-23: Comparison of static method predictions of toe capacity of H-pile to measured toe capacity.

The predicted axial pile capacities presented above, are summarized in Table 4-3 and Table 4-4, for the sheet pile and H-pile, respectively.

Table 4-3: Predicted axial capacities for sheet pile wall tested at field test site.

Prediction Method		Total Capacity		Shaft Capacity		Toe Capacity	
		Q_c (kip)	Q_c/Q_m	Q_c (kip)	Q_c/Q_m	Q_c (kip)	Q_c/Q_m
Meyerhof	Unplugged	38.37	1.12	32.08	1.04	6.3	1.75
	Plugged	87.21	2.54	27.00	0.88	60.21	16.73
Beta	Unplugged	48.11	1.40	41.67	1.36	6.44	1.79
	Plugged	96.66	2.82	35.07	1.14	61.59	17.11
LCPC	Unplugged	61.88	1.80	58.47	1.90	3.41	0.95
	Plugged	81.77	2.38	49.22	1.60	32.56	9.04
Nottingham & Schmertmann	Unplugged	101.46	2.96	96.24	3.13	5.22	1.45
	Plugged	132.49	3.86	82.64	2.69	49.86	13.85
DeRuiter & Beringen	Unplugged	137.49	4.01	133.96	4.36	3.53	0.98
	Plugged	146.51	4.27	112.76	3.67	33.75	9.38
Elsami & Fellenius	Unplugged	158.17	4.61	149.51	4.87	8.66	2.41
	Plugged	122.08	3.56	74.69	2.43	47.4	13.17

Notes: Q_c = calculated value using static methods. Q_m = measured value corresponding to Davisson's failure criterion (total = 34.3 kip, shaft = 30.7 kip, toe = 3.6 kip). Qc/Q_m = the ratio of calculated to measured.

Table 4-4: Predicted axial capacities for H-pile tested at field test site.

Prediction Method		Total Capacity		Shaft Capacity		Toe Capacity	
		Q_c (kip)	Q_c/Q_m	Q_c (kip)	Q_c/Q_m	Q_c (kip)	Q_c/Q_m
Meyerhof	Unplugged	16.58	0.74	14.14	0.68	2.44	1.36
	Plugged	32.04	1.42	9.78	0.47	22.26	12.37
Beta	Unplugged	40.42	1.80	37.21	1.80	3.21	1.78
	Plugged	27.97	1.24	25.75	1.24	2.22	1.23
LCPC	Unplugged	42.71	1.90	41.89	2.02	0.82	0.46
	Plugged	36.49	1.62	28.98	1.40	7.51	4.17
Nottingham & Schmertmann	Unplugged	69.25	3.08	67.40	3.26	1.85	1.03
	Plugged	64.61	2.87	47.73	2.31	16.88	9.38
DeRuiter & Beringen	Unplugged	100.80	4.48	99.84	4.82	0.96	0.53
	Plugged	77.87	3.46	69.08	3.34	8.79	4.88
Elsami & Fellenius	Unplugged	113.13	5.03	107.95	5.21	5.19	2.88
	Plugged	122.08	5.43	74.69	3.61	47.40	26.33

Notes: Q_c = calculated value using static methods. Q_m = measured value corresponding to Davisson's failure criterion (total = 22.5 kip, shaft = 20.7 kip, toe = 1.8 kip). Qc/Q_m = the ratio of calculated to measured.

The various static methods used to predict total axial pile capacity of the sheet pile wall (Table 4-33) led to ratios of calculated-to-measured pile capacities (Q_c/Q_m) ranging from 1.11 to 4.61 for the unplugged condition assumption, and from 2.38 to 4.27 for the plugged condition assumption. The range of Q_c/Q_m ratios for the toe capacity of the sheet pile wall were closer to unity for estimates that considered the unplugged condition. The Q_c/Q_m ratios for the shaft

capacity were close to unity for the SPT based methods. In contrast the CPT-based static methods yielded Q_c/Q_m ratios for the shaft capacity that ranged from 1.4 to 3.6 and from 2.0 to 5.2 for the plugged and unplugged assumptions, respectively. Confirmation of plugging phenomenon for the sheet pile at the field site on the basis of the above static method predictions is not possible. Based on measured CPT tip resistances, the soil near the toe of the sheet pile (17 feet depth) was a soft, low plastic sandy silt that may not be as conducive to plug formation. Based on various static methods used to predict total axial pile capacity of the H-pile (Table 4-4), the ratios of calculated-to-measured pile capacities (Q_c/Q_m) were found to range from 0.74 to 5.03 for the unplugged condition assumption, and from 1.24 to 5.43 for the plugged condition assumption. Occurrence of the plugging phenomenon for the H-pile based on these Q_c/Q_m ratios is equally difficult to assess.

In general, it is recommended to use the lowest capacity value computed from the two extreme conditions of unplugged and fully plugged. For both piles tested at the field test site the lowest toe capacity estimates were found to correspond to the unplugged condition, while the lowest shaft capacity estimates were obtained using the plugged condition. Using this suggested approach for capacity estimates of both the toe and the shaft capacity of sheet piles will be conservative and help minimize over-estimation of the axial load capacity.

This full-scale pile load test program highlights the level of uncertainty associated to predicting the plugged or unplugged behavior for sheet pile walls under static loading. Use of the plugged condition assumption for pile toe capacity should only be used if there is reasonable assurance (or field evidence form a project specific load test) that a soil plug will form. Further research is needed and recommended to improve our understanding of the plugging phenomenon for sheet pile walls and to help develop design guidelines that can possibly allow incorporation of any beneficial load capacity contribution associated to plug formation.

4.7 Experimental load transfer curves and associated predictions

4.7.1 Sheet pile

Using the different elevations of strain gage instrumentation on the sheet piles (See Figure 4-6), the load transfer curves were obtained. The T-Z curves obtained for the eight levels of strain gages are shown in Figure 4-24. These side shear load transfer curves although useful do not correspond to the main geotechnical layers encountered at the field test site. Therefore, a second set of load transfer curves was developed based on the main soil layers present along the sheet pile wall as shown in Figure 4-25.

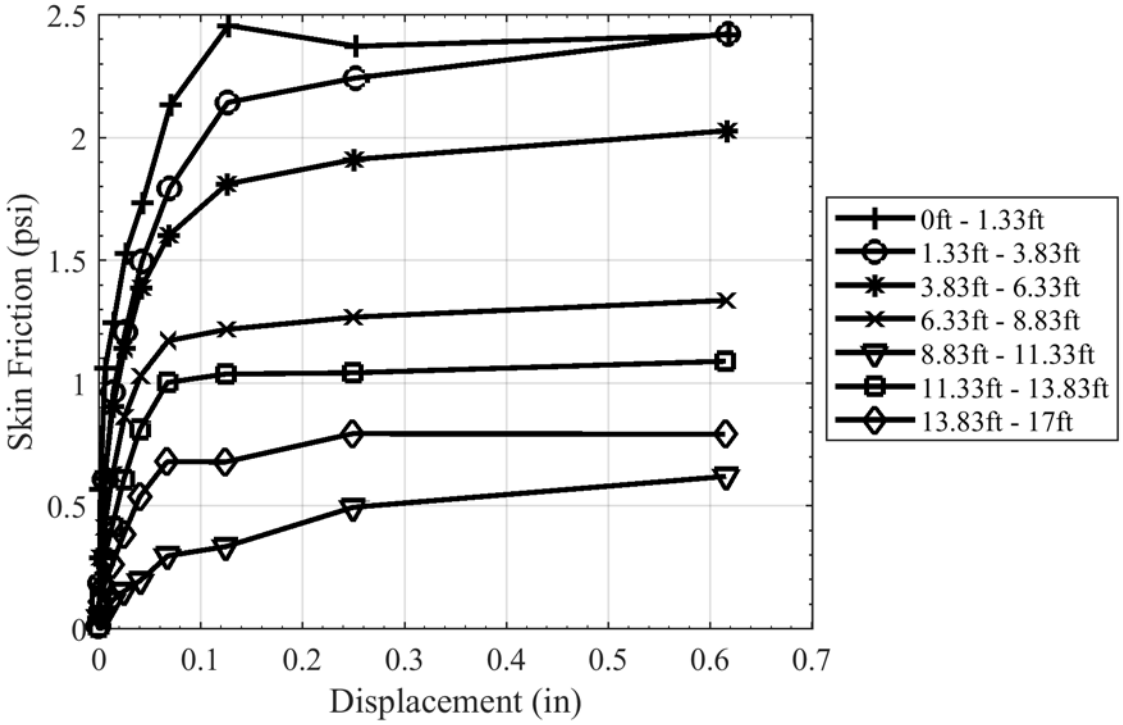

Figure 4-24: Experimental T-Z load transfer curves for field axial load test of sheet pile wall based on strain gage layout.

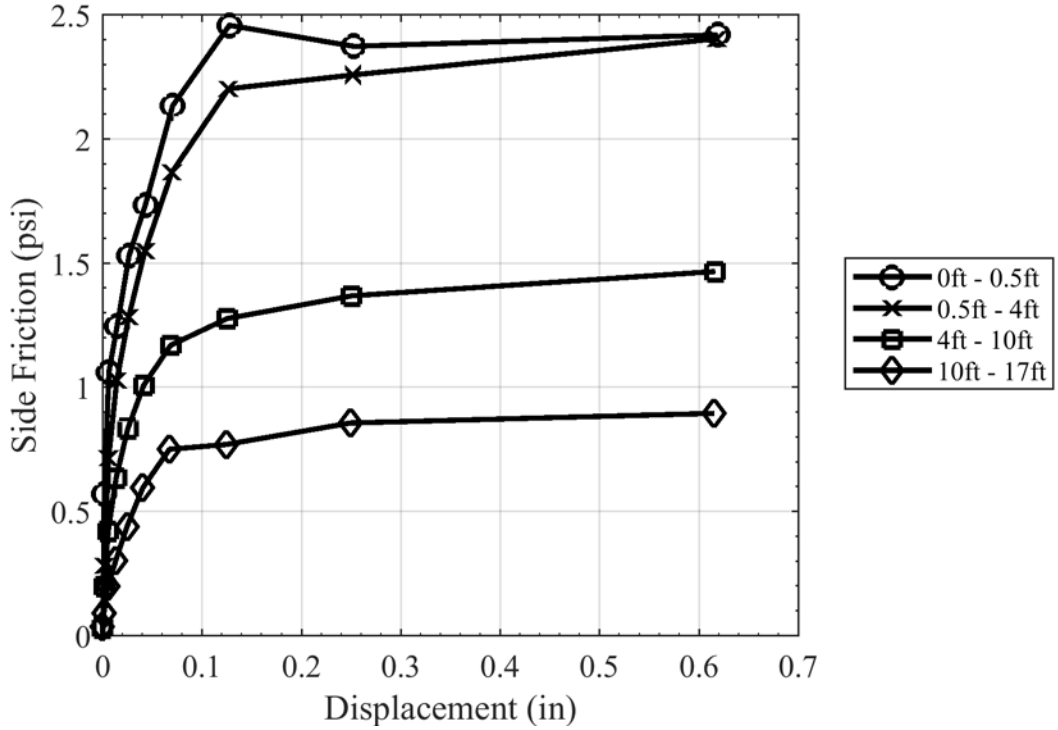

Figure 4-25: Experimental T-Z load transfer curves for field axial load test of sheet pile wall based on geotechnical stratigraphy in Figure 4-4.

The T-Z curves in this figure show the peak side friction does not increase with depth. This is as expected given this site consists primarily of low plastic fine grained soils with soft to medium stiff consistency. The amount of displacement required for mobilization of the peak side friction resistance was found to be between 0.15 in (3.8 mm) and about 0.5 in (12 mm). This level of relative shaft displacement required to mobilize peak side friction is higher than normally expected for steel deep foundations installed in fine grained soils. For example, empirical load transfer curves reported by Coyle and Reese (1966) for piles installed in the San Francisco Bay mud suggest full peak side friction mobilization occurs at relative displacements between 0.03 in (0.75 mm) and 0.07 in (1.8 mm).

The experimental load transfer curve obtained for the mobilization of the toe capacity is shown in Figure 4-26. This plot shows that the mobilization of the full toe capacity (≈ 3.6 kip) required only a small toe displacement of about 0.1 inches (2.5 mm). This observation suggests no plugging at the toe of the sheet pile wall since toe capacity mobilization usually requires displacements between 5 to 10% of the toe width or diameter. A plugged toe condition would represent an equivalent pile width at the toe of about 12 in (305 mm) which would require a much larger toe displacement for toe capacity mobilization (between 0.6 to 1.2 in). Furthermore, the larger toe area associated to the plugged condition would yield a much larger toe force than the low value measured of 3.6 kips.

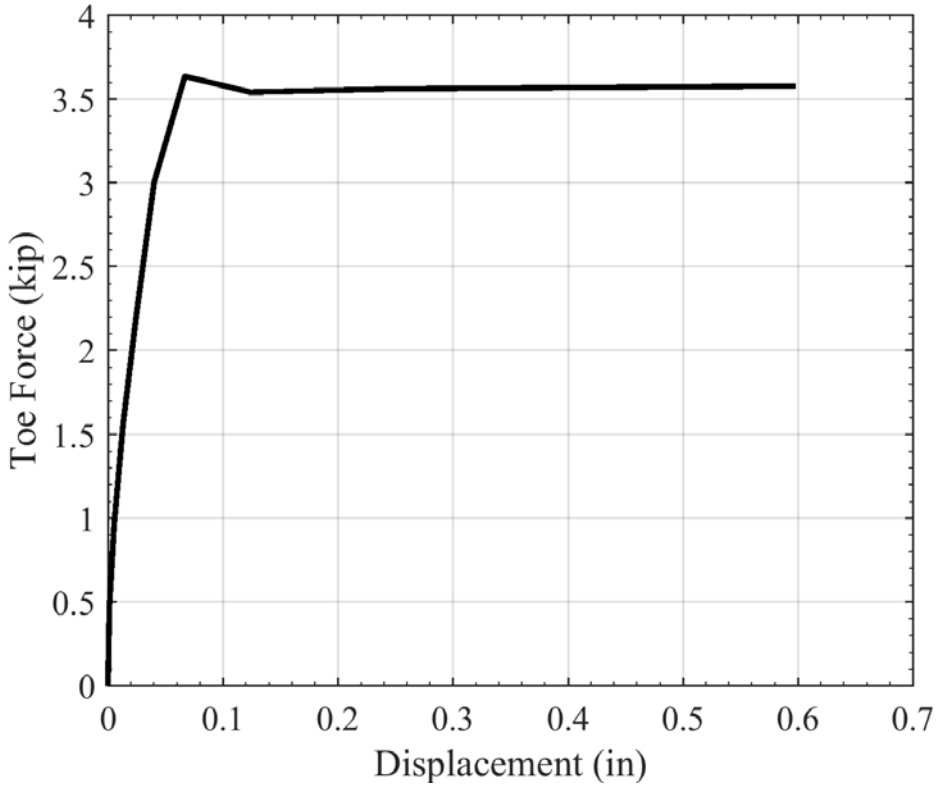

Figure 4-26: Experimental pile tip load-displacement (Q-Z) load transfer curve for field axial load test of sheet pile.

The predicted load-settlement curve obtained using the load transfer method with the experimental T-Z and Q-Z load transfer curves reported above, is shown in Figure 4-27. This curve shows the prediction is quite good given it is based on measured load transfer curves.

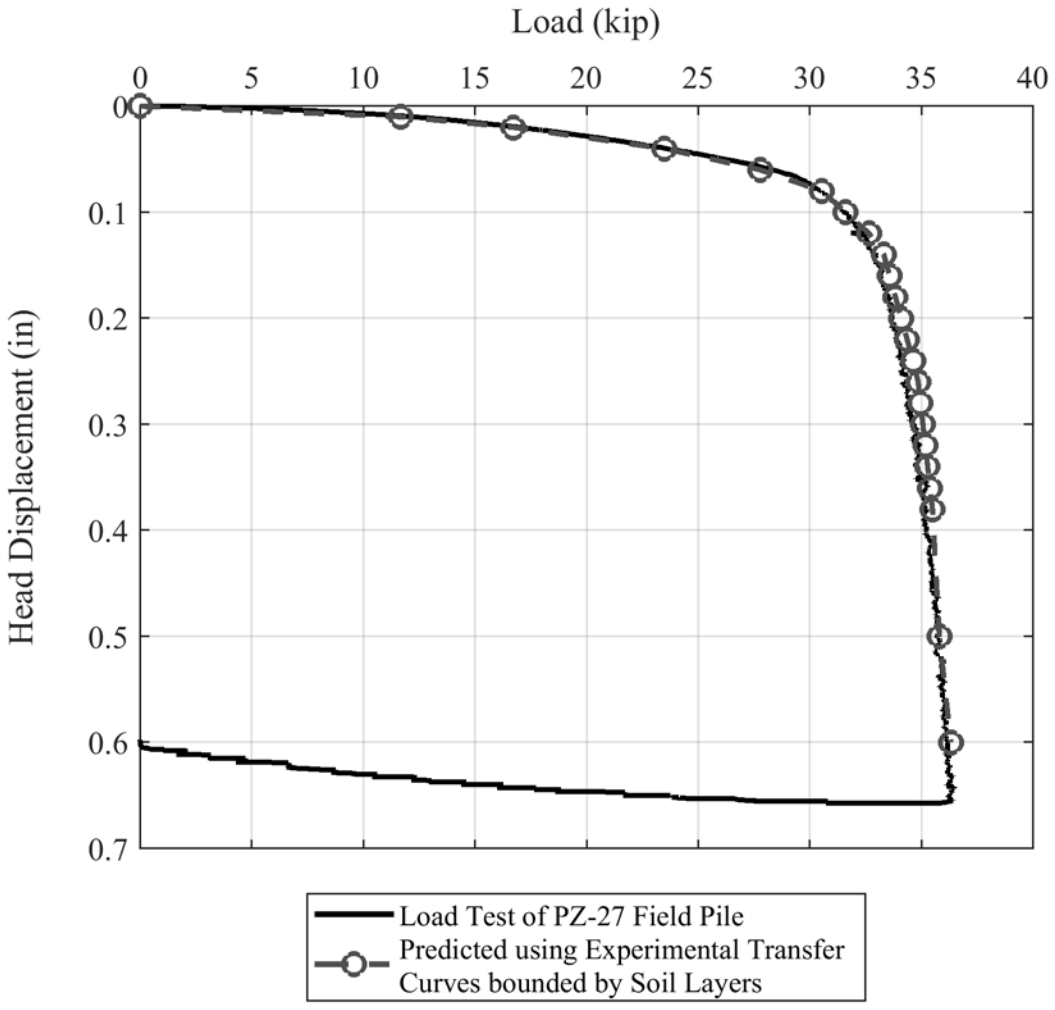

Figure 4-27: Settlement prediction for sheet pile wall using experimental load transfer curves.

4.7.2 H-pile

Considering the geotechnical conditions for both test piles were similar, and the interface behavior that controls side friction T-Z curves should be similar given it is the same pile material and surface roughness (hot-rolled steel from same company; Skyline) a load transfer prediction was made for the H-pile using the experimental load transfer curves measured for the sheet pile. To correct for the difference in cross sectional area between the two pile types, the magnitude of the Q-Z curve was scaled proportional to the areas.

The predicted load-settlement curve for the H-pile using the load transfer method with the experimental T-Z and Q-Z load transfer curves reported for the sheet pile (previous subsection), is shown in Figure 4-28. The comparison indicates that the prediction is reasonably strong, especially given it is based on load transfer curves measured on a different type of pile located about 15 feet away. The differences are attributed to inherent differences in the geotechnical conditions at the location of both test piles and expected differences in the way the shaft and toe contributions are mobilized given differences in cross section.

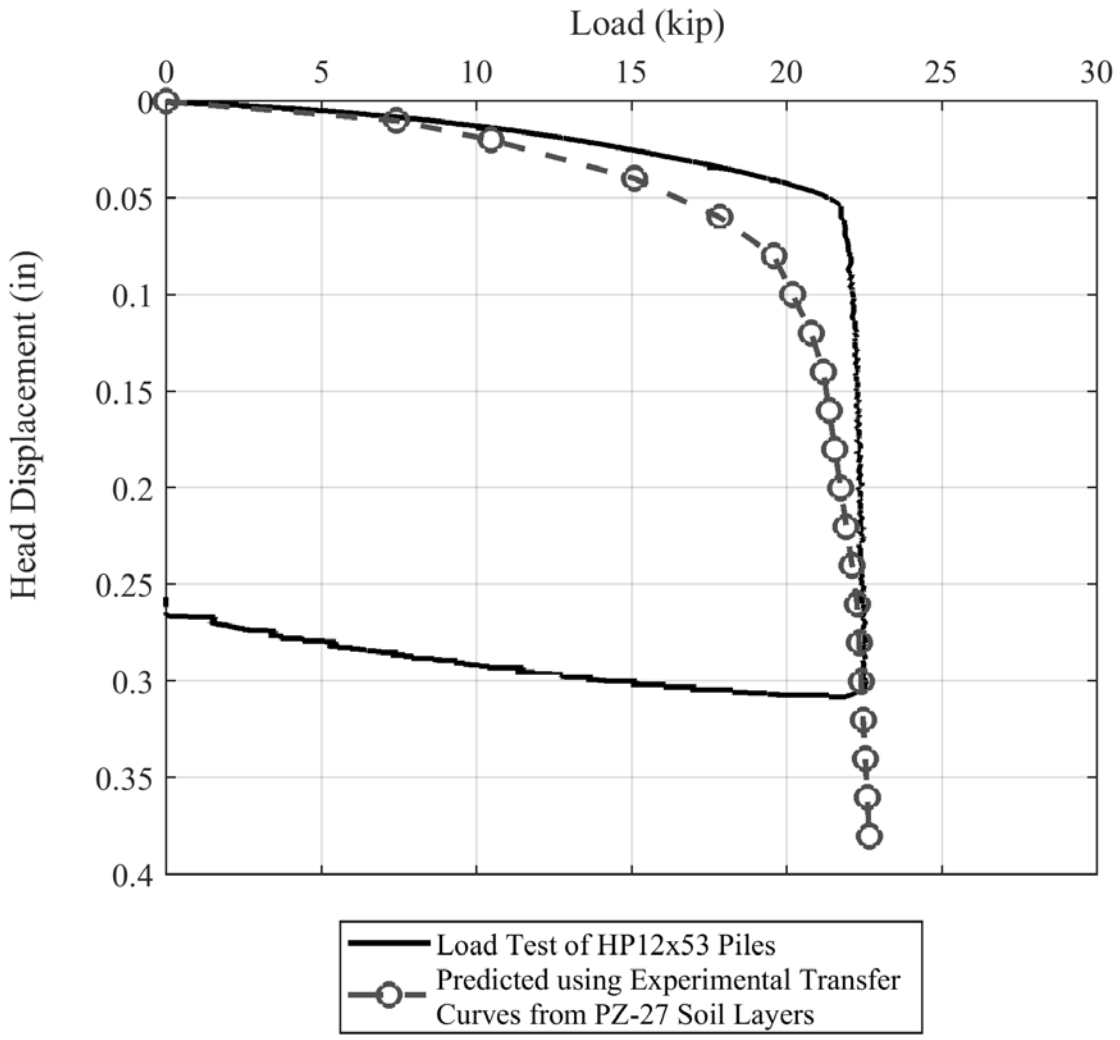

Figure 4-28: Settlement prediction for H-pile using experimental load transfer curves from sheet pile wall.

4.8 Summary

A full-scale axial load test program was conducted on an instrumented sheet pile wall as well as a reference H pile installed at a field test site located In Matthews, NC. The test piles were installed at a relatively flat site at a separation of approximately 15 feet from each other. Piles were installed using similar procedures to the same final embedment depth of 17 feet. Geotechnical conditions at the test site were characterized with a detailed field program that included drilling, SPT tests, CPT soundings, and MASW geophysical tests. Despite inherent variability of geotechnical site conditions, the soil conditions for both test piles were generally very similar and consisted of fine grained residual soils described as low plastic, medium stiff, sandy clays and silts (CL to ML) that extended to a depth of about 20 feet. Below 20 feet depth, that is below the depth of the tip of the test piles, the residual soils become coarser grained as they were found to consist of medium dense to dense silty sand. The groundwater level at the site fluctuated from about 5 to 12 feet depth depending on seasonal climate conditions.

The field load tests allowed assessment of the axial load capacity of PZ-27 sheet pile walls under field conditions considered representative of the NC Piedmont geology. The axial load tests included dynamic measurements acquired during installation that allowed for PDA and CAPWAP analyses. Strain gage installations on the test piles permitted for evaluation of the mobilization of shaft and toe resistance during the static axial load testing, in addition to the measurement of the total axial load capacity. A key aspect of the field test program, not part of the original scope of the NCDOT project, is the inclusion of an axial load test on a reference H-pile for comparison.

The field load test program contributes to the state of knowledge particularly given the scarcity of case histories involving full-scale axial load tests on instrumented sheet piles. The field load test program helps demonstrates strong potential for safely considering the axial load contribution from sheet pile walls. Particularly the side-by-side comparison with the H-pile further demonstrates how sheet piles can provide adequate load bearing capacity/ axial stiffness that is comparable to values contributed by the commonly used H pile deep foundation.

The prediction of the axial capacity of the sheet pile wall was found to be reasonable using the same procedures commonly used for capacity estimates used for commonly used driven piles such as H-piles. The level of accuracy of the axial capacity predictions using methods such as PDA, CAPWAP, and static methods was found to be reasonable and similar to the levels of accuracy obtained for the comparison H-pile.

A key design consideration for estimating the axial capacity of sheet pile walls is the plugging phenomenon. The axial test results did not confirm plug formation in the sheet pile or H pile. For both piles tested at the field test site the lowest toe capacity estimates were found to correspond to the unplugged condition, while the lowest shaft capacity estimates were obtained using the plugged condition.

For design purposes, it is recommended to estimate the axial capacity of sheet piles as the sum of the shaft and toe capacities computed as the lesser value obtained by assuming the two extreme conditions of being unplugged or fully plugged. This suggested approach for capacity estimation is conservative and should help minimize over-estimation of the axial load capacity.

Finally, this full-scale pile load test program highlights the level of uncertainty associated to in predicting the plugged or unplugged behavior for sheet pile walls under static loading. Use of the plugged condition assumption for pile toe capacity should only be used if there is reasonable assurance (or field evidence form a project specific load test) that a soil plug will form. Further research is needed and recommended to improve our understanding of the plugging phenomenon for sheet pile walls and to help develop design guidelines that can possibly allow incorporation of any beneficial load capacity contribution associated to plug formation.

5 Parametric study of a sheet pile wall abutment

5.1 Introduction

This chapter presents the results of a parametric study performed to assess possible technical and economical advantages of incorporating sheet pile elements as partial or total axial load bearing elements in a typical NCDOT short span bridge. The parametric analyses are based on simplified analytical models of several bridge abutment configurations presented by the PI's as part of the original proposal for this project. Figure 5-1 shows the five abutment configurations considered. This figure includes the standard abutment (Figure 5-1(a)) with a row of H piles serving as the commonly used deep foundation for these types of bridges, as well as different potential configurations where H piles are replaced by axial load bearing sheet piles, shown in Figure 5-1(b) through Figure 5-1(e). The deep foundation elements shown in this figure are the HP 12x53 and PZ-27 sections that are commonly used in NCDOT bridge projects, as mentioned earlier in this report. The cross-section details and geometric properties were described earlier in this report.

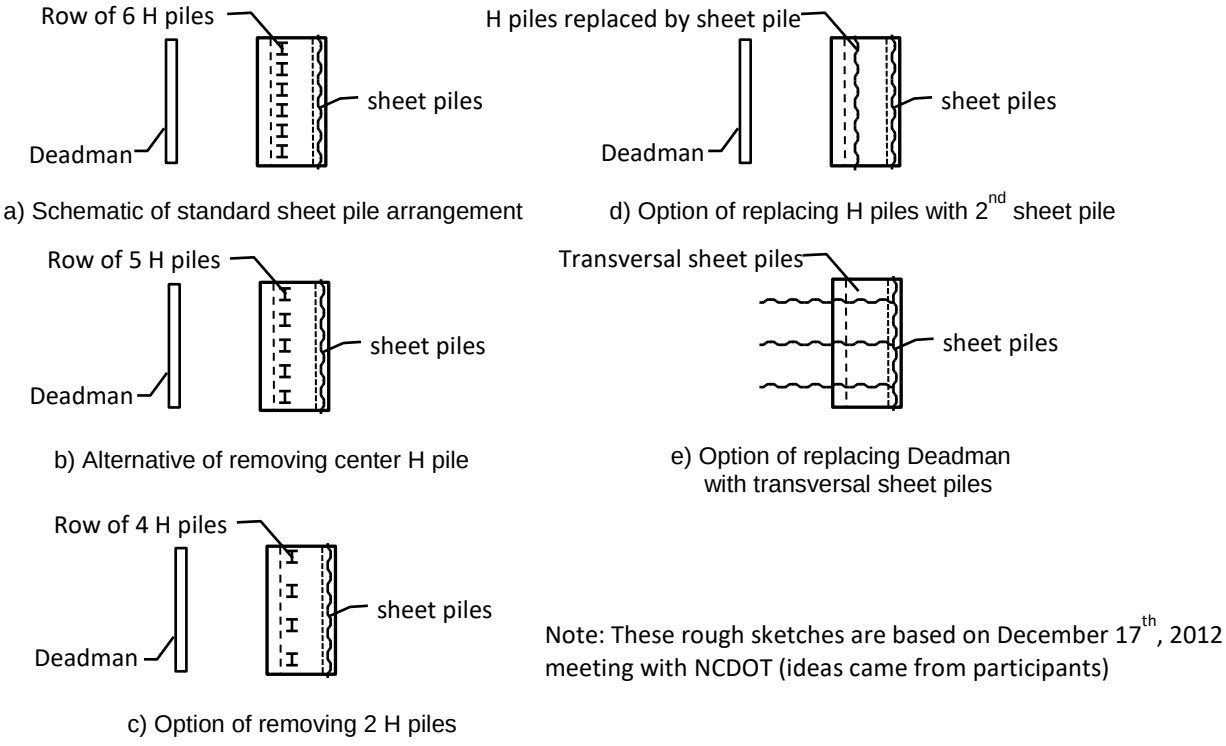

Figure 5-1: Different bridge abutment configurations considered in parametric study.

The parametric study involved a series of analyses performed for a fictitious bridge that is based on the Task #1 interim report that reviewed and summarized a total of fifteen NCDOT bridges. As suggested by the Steering and Implementation Committee for this research project, the dimensions and geotechnical conditions of the fictitious bridge were selected to be representative of a short span bridge in the NC Blue Ridge Mountains region.

5.2 Description of representative bridge

The representative bridge used for the parametric analysis has a span of 60 feet and a width of 40 feet. The bridge is shown schematically in Figure 5-2.

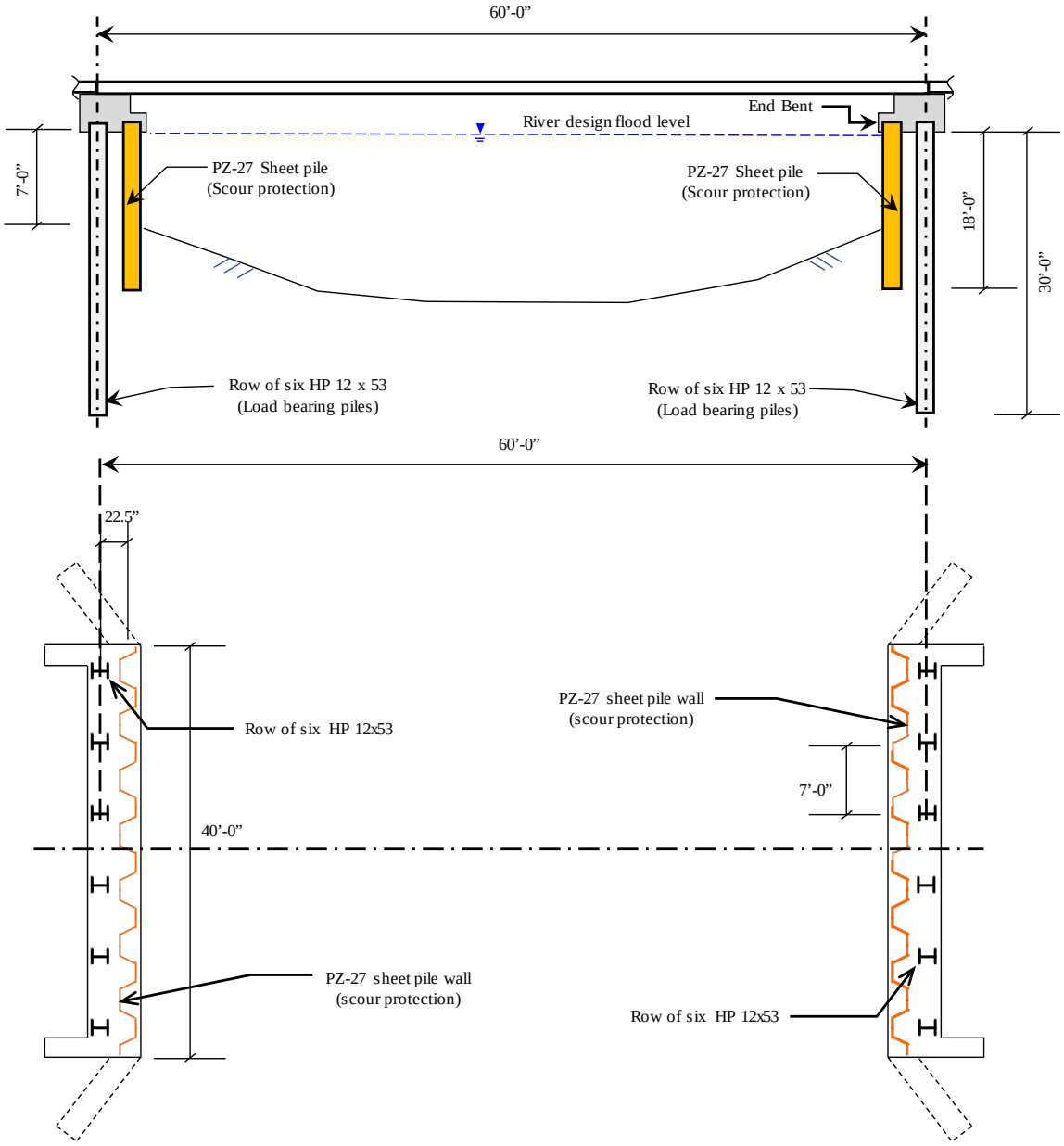

Figure 5-2: Schematic of representative bridge used in parametric study.

The abutment of the representative bridge has a total width of 40 feet and the standard configuration currently used by NCDOT, as shown in Figure 5-1. For the representative design, the configuration of the abutment has six HP 12x53 as the sole elements for carrying the axial load from the bridge superstructure. These piles are typically driven to refusal. Additionally,

this standard abutment configuration has a continuous row of PZ-27 sheet piles for scour protection, and a deadman anchor to provide resistance to lateral loads. For the parametric study, it was assumed that the H piles were driven to refusal to a bedrock with an embedment depth of 30 feet. The PZ-27 sheet piles were assumed to have an embedment depth of 18 feet and the critical scour depth was considered to be 7 feet. These dimensions were selected based on the survey of bridge abutment designs performed in the Task #1 interim report. Simplified geotechnical conditions were assumed with a uniform medium dense sand having a total unit weight of 120 pcf and an effective friction angle of 32 degrees. A schematic view of the standard configuration of the bridge abutment is shown in Figure 5-3.

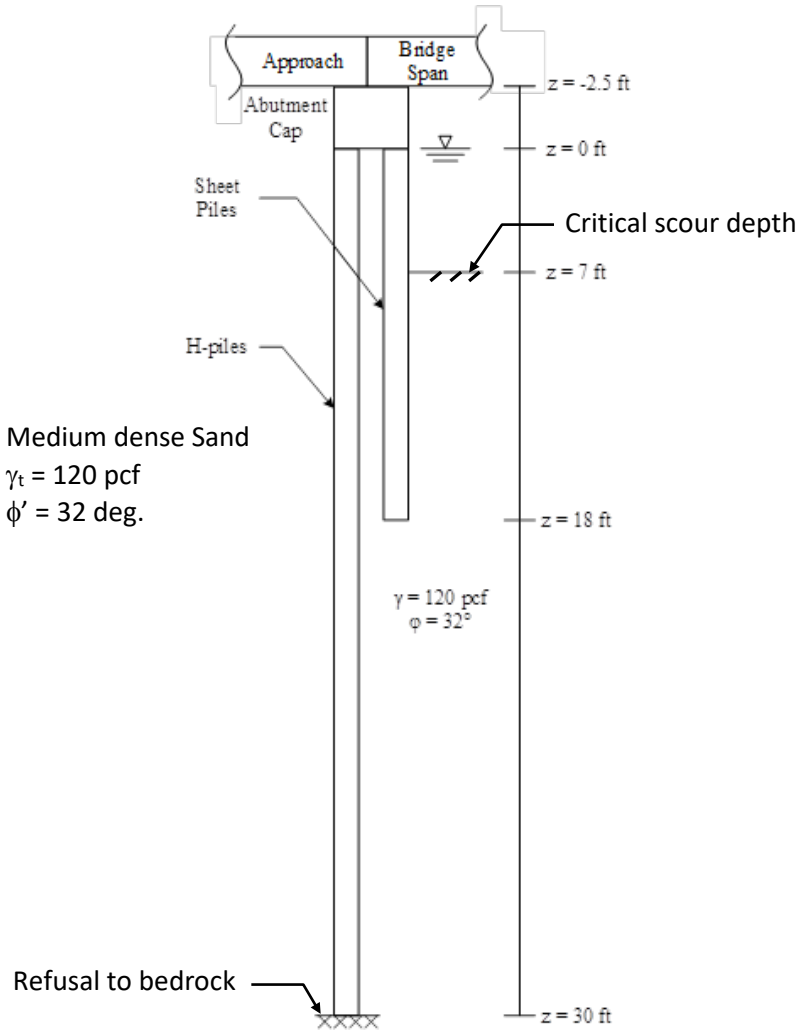

Figure 5-3: Abutment geometry for representative bridge used in parametric study.

5.3 Axial capacity estimates of abutment piles

The axial capacity of the H piles and sheet piles can be estimated using an effective stress based method and the procedure outlined by Yandzio (1998) that was described in Chapter 1. This approach requires determination of the vertical stresses along the length of the different piles.

The computed vertical stresses are shown in Figure 5-4. These values were computed for an effective unit weight of 57.6 pcf for the sand and consider the differences in embedment and surface loading of the active (or side towards inside of abutment fill) and passive (or river side) sides. The designation of active and passive sides refers to the two extreme soil states that result in the active and passive zones shown in Figure 5-5. These two zones are based on assuming a simplified failure mechanism, as recommended by Yandzio (1998).

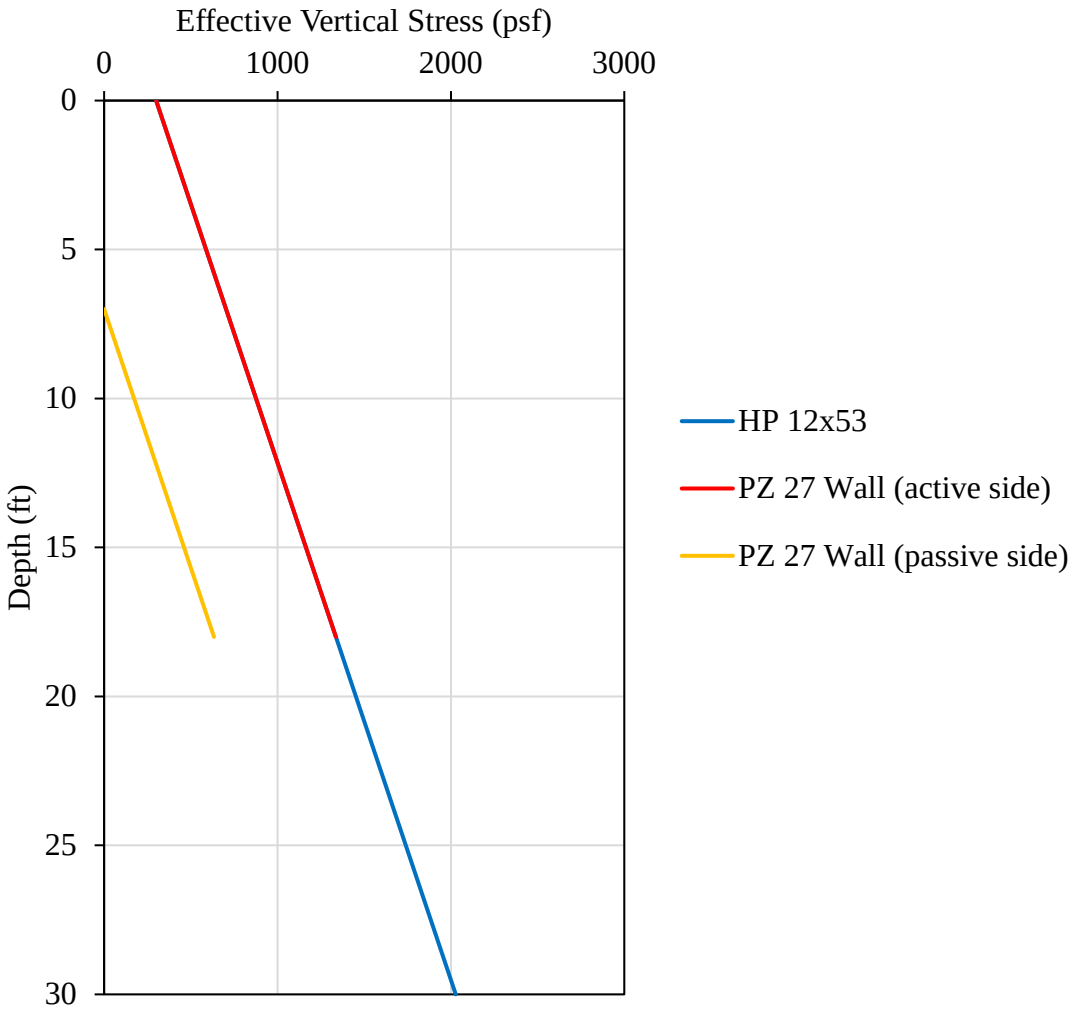

Figure 5-4: Effective vertical stresses on piles in representative bridge used in parametric study.

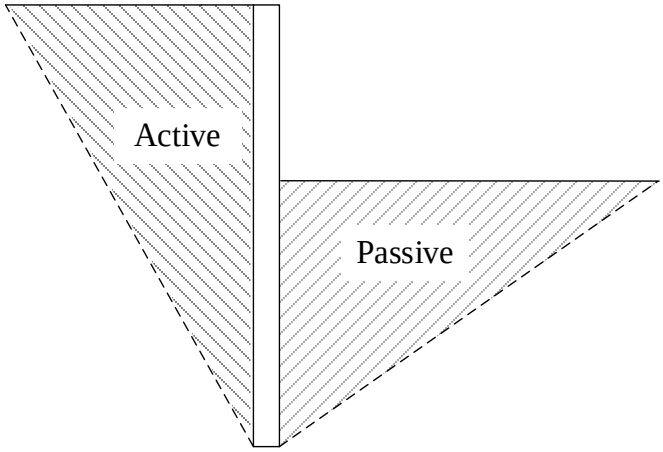

Figure 5-5: Simplified failure mechanism showing active and passive zones for a sheet pile wall.

Following recommendations by Yandzio (1998), the side friction (or skin friction) along the active side the sheet pile should be neglected above the so called point of stability. This point of stability can be determined from moment equilibrium and it corresponds to the first inflection point in the moment diagram along the length of the sheet piles where the moment is zero. For the conventional abutment configuration, and the assumed geometry and soil conditions of the representative bridge, the point of stability was found to be at about 11 feet below the head of the sheet piles (Figure 5-6).

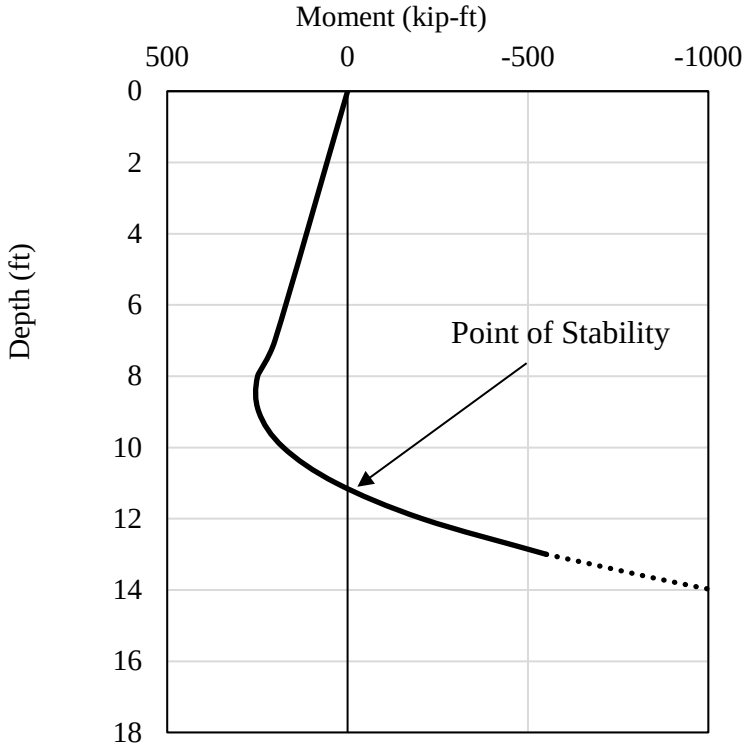

Figure 5-6: Calculated point of stability for conventional abutment configuration of representative bridge.

The axial capacity of the sheet pile, like any deep foundation, is the sum of the tip resistance (q_t) and side friction (f_s). However, following the recommendations by Yandzio (1998), contributions from side friction are only considered at the locations shown in Figure 5-7. This figure also shows the end bearing and side friction contributions for a conventional H-pile.

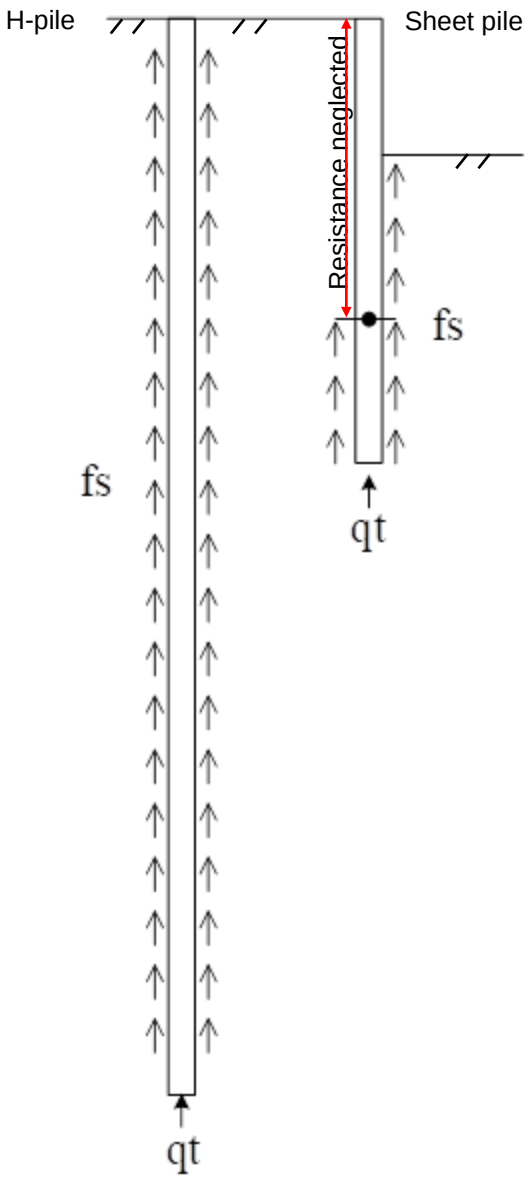

Figure 5-7: Locations where unit side friction is considered based on Yandzio (1998).

Using the effective stress approach, the maximum unit side friction (fs) can be computed using the popular beta method, as follows:

$$fs_{max} = \beta \cdot \sigma_v' \quad \text{.....(5.1)}$$

Where σ_v' = the vertical effective stress at the location where f_s is being computed, and β is a coefficient that is related to the lateral earth pressure coefficient (k_s) and the interface friction angle between the surrounding soil and the material of the sheet pile. For conventional deep foundations, the coefficient of lateral earth pressure is typically assumed to be slightly below or slightly above the at-rest coefficient depending on the installation procedure and whether the pile is a non-displacement or displacement pile (See for example Hannigan et al., 2016). The interface friction angle for most pile types is considered to be between 1/2 and 2/3 of the soil effective friction angle, which correspond to the lower bound of the range associated with smooth pile materials and the upper bound of range for pile materials that have a rough surface topography. For the case of sheet piles, Yandzio (1998) proposed estimating the interface friction angle as 1/2 ϕ' for the passive side and 2/3 ϕ' for the active side:

$$\delta = \frac{1}{2}\phi' \ (passive) \ to \ \frac{2}{3}\phi'(active) \quad \text{.....(5.2)}$$

Where, ϕ' is the effective friction angle (equal to 32 degrees for the representative bridge abutment).

Then taking the lateral earth pressure coefficient (k_s) needed to compute the beta coefficient according to Yandzio (1998) should be based on whether the skin friction is computed for the active or passive zones shown in Figure 5-5. Therefore, the beta coefficient for axially loaded sheet piles, as adapted by Yandzio (1998) and described in Chapter 1, is computed as:

$$\beta = k_s \cdot \tan(\delta) \text{.....(5.3)}$$

Where k_s = the lateral earth pressure coefficient that can be equal to k_a if f_s is being evaluated in the active wedge, or k_p is it is being evaluated along the passive wedge. Note that for H-piles it was assumed that k_s = k_o (the at-rest coefficient).

Using the beta method with the modifications proposed by Yandzio (1998), the resulting unit side friction (or skin friction) for the sheet pile of the representative bridge is shown in Figure 5-8(a). Note that the side friction contribution for the active side is zero from the ground surface to the depth of the Point of Stability, which for the abutment of the representative bridge is equal to 11 feet. The side friction for the H-pile is shown in Figure 5-8(b).

The unit toe resistance for the sheet pile toe was estimated based on the average vertical stress magnitude computed for the location of the sheet pile toe, shown in Figure 5-3, and a bearing capacity coefficient (N_t). For the geometry and soil conditions considered in the parametric study, the unit toe resistance of the sheet pile was estimated to be about 19 ksf. This value

considered the average vertical stress magnitude at the toe and a bearing capacity coefficient of Nt = 30. For the H-piles that are driven to bedrock, the unit toe resistance was estimated to be about 406 ksf. This value is based on the vertical stress level at a 30 feet depth and an assumed bearing capacity coefficient of 200, which is considered a conservative estimate for bedrock that is in a partly weathered condition.

From the above considerations, the estimated skin and toe axial capacities for an HP 12 x 53 pile are 27.4 and 43.7 kip, respectively. These values yield an ultimate axial load capacity of about 71.1 kip for the H-pile assuming an unplugged condition. Similarly, a PZ-27 sheet pile wall of 40 feet width installed to the depth shown in Figure 5-3 results in skin and toe axial capacities of 33.8 and 41.9 kip, respectively. These values result in an ultimate axial capacity of 75.7 kip also assuming an unplugged condition.

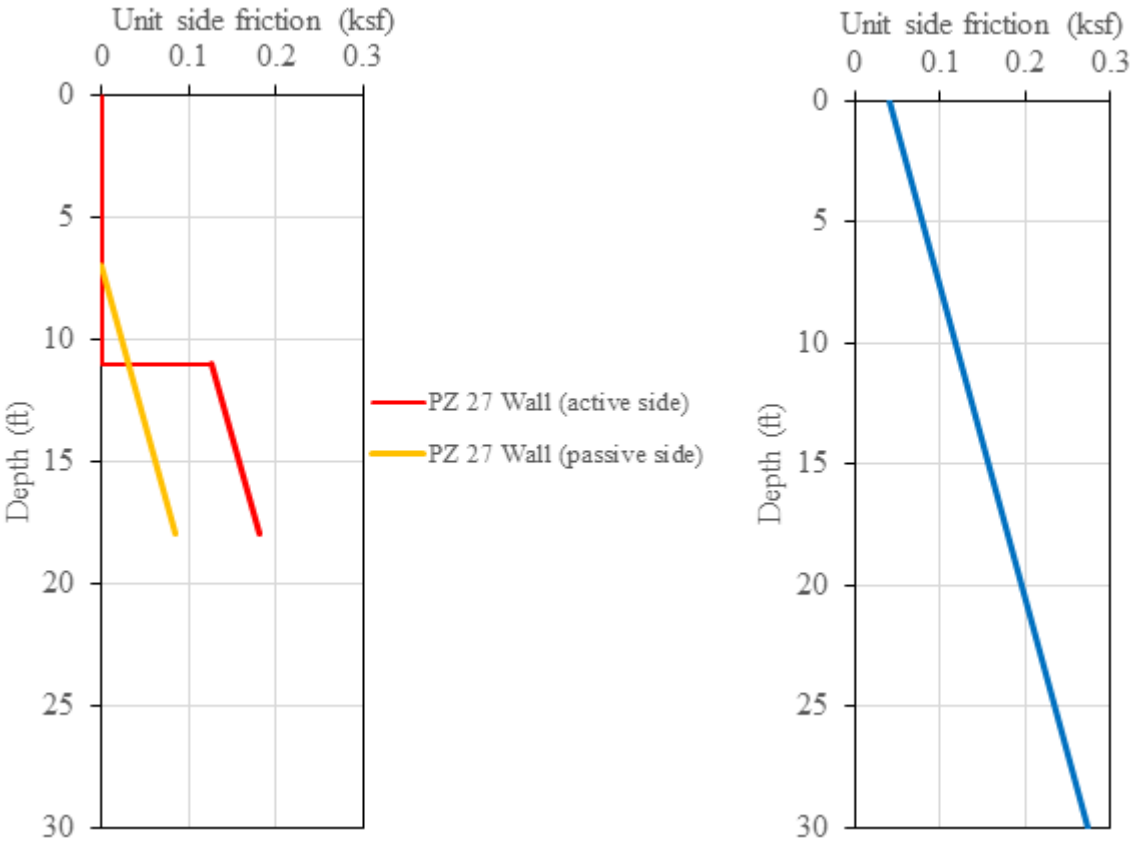

a) PZ-27 sheet pile **b) H-pile**

Figure 5-8: Unit side friction distributions for abutment of representative bridge based on the beta method.

Using the estimated axial toe and skin friction capacities for both piles it is possible to compute total axial capacity values for the different abutment configurations shown in Figure 5-1. The axial capacities are summarized in Table 5-1.

Table 5-1: Summary of axial capacities for different abutment configurations of representative bridge.

Configuration	Description	Total Axial Capacity (kips)	Comments
Baseline case (Figure 5-1a)	Six H-piles; neglecting any sheet pile contribution	426.3	- n.a.
Baseline + sheet pile (Figure 5-1a)	Six H-piles including contribution of PZ-27 sheet pile wall (40 ft wide, and 18 ft length)	502.0	- Would require structural design of sheet pile connection to abutment seat.
Five H-piles + sheet pile (Figure 5-1b)	Five H-piles including contribution of PZ-27 sheet pile wall (40 ft wide, and 18 ft length)	431.0	- Would require structural design of sheet pile connection to abutment seat.
Four H-piles + ***extended*** sheet pile (Figure 5-1c)	Four H-piles including contribution of PZ-27 sheet pile wall (40 ft wide, and 23 ft length)	436.5	- Sheet piles driven deeper by 5 ft for new L = 23 ft. - Would require structural design of sheet pile connection to abutment seat.
No H-piles + ***Two rows of*** sheet piles (Figure 5-1d)	No H-piles + ***Two rows of*** sheet piles extended by 7 feet (L = 25 ft)	432.2	- Two rows of sheet piles (40 ft wide, and embedded 25 ft). - Assumed simplistically same effective stress distribution as H-pile.
Four rows of sheet piles (Figure 5-1e)	No H-piles and four rows of sheet piles (driven to bedrock)	773.6	- Four rows of sheet piles (40 ft wide, and embedded to bedrock). - Assumed conservatively that sheet pile walls oriented perpendicular to bridge abutment facing solely provide lateral stability and do not contribute to the axial bearing capacity. - Increased lateral capacity of this configuration compared to dead man option, was assumed allowed inclusion of shaft resistance of full length of active side.

Note: Capacity values are for representative bridge geometry and simplified geotechnical conditions in Figure 5-1.

5.4 Cost comparison and discussion

Based on total axial capacity considerations, several of the proposed alternative abutment designs (Figure 5-1) were found to be feasible with the elimination of one or more bearing H-

piles. However, as listed in Table 5-1, most configurations required that the sheet pile wall be driven to a deeper embedment depth in order to yield estimated axial capacities equal to or greater than the baseline design case. While these different configurations may be technically feasible, the cost of each configuration needs to be considered before pursuing the use of these alternative abutment designs.

A simplified cost comparison was performed by based on estimated cost for the HP 12x53 and the PZ-27 sheet piles of $45 per linear foot and $30 per square foot, respectively. These unit costs were based on examining recent bid documents and contracts for various NCDOT bridge projects that utilized bearing piles and sheet pile facing. It is assumed these unit costs are installed.

For the original abutment design considered in this parametric study, the six HP 12x53 piles would cost approximately $8,100, based on a total of 180 linear feet of H-piles. The 40 foot wide PZ-27 sheet pile wall has a total area of 720 ft^2, which corresponds to total cost of $21,600. Consequently, the estimated cost for the original abutment (baseline) is $29,700. A comparison of the estimated costs for the different configurations presented in Table 5-2 are shown below.

Table 5-2: Cost comparison for the different abutment configurations of representative bridge.

Configuration	Description	Total Axial Capacity (kips)	Estimated Cost of Foundation Elements
Baseline case (Figure 5-1a)	Six H-piles; neglecting any sheet pile contribution	426.3	$ 29,700
Baseline + sheet pile (Figure 5-1a)	Six H-piles including contribution of PZ-27 sheet pile wall (40 ft wide, and 18 ft length)	502.0	$ 29,700
Five H-piles + sheet pile (Figure 5-1b)	Five H-piles including contribution of PZ-27 sheet pile wall (40 ft wide, and 18 ft length)	431.0	$ 28,350
Four H-piles + ***extended*** sheet pile (Figure 5-1c)	Four H-piles including contribution of PZ-27 sheet pile wall (40 ft wide, and 23 ft length)	436.5	$ 33,000
No H-piles + ***Two rows of*** sheet piles (Figure 5-1d)	No H-piles + ***Two rows of*** sheet piles extended by 7 feet (L = 25 ft)	432.2	$ 60,000
Four rows of sheet piles (Figure 5-1e)	No H-piles and four rows of sheet piles (driven to bedrock)	773.6	$ 36,000

Note: Applies to representative bridge geometry and simplified geotechnical conditions in Figure 5-1.

The above cost estimates do not take into account possible cost savings when only using one contractor and hammer if only sheet piles are installed. The axial capacities, and associated cost estimates, for the chosen geometry and simplified soil conditions, suggest that including

the axial contribution of the PZ-27 sheet pile wall in the abutment design does yield technically and economically feasible alternatives. However, the current analysis suggests that only the alternatives that involve reducing, but not completely eliminating, the number of H-piles in the abutment design could result in potential cost savings. This cost analysis was based on simplifying assumptions and is limited to a single geometry case study. It is important to emphasize that this short simplified economic study only considers material cost and that the cost of labor and mobilization of different driving equipment (e.g., impact vs. vibratory), or consideration of a specialty contractor, could change the preliminary findings produced through this simplified analysis. Furthermore, analyses performed with extended sheet pile designs assume that all sheet piles in the abutment are driven to the same embedment depth, while potentially optimal designs could be developed where only select sheet piles in the wall are driven to a deeper depth to develop the necessary axial load capacity. Thus, a more detailed study of the potential impact on the cost of alternative abutment designs is warranted before developing conclusions on the suitability of any of the alternative designs proposed.

6 Proposed preliminary design recommendations

The reported case histories described in the literature review chapter and the two experimental programs performed for this project confirm the feasibility of using steel sheet piles as axial load bearing elements in bridge abutments of short and medium spans. The axial load test results show that sheet pile walls (PZ-27) have similar axial load capacity and axial stiffness as steel H piles typically used by NCDOT for bridge abutments.

Based on the test results, and the literature review, it is recommended to use conventional static methods for estimating the axial capacity contributions from shaft and toe resistances. This study evaluated six static methods with similar levels of accuracy. For example, the beta (effective stress approach) or the alpha methods (total stress approach) have been reported in the literature as suitable methods for estimating axial capacity of sheet pile walls. Several suitable static methods can be found in the FHWA driven pile manual by Hannigan et al. (2016). This reference also provides guidance regarding suitable minimum values for global factors of safety for ASD design, or resistance factors for LRFD design.

The experimental components of this study confirmed that the plugging phenomenon plays an important role in the final axial capacity mobilized by the sheet pile wall. However, since the occurrence of plugging at a specific project is dependent on a number of conditions (i.e., geometry, geotechnical, and other project specific details) and cannot be predicted in a reliable way, it is recommended that for design purposes that the shaft and toe capacities be taken as the lesser value obtained from considering the two extreme conditions of unplugged condition and fully plugged, as follows:

$$Q_s = Minimum\ (Q_{s\ unplugged}, Q_{s\ plugged}) \quad (6.1)$$

$$Q_t = Minimum\ (Q_{t\ unplugged}, Q_{t\ plugged}) \quad (6.2)$$

The shaft capacity (Q_s) and toe (Q_t) values for the unplugged and plugged conditions can be computed using the static method of choice and should consider the differences in shaft and toe areas for both conditions (Shown in Figure 3-20 for the laboratory load test program).

Regarding plugging, Yandzio (1998) indicated that for toe capacity the unplugged condition should be used when estimating this capacity component. No comments were made in this reference regarding plugging of the shaft.

Finally, we also recommend incorporating the recommendations reported by Yandzio (1998) for sheet piles located at the face of the abutment. In this reference, it is recommended that any contribution to shaft capacity along the face of the sheet pile that is located in the active side and above the point of stability (or point of zero bending moment) be neglected. Further details on this were presented in Chapter 5.

7 Summary and Conclusions

The work described in this report was undertaken to investigate the feasibility of incorporating sheet pile walls as primary axial load bearing elements of bridge abutments. Currently sheet pile walls are used to protect the bridge abutment and foundations against erosion and scour. Incorporation of the sheet pile walls for the double function of scour protection and axial load bearing has the potential to significantly reduce construction cost and time. The literature review performed for this study indicates there is ample positive case histories in Europe supporting this alternative design approach.

The need for this research project was motivated to a great extent due to the scarcity of full-scale axial load tests on instrumented sheet piles that has hindered implementation of this design alternative in the U.S. Therefore, one of the main goals of this study was to help fill this gap of knowledge gap through a comprehensive experimental program to investigate the axial load behavior of sheet piles through full-scale axial load tests on well-instrumented sheet piles. The project encompassed two test programs involving full-scale instrumented test piles. The first test program involved axial load tests under controlled conditions (e.g., controlled soil backfill, detailed geotechnical characterization, etc.) performed at a geotechnical test pit at UNC Charlotte. The second test program involved axial load tests at a field test site that allowed comparison of the axial stiffness and load capacity of a sheet pile wall and an H-pile. The second test program involved geotechnical conditions that are similar to those encountered in NCDOT bridge abutments in the Piedmont region. Based on the research findings, the axial load capacity and axial stiffness of the sheet pile walls were found to be considerable and comparable to the values measured for H-piles installed under similar conditions and dimensions. Therefore, there is strong potential for incorporating the axial load bearing capacity of sheet piles for abutment bridge design that could result in substantial savings in terms of time and money.

Additionally, the project assessed the suitability of analysis and design procedures commonly used in practice for conventional deep foundations to the case of axially loaded sheet pile walls. It was found that deep foundation methodologies for analysis and design of conventional driven piles were found to be applicable to assess axial load capacity of sheet piles. The methods evaluated included static methods based on geotechnical in-situ tests such as SPT and CPT, and methods based on dynamic measurements obtained during pile installation such as PDA and CAPWAP. The level of accuracy of the different methods evaluated showed the level of uncertainty for the sheet pile capacity estimates was comparable to the levels obtained for the comparable H-pile used in the field test program. The applicability of load-transfer methods to predict load-settlement curves, and axial load transfer mechanisms, for sheet piles was also assessed using the results of the different axial load tests. Load-settlement curves predicted using load transfer analyses showed good agreement with the measured behavior during load tests.

An important design consideration for axial capacity determination of sheet pile walls is the formation or not of a plugged condition which can significantly increase the axial load capacity of a sheet pile wall. For preliminary design purposes it is recommended that the axial capacity of a sheet pile be estimated as the lowest value for the shaft and toe resistances computed using a plugged and unplugged condition. This conservative approach is consistent

with the design approach used for H piles and open pipe piles where the plugging phenomenon has also been reported as being a complex problem difficult to predict a priori.

The project also evaluated potential cost savings through a short parametric analysis that studied the axial load capacities of different abutment design configurations and the associated material costs for each design configuration. The parametric analyses show that significant cost and time savings are possible if alternative abutment configurations are used where even all H-piles can be eliminated and replaced with one or more sheet piles walls.

Suggestions for future work:

In order to incorporate sheet piles as primary load bearing elements as an alternative bridge abutment design approach there are important technical aspects that need to be addressed. The following recommendations for research needs are proposed:

- A study to define suitable structural design details for the connection of sheet pile walls to the bridge abutment.
- Develop a design approach similar to the one proposed by Yandzio (1998) for the UK, to deal with possible gap formation on the active side of the sheet pile wall and the bridge abutment fill. This study could also look into gap formation associated to cycles of expansion and contraction of the bridge superstructure that can be significant in integral bridge abutments.
- This study focused on axial loading. However, it is important to expand the scope to include a more general loading condition expected in bridge abutments. For example, the performance of sheer pile supported abutments to combined axial, latera, and bending moment as well as monotonic and dynamic loading conditions.
- The sheet pile design shall include design considerations related to bridge design requirements related to minimum longitudinal and flexural rigidity expected from the abutment foundation system.

CITED REFERENCES

Abbondanza, D. "Steel Innovation: Changing the Economics of Below Grade Foundations." Proc., International Foundation Congress and Equipment Expo, ASCE, 57-64.

API (1993). Recommended Practice for Planning, Designing and Constructing Fixed Offshore Platforms-Load and Resistance Factor Design, American Petroleum Institute, Washington.

Baguelin, F., Frank, R., and Jezequel, J.-F. (1975). "Quelques résultats théoriques sur l'essai d'expansion dans les sols et sur le frottement latéral des pieux." Bull. Liaison Labo. P. et Ch.(78), 131-136.

Bustamante, M. G., and Gianeselli, L. (1991). "Predicting the bearing capacity of sheet piles under veritical load." Proceedings of the 4th International Conference on Piling and Deep Foundations, Deep Foundations Institute, Italy, pp. 8.

Bustamante, M.G., and Gianeselli, L. (1982). Pile Bearing Capacity Prediction by Means of Static Penetrometer CPT. Proceedings of the 2nd European Symposium on Penetration Testing, ESOPTII, Amsterdam, 2, pp. 493-500.

Carle, R., and Whitaker, S. (1989). Sheet Piling Bridge Abutments. Deep Foundations Institute Annual Meeting, Maryland, pp. 1-16.

Coyle, H. M. and Reese, L. C. (1966). “Load Transfer for Axially Loaded Piles in Clay.” Journal of Soil Mechanics and Foundations Division, ASCE, Vol. 92, No. SM2.

Engineering, L. (2011). "Plans for Lone Star Canal at Double Bayou Aqueduct Replacement Project." Project P00644 Aqueduct Replacement, Beaumont, Texas, 18 p.

Evans, R. (2010), “Modified sheet pile abutments for low volume road bridges’, MS thesis, Iowa State University.

Evans, R., White, D., and Klaiber, W. (2012). "Modified Steel Pile Abutments for Low-Volume Road Bridges." IHRB Project TR-568, Iowa Department of Transportation, Ames, Iowa, 294 p.

Everett, J. (1991). "Load transfer functions and pile performance modelling." Geotechnics in the African environment, Blight et al., Balkema, Rotterdam, 229-234.

FHWA (Federal Highway Administration). (2012). *Evaluating Scour at Bridges,* FHWA Publication No. FHWA-HIF-12-003, HEC No. 18, April, 2012, 340 p.

Frank, R. (1975). "Etude Theorique Du Comportement Des Pieux Sous Charge Verticale; Introduction De La Dilatance." Ph.D., University Paris VI (Pierre et Marie Curie University).

Goble, G.G., Likins, G.E., and Rausche, F. (1975). *Bearing Capacity of Piles from Dynamic Measurements.* Final report, Department of Civil Engineering, Case Western Reserve University, .Cleveland, Ohio.

Goldsmith, Richard, Milton, D.J., and Horton, J.W., Jr. (1998). “Geologic map of the Charlotte 1 degree x 2 degrees quadrangle, North Carolina and South Carolina”, U.S.G.S. Miscellaneous Investigations Series report and map I-1251-E.

Guo, W. D. (1996). "Analytical and Numerical Solutions for Pile Foundations." Ph.D., The University of Western Australia.

Hannigan, P.J., Rausche, F., Likins, G.E., Robinson, B.R., and Becker, M.L. (2016). “Geotechnical Engineering Circular No. 12 – Design and Construction of Driven Pile Foundations”, FHWA NHI-16-009, Volumes 1 and 2, 517 p.

Hirayama, H. (1990). "Load-settlement analysis for bored piles using hyperbolic transfer functions." Soils and Foundations, 30(1), 55-64.

Jeong, S., Ko, J., Won, J., and Lee, K. (2015). "Bearing capacity analysis of open-ended piles considering the degree of soil plugging." Soils and Foundations, 55(5), 1001-1014.

Kodikara, J., and Johnston, I. (1994). "Analysis of compressible axially loaded piles in rock." International journal for numerical and analytical methods in geomechanics, 18(6), 427-437.

Lunne, T., Robertson, P. K., and Powell, J. J. M. (1997). Cone Penetration Testing in Geotechnical Practice, Chapman & Hall, 2-6 Boundary Row, London SE1 8HN, UK.

McShane, G. (1991). "Steel sheet piling used in the combined role of bearing piles and earth retaining members." Proceedings of the 4th International Conference on Piling and Deep Foungations, Deep Foundations Institute Stresa, Italy, April 7-12, pp. 49-55.

Meyerhof, G.G. (1976). Bearing Capacity and Settlement of Pile Foundations, American Society of Civil Engineers (ASCE), Journal of Geotechnical Engineering, Vol. 102, No. 3, pp. 195-228.

Mullins, G., Lewis, C. L., and Justason, M.D. (2002), “Advancements in statnamic data regression techniques”, ASCE GSP No. 116, Vol. 2, pp. 915-930.

O'Neill, M. W., and Raines, R. D. (1991). "Load transfer for pipe piles in highly pressured dense sand." Journal of Geotechnical Engineering, 117(8), 1208-1226.

Poulos, H. G. (1989). "Pile behaviour—theory and application." Geotechnique, 39(3), 365-415.

Randolph, M. F., and Wroth, C. P. (1978). "Analysis of deformation of vertically loaded piles." Journal of Geotechnical and Geoenvironmental Engineering, 104(ASCE 14262).

Rausche, F. and Beim, J.W. (2012) “Analyzing and Interpreting Dynamic Measurements taken During Vibratory Pile Driving,” *In Proceedings from Testing and Design Methods for Deep Foundations*, IS-Kanazawa: Kanazawa, Japan, September, pp. 123-131

Rice et al., 2014 Report for Task # 1 of NCDOT Project No. RP 2014-08

Rice, C. D., Pando, M. A., Whelan, M. J., and Ogunro, V. O. (2014). "Vertical Load Capacity of Steel Sheet Piles for Bridge Abutments- Preliminary Assessment for Sand Conditions." 9th International Conference on Short and Medium Span Bridges, Calgary, Alberta, Canada, pp 1-10.

Rybak, J., and Zyrek, T. (2013). "Experimental Validation of Sheet Pile and Combined Pile Axial Capacity Computation." Vplyv Vody na Geotechnicke KonstruckcieBratislava, 8 p.

SACILOR (n.d., no date given). "Steel Sheet Piling in Inland Structures." Hayange, France, 53 p.

SACILOR (n.d., no date given). "Steel Sheet Piling in Inland Structures." Hayange, France, 53 p.

Skyline Steel LLC (2009). "Roads and bridge abutments in sheet piles." Skyline Steel LLC, 8 p.

Sylvain, M. S., Pando, M. A., Whelan, M. J., Ogunro, V. O., and Park, Y. (2016). “Design and application of a low-cost, 3D printed crosshole seismic system- Preliminary assessment.” Geotechnical and Geophysical Site Characterisation 5, Gold Coast, Queensland, Australia, 941-946.

Sylvain, M. S., Pando, M. A., Whelan, M. J., Ogunro, V. O., Park, Y., and Koch, T. (2015). "Large Scale Laboratory Testing to Evaluate Axial Load Capacity of Sheet Piles for Bridge Abutments." From Fundamentals to Applications in Geotechnics: Proceedings of the 15th Pan-American Conference on Soil Mechanics and Geotechnical Engineering, Buenos Aires, Argentina, 290-297.

Sylvain, M. S., Pando, M. A., Whelan, M. J., Rice, C. D., Ogunro, V. O., Park, Y., and Koch, T. (2017). "Case History of a Full Scale Axial Load Test of Sheet Piles." Geotechnical Frontiers 2017, Orlando, FL, 355-365.

Taenaka, S., Otani, J., Tatsuta, M., and Nishiumi, K. "Vertical bearing capacity of steel sheet piles." Proc., 6th International Conference on Physical Modelling in Geotechnics-Physical Modelling in Geotechnics-6th ICPMG'06.

Underwood, C. A., and Greenlee, R. M. (2010). "Steel Sheet Pile Used as Permanent Foundation and Retention Systems-Design and Construction." Proc., Earth Retention Conference 3, ASCE, 129-136.

Vijayvergiya, V. (1977). "Load-movement characteristics of piles." Proc., Ports'77. 4 th annual symposium of the American Society of Civil Engineers, Waterway, Port, Coastal and Ocean Division, Long Beach, California, v. 2, 269-284.

Yandzio, E. (1998), “Design Guide for Steel Sheet Pile Bridge Abutments”, The Steel Construction Institute, SCI Publication No. 187, ISBN 1859420648, 127 p.

Appendices

Appendix A – Additional Information Load tests at the UNC Charlotte Geotechnical Test Pit.

Appendix B – Additional Information Field Load Tests at Facility of ICE in Matthews, NC.

Appendix C – Additional Information for parametric study for typical NCDOT short span bridge.

Table of Appendix Contents

List of Appendix Figures

List of Appendix Table

A. Appendix A

Additional Information Load tests at the UNC Charlotte Geotechnical Test Pit.

A.1 Additional information backfill soil

Figure A-1: Photos of backfilling of UNCC geotechnical test pit.

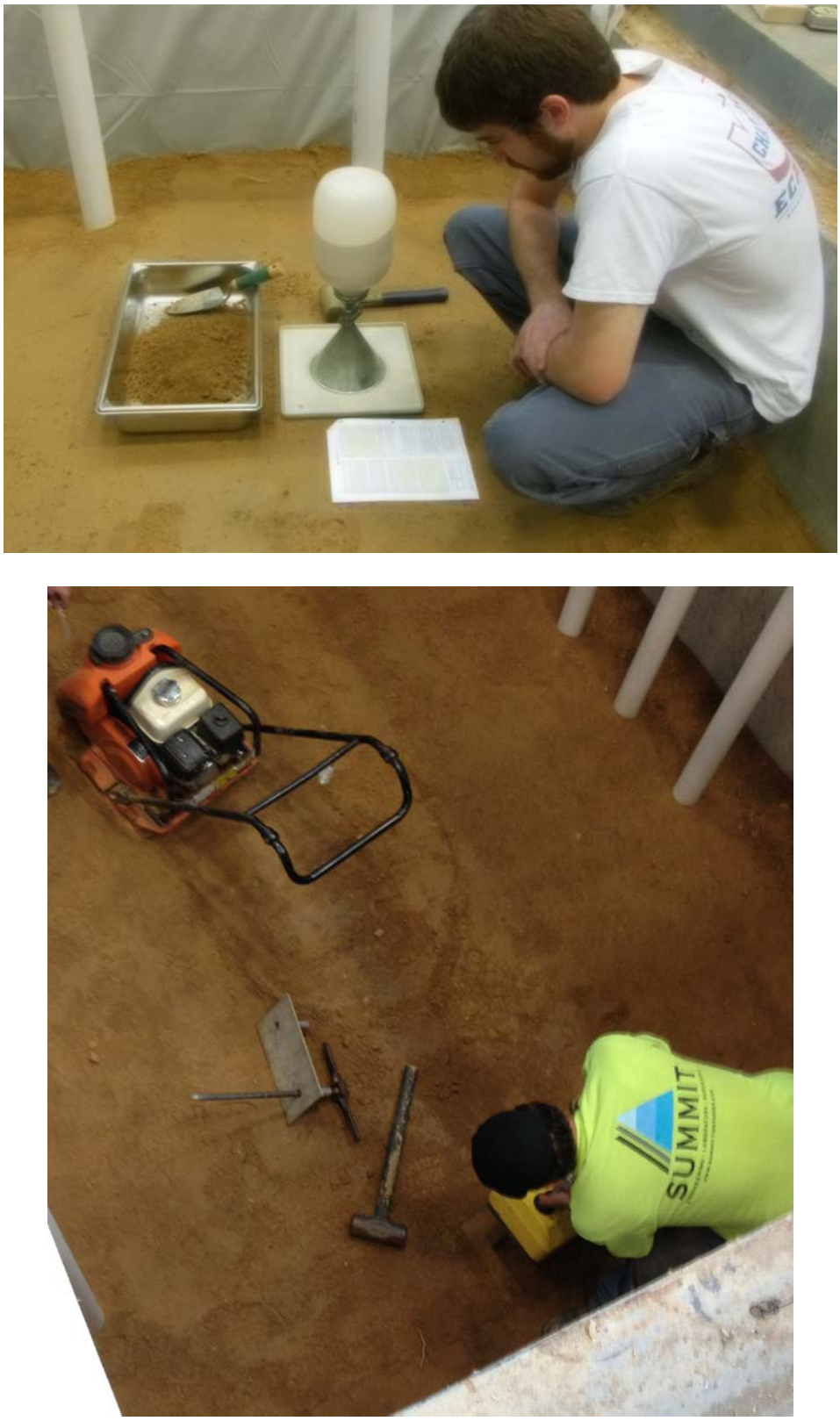

Figure A-2: Photos of compaction density and moisture control of UNCC geotechnical test pit.

A.2 Compaction tests and compaction control of backfilling of geotechnical test pit

Figure A-3 shows results of two compaction tests carried out for the SW-SC backfill soil using the Standard Proctor compaction energy. .

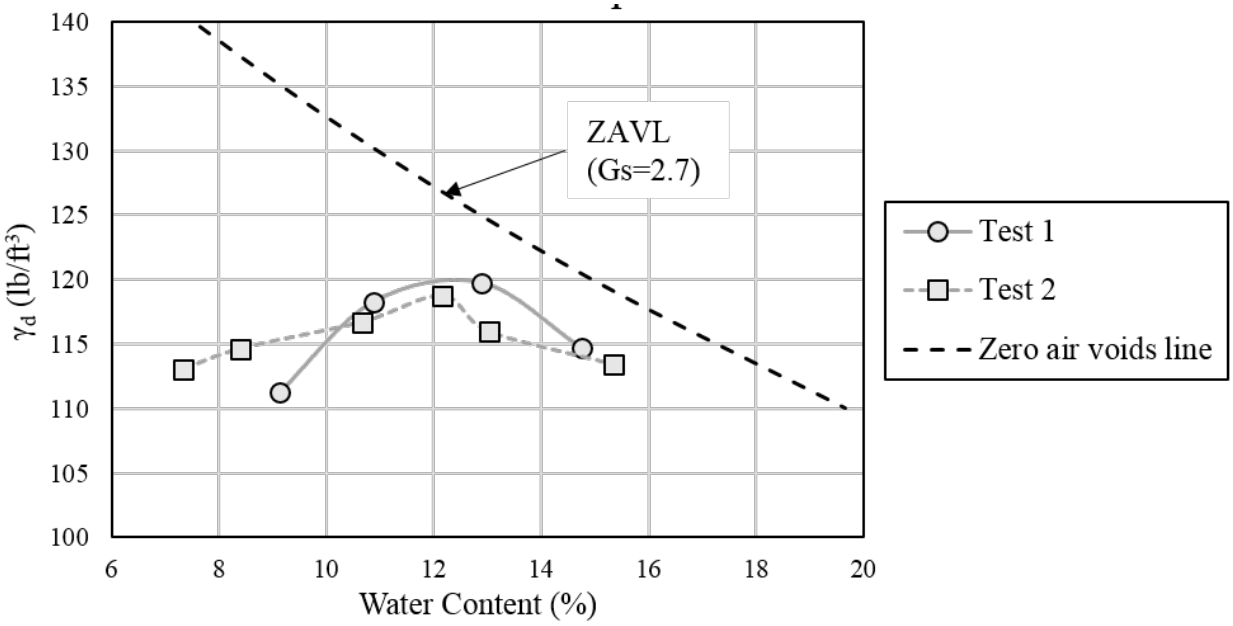

Figure A-3: Standard Proctor Compaction test results for SW-SC backfill.

During backfilling of the geotechnical test pit compaction control was performed using: Nuclear gauge, Sand-cone, and Drive-Cylinder methods. The Nuclear gauge test and Drive-Cylinder test were performed by SUMMIT Engineering. Results from these tests were used to measure the as-constructed relative compaction as well as the placement water content. As mentioned in the body of the report the backfill was placed in layers and compacted using hand tampers and a vibratory plate compactor.

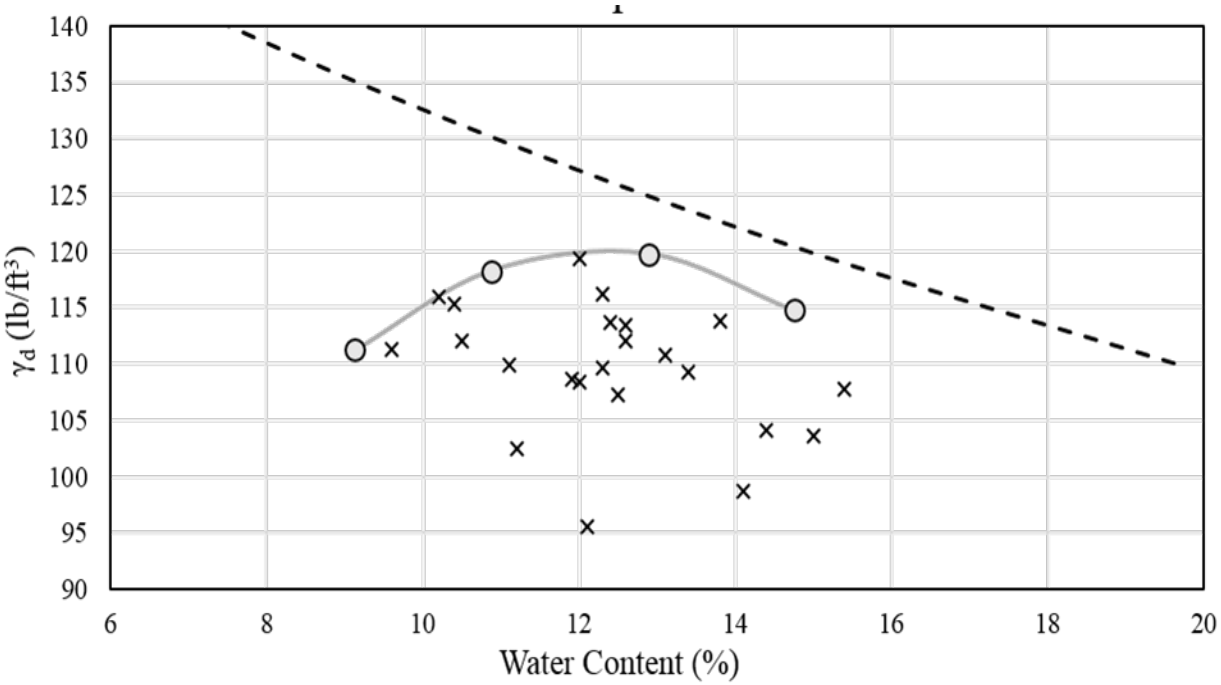

Figure A-4: As compacted dry unit weight and moisture content values measured for the SW-SC backfill during backfilling of the geotechnical test pit.

A.3 In-situ tests at geotechnical test pit

After backfilling and compaction of the geotechnical test pit several in-situ tests were performed to assess to characterize the soil. As mentioned in the main body of the report, these tests included SPT, SCPTu, DMT, and geophysical tests MASW and CHT. The location of tests is shown in Figure A-5.

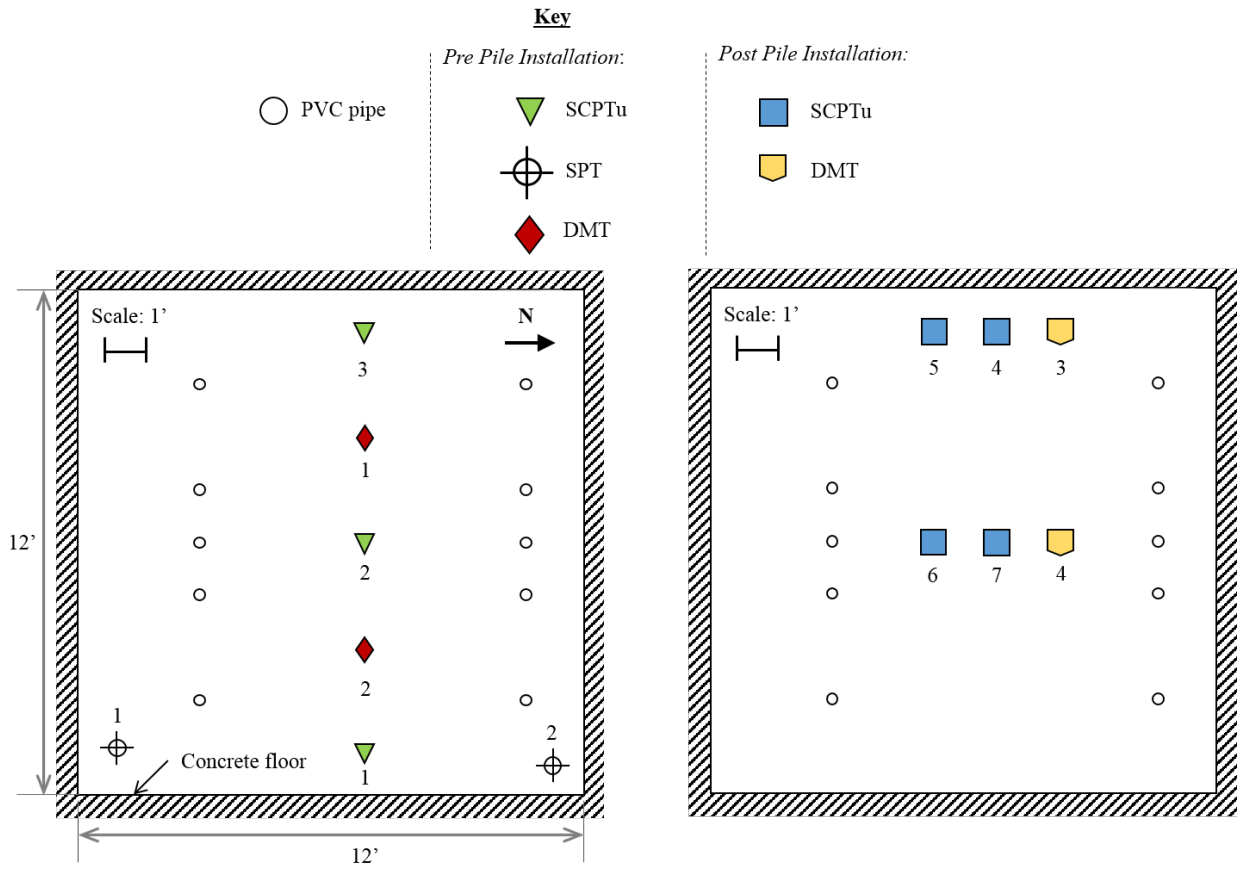

Note: Left figure corresponds to test prior to installation of sheet piles and figure to the right corresponds to locations of tests after sheet pile installation.

Figure A-5: Plan view of geotechnical test pit showing location of in-situ tests that involved a vertical sounding.

Figure A-6: Photos of geotechnical drilling with SPT testing by S&ME (Charlotte office).

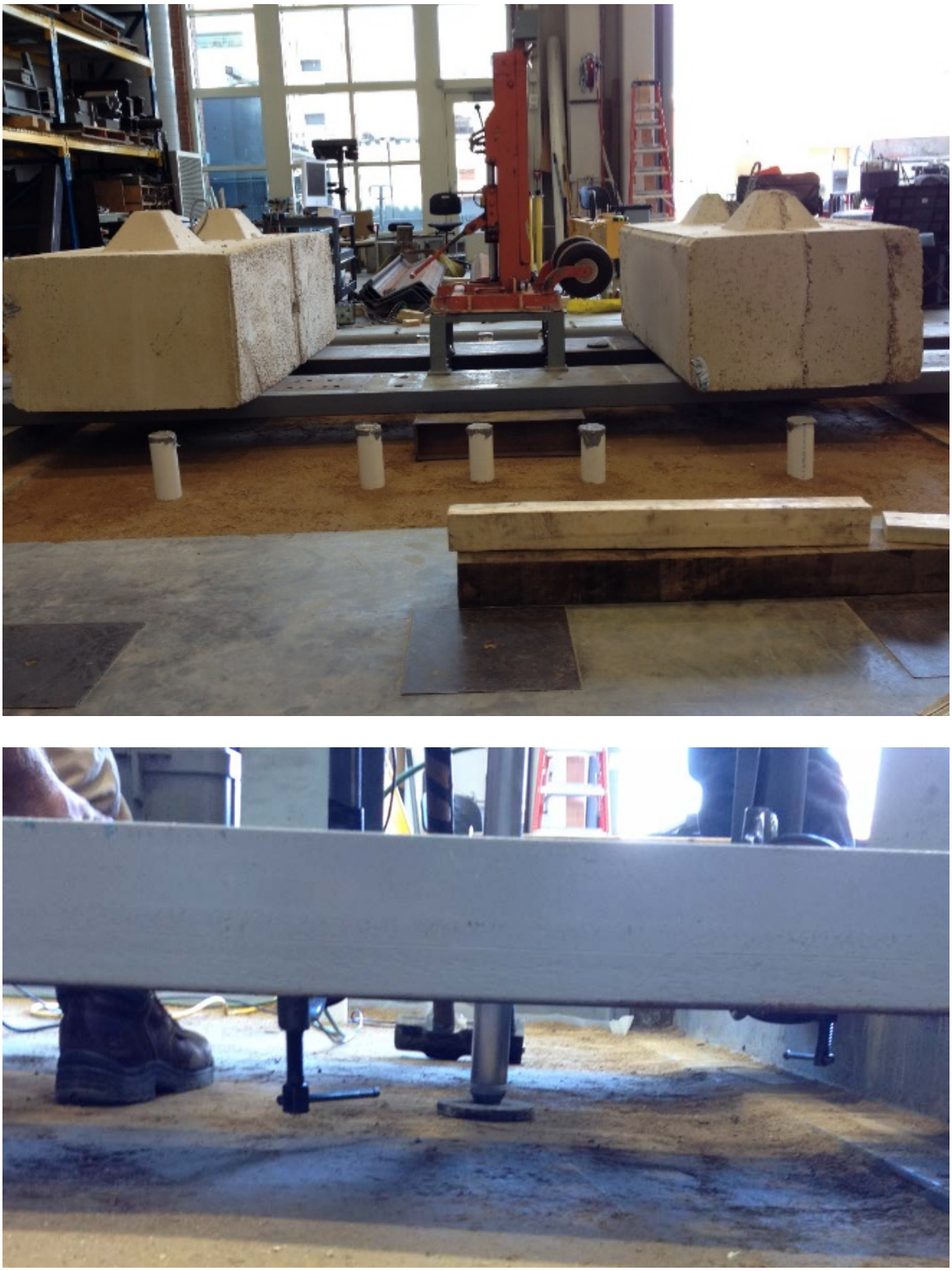

Figure A-7: Photos showing setup used for of borehole drilling with SCPTu testing done by S&ME (Charleston office).

Figure A-8: Photos of DMT testing prior to sheet pile installation.

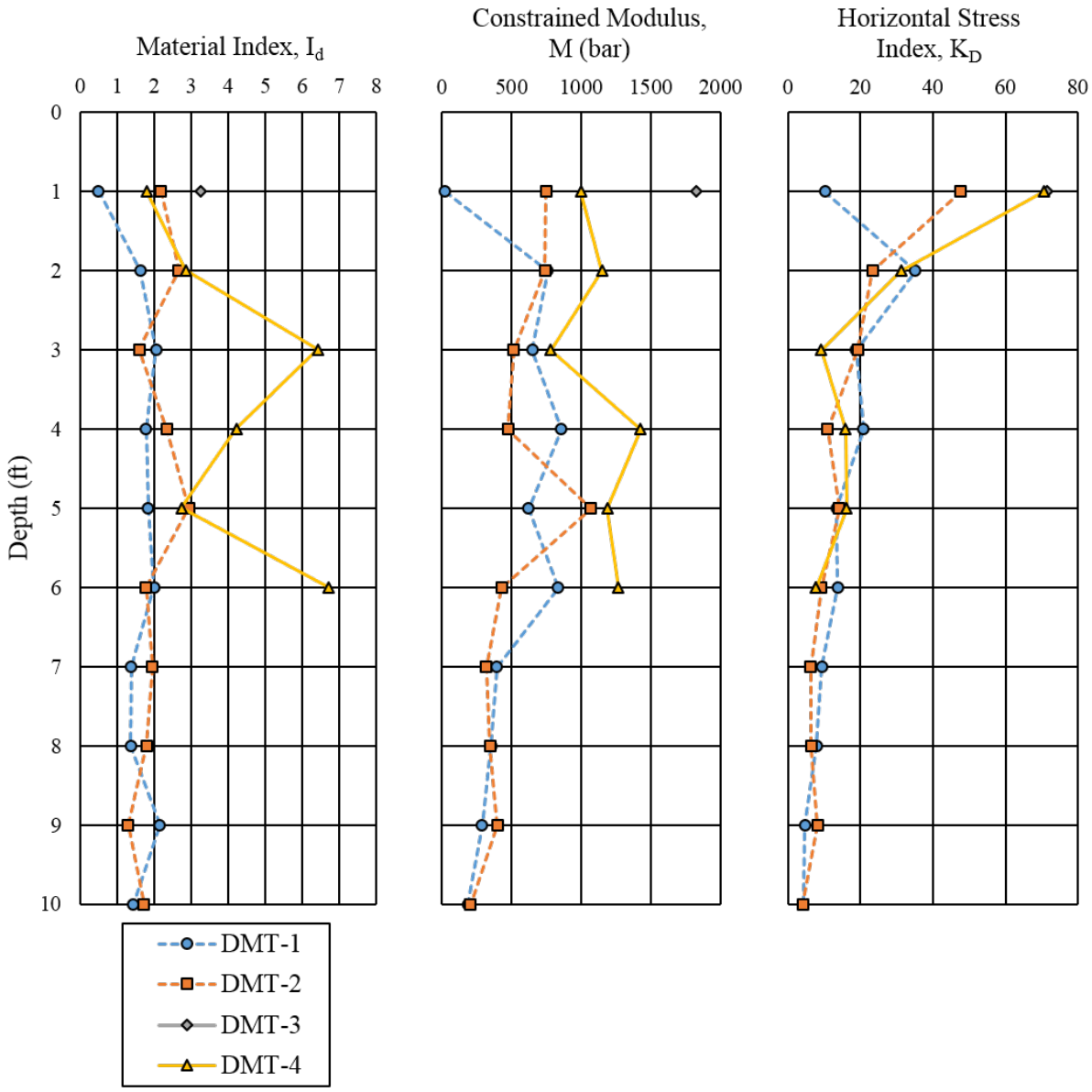

Figure A-9: Summary plot of DMT Material Index results from four DMT soundings.

A.4 Geophysical tests:

MASW testing: MASW testing was performed thanks to the assistance of the Charlotte office of S&ME. Select photos of MASW testing are provided in figure below.

(a) Hammers used for MASW testing

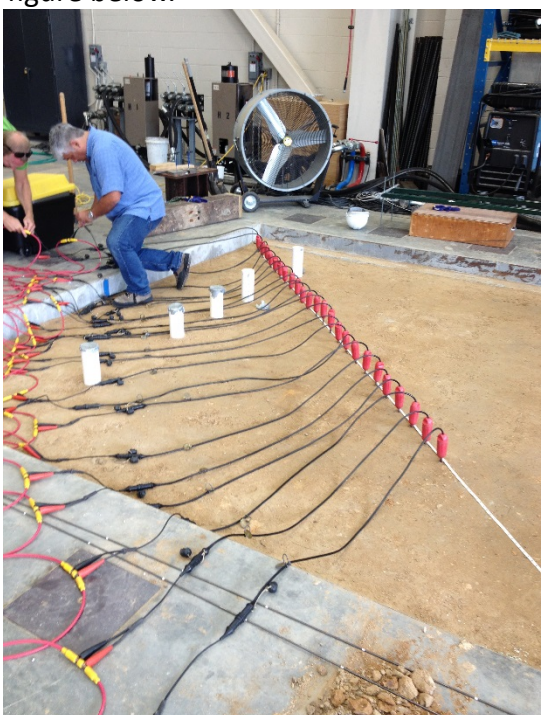

(b) MASW testing

(c) 14 Hz geophone array

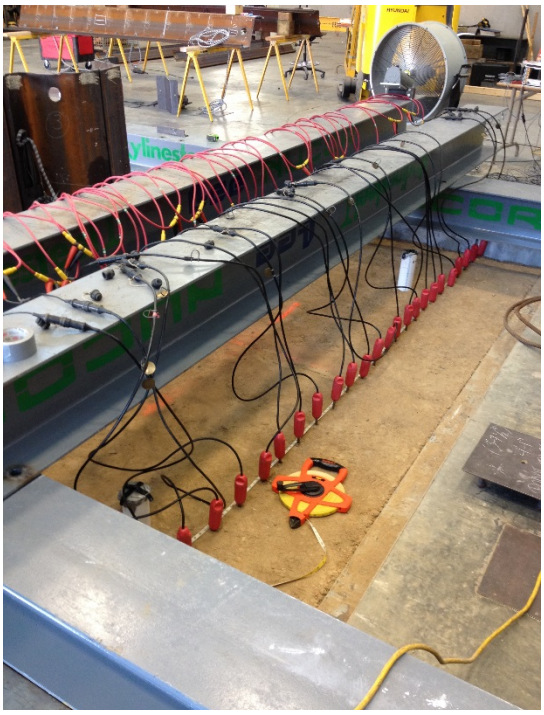

(d) 100 Hz geophone array

Figure A-10: Photos of MASW testing at UNCC Highbay.

Crosshole testing: MASW testing was complemented with crosshole testing performed with a system developed in-house that are shown in Figure A-11 through Figure A-12 (additional details in Sylvain et al. 2016).

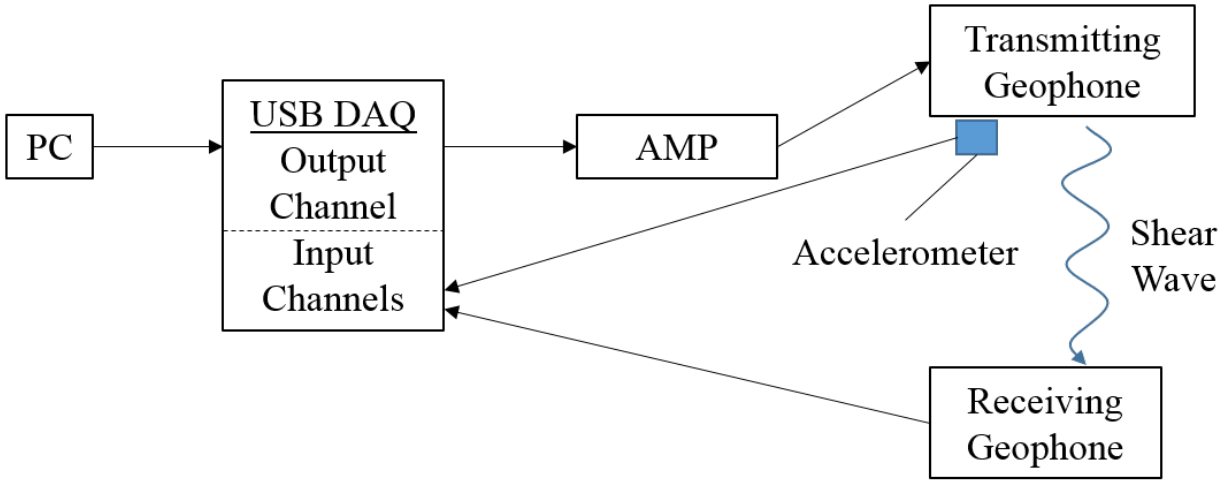

(a) Layout of system components for crosshole testing

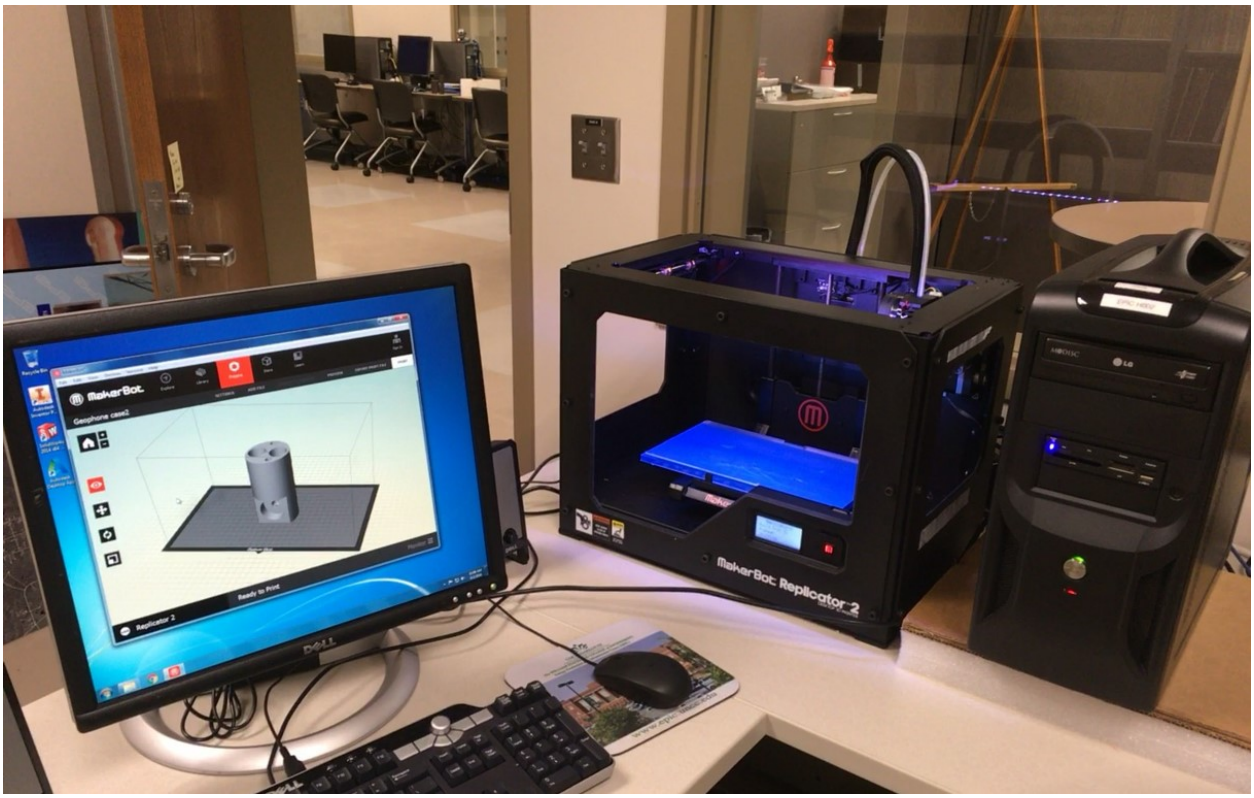

(b) 3D printing for geophone casing for crosshole test

Figure A-11: Developed crosshole test system at UNCC.

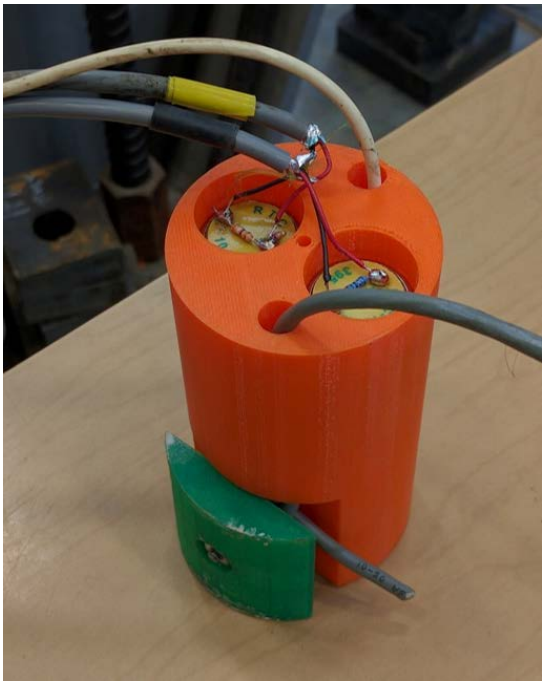

(a) 3D printed crosshole sensor casing (V.2 Improved sensor)

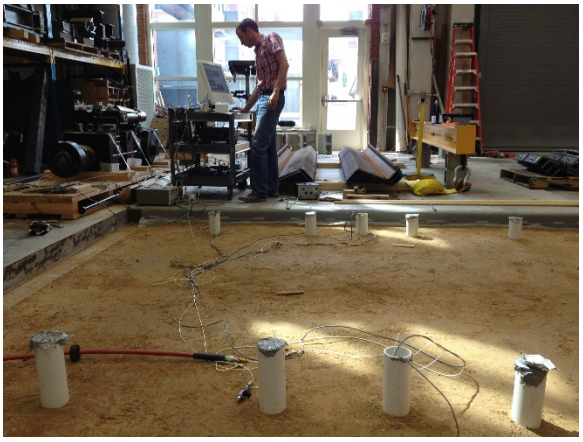

(b) Collecting crosshole data

(c) Observing crosshole data and modifying computer program

Figure A-12: Photos of Equipment and crosshole testing at UNCC Highbay.

<u>Summary of geophysical test results</u>:

A summary of the interpreted shear wave profiles obtained from the different test methods (SCPTu, MASW, and crosshole) is presented in Figure A-13.

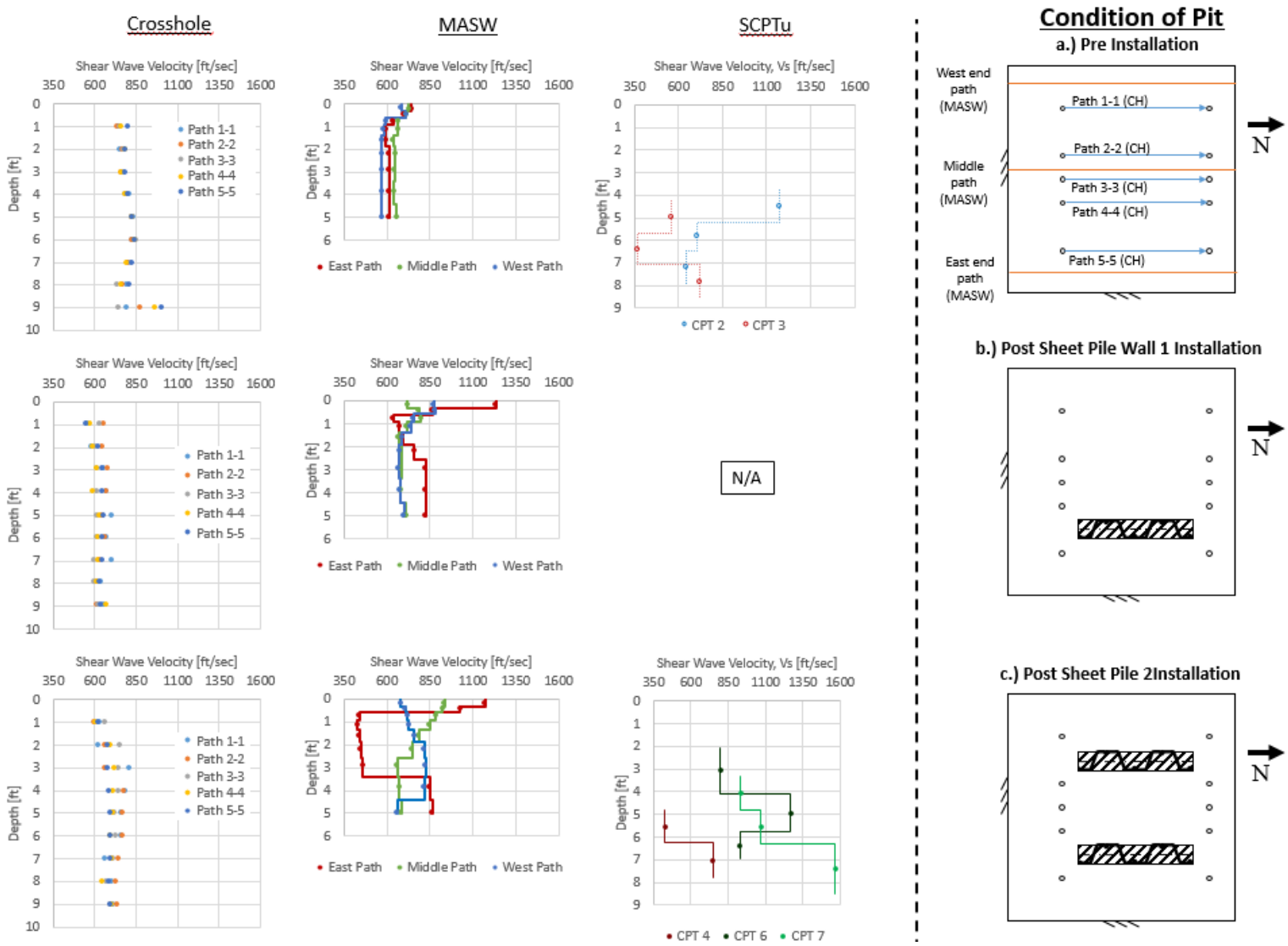

Figure A-13: Comparison of shear wave velocity measurement of compacted backfill at UNCC Highbay.

A.5 Additional laboratory tests

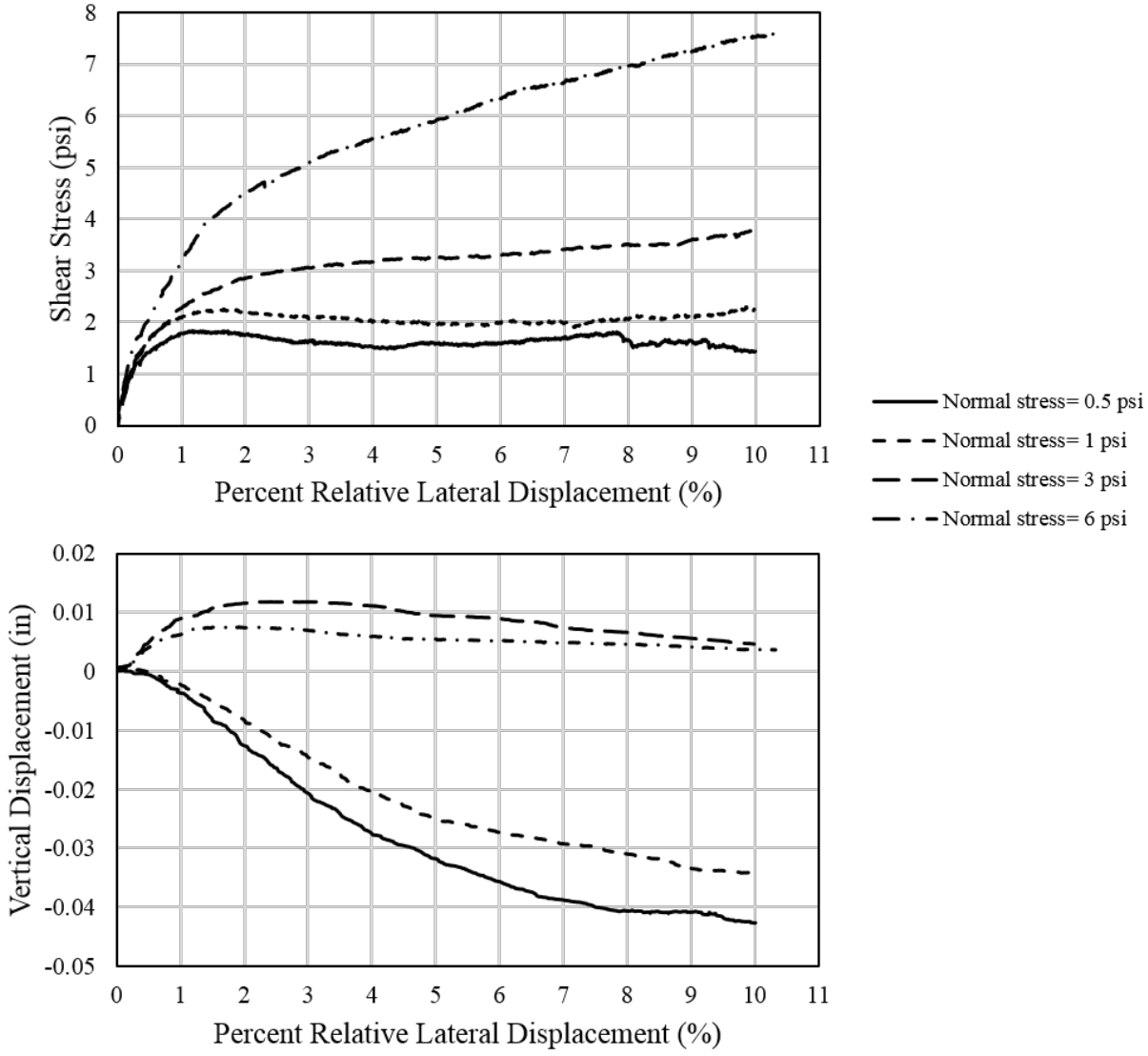

Figure A-14: Direct shear test results for compacted backfill.

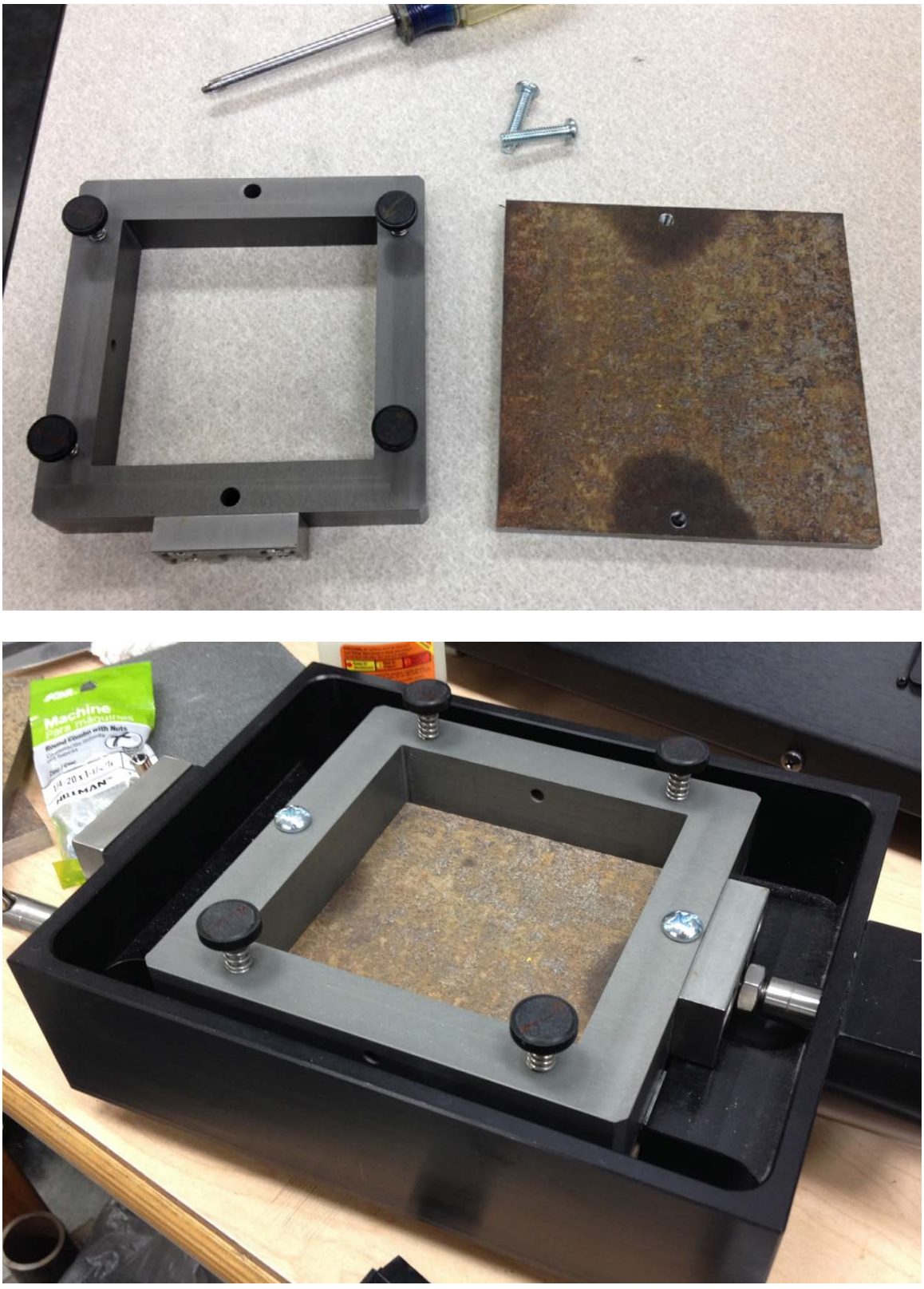

Figure A-15: Interface shear test setup (Steel coupon, top box, assembled box).

A.6 Instrumentation of Tested Piles

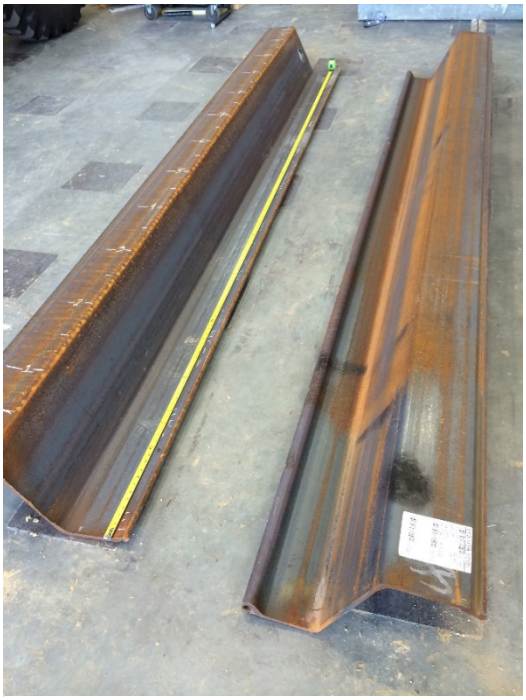

(a) Test sheet piles

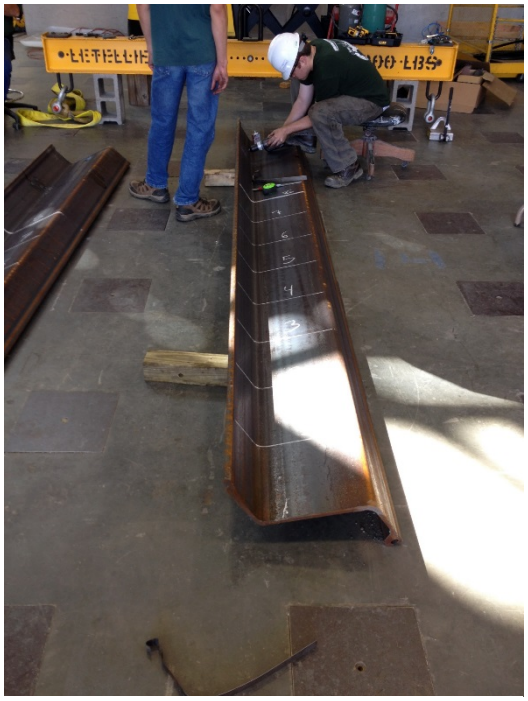

(b) Marking piles for sensors

(c) Welding for sensor protection

(d) Instrumented sheet piles

Figure A-16: Photos of Highbay test piles.

A.7 Pile Installation

Figure A-17: Photo of ICE 6E vibratory hammer used at UNCC High bay.

Figure A-18: Driving with ICE Model 6E vibratory hammer.

B. Appendix B

Additional Information Field Load Tests at Facility of ICE in Matthews, NC

B.1 Photos of site and in-situ testing

Figure B-1: Field site visit during site selection process.

Figure B-2: Field site after site characterization testing.

(a) CME 550X rig used for SPT and CPT testing

(b) Conducting SPT boring

(c) Loose soil encountered during SPT boring

Figure B-3: Images of SPT borings conducted at ICE field site.

(a) CME 550X rig used for pushing SCPTu cone and rods

(b) SCPTu cone with saturated porous element around pore pressure sensors

(c) Placing SCPTu cone prior to sounding

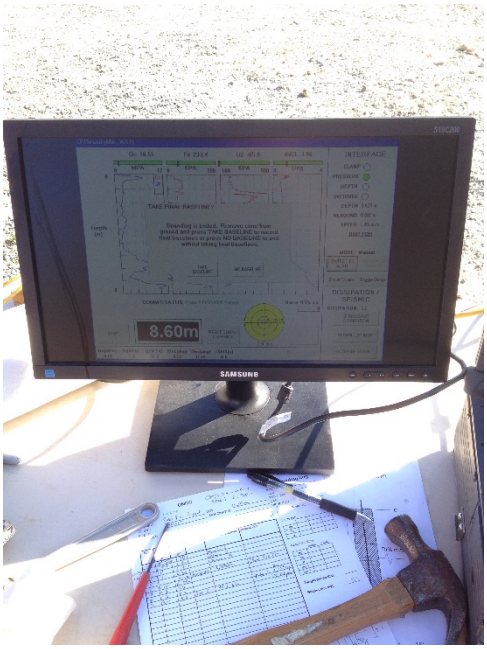

(d) Results from SCPTu test at end of sounding

Figure B-4: Images of SCPTu soundings conducted at ICE field site.

B.2 Photos of MASW testing

S&ME performed MASW testing was performed at the field test site as shown in the photos in Figure B-5.

(a) MASW equipment

(b) MASW seismic source

(c) Array for MASW

(d) Additional array for MASW

Figure B-5: Images of MASW conducted at ICE field site.

B.3 Boring logs

Boring logs for the geotechnical boreholes performed by S&ME at the field test site are shown in Figure B-6 through Figure B-8.

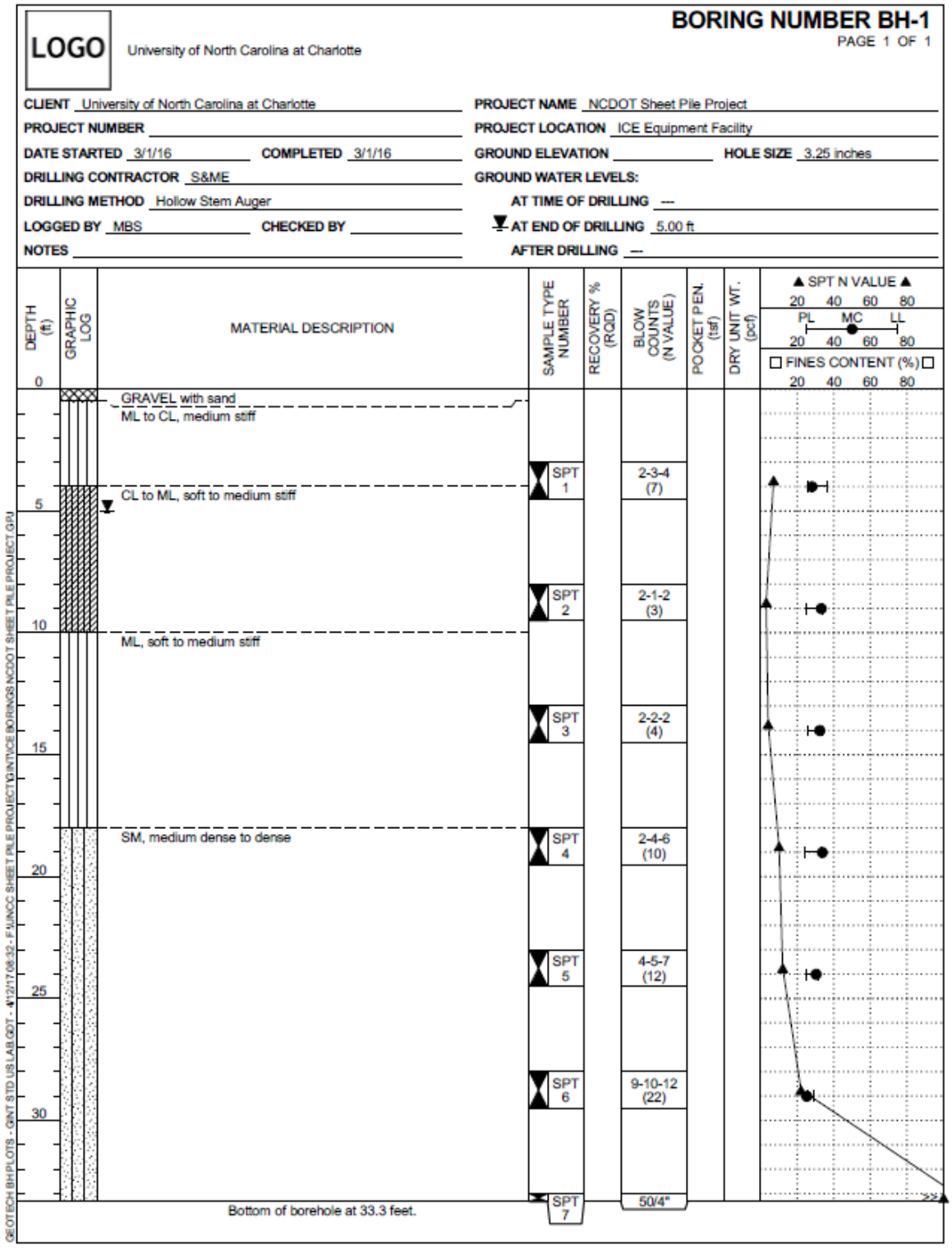

Figure B-6: Boring log for borehole BH-1.

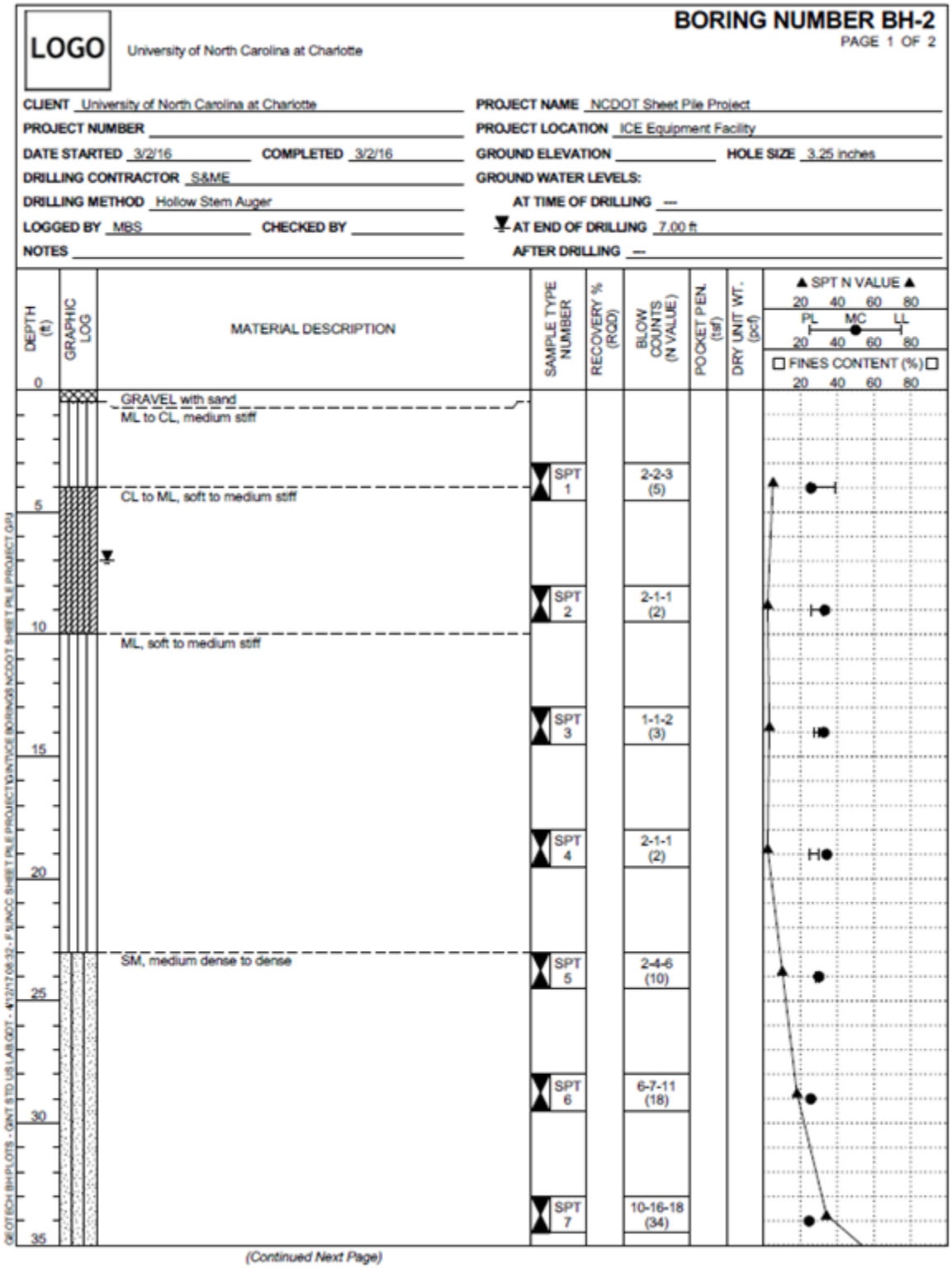

Figure B-7: Page 1 of 2 of Boring log for borehole BH-2

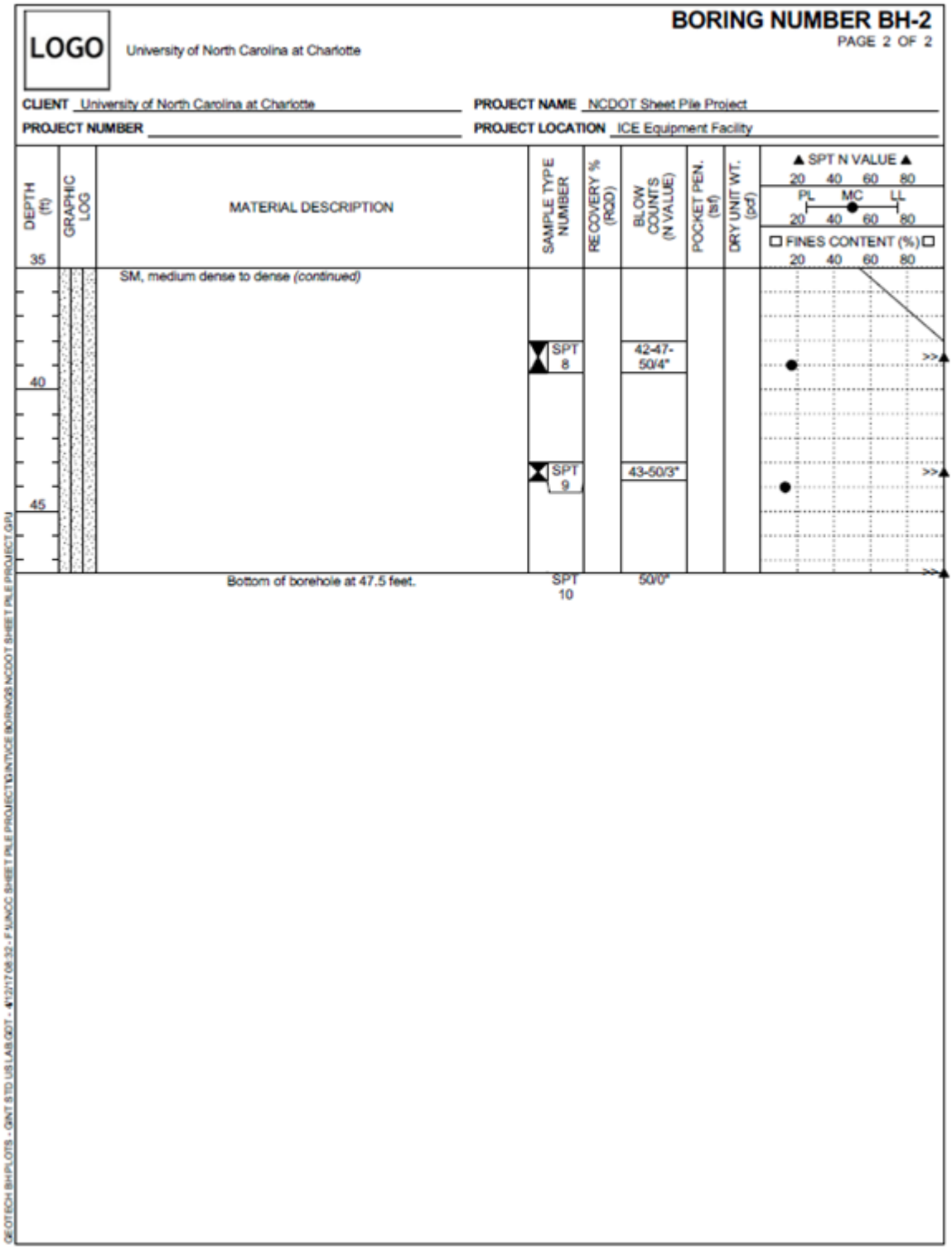

Figure B-8: Page 2 of 2 of Boring log for borehole BH-2

B.4 Test pile instrumentation

As-built layouts of the instrumentation for the sheet pile and H-pile are shown in Figures B-9 and Figure B-10, respectively.

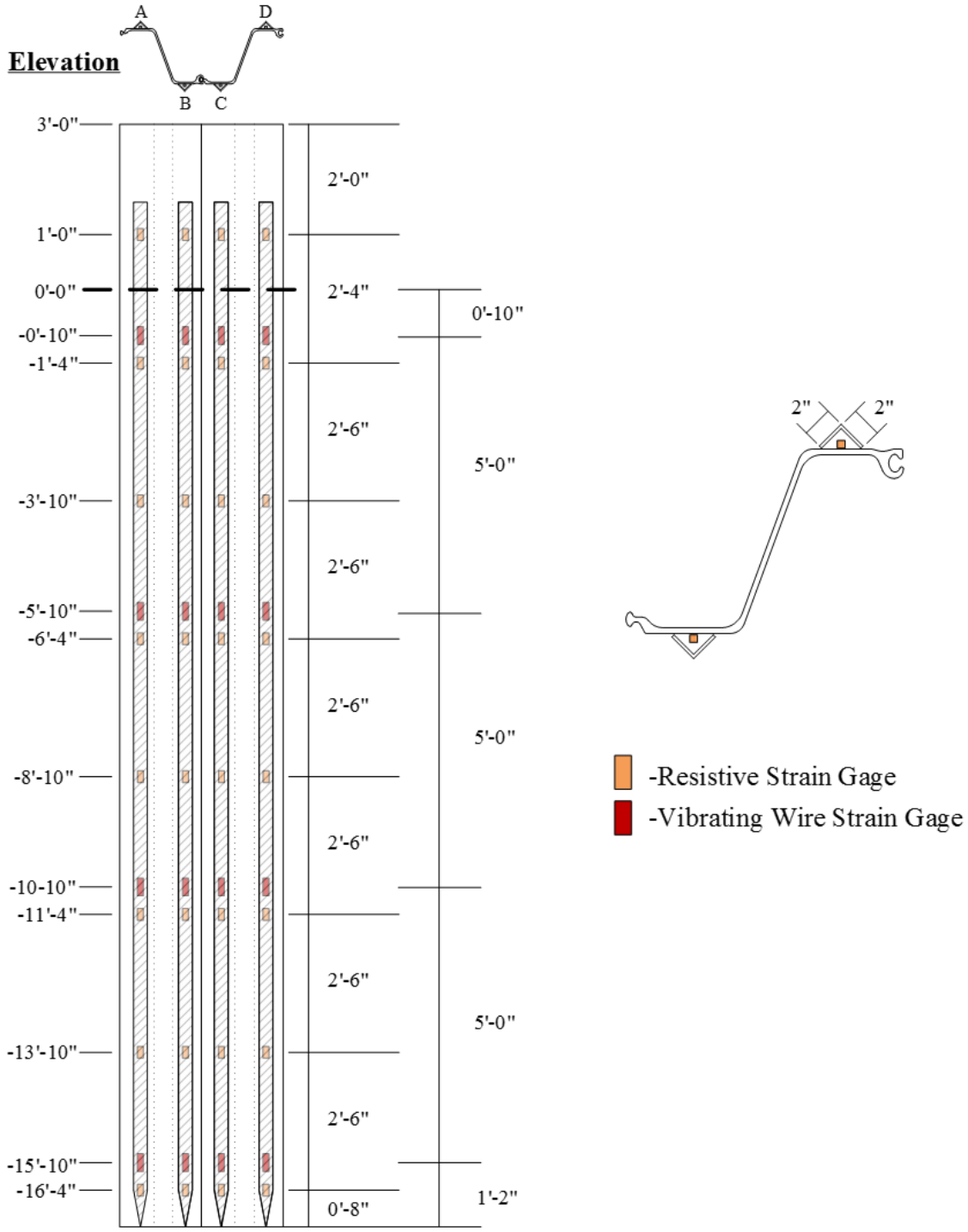

Figure B-9 Layout of instrumentation for sheet pile tested at field site.

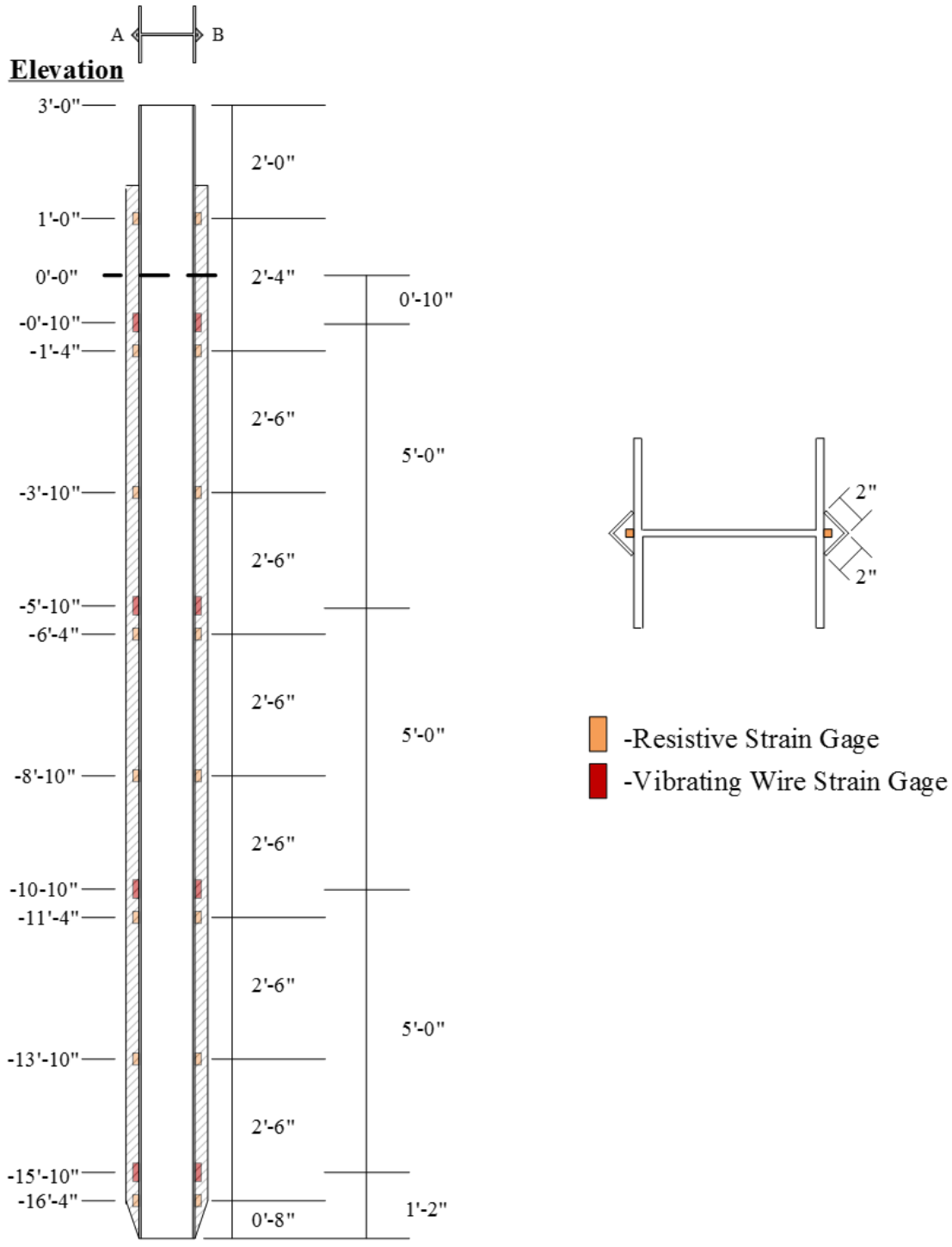

Figure B-10 Layout of instrumentation for H-pile tested at field site.

A photo showing the instrumented H pile, including measures to protect gages and cables, is shown in Figures B-11.

Figure B-11 Photo of instrumented H-pile for field load testing program.

A photo showing the instrumented sheet pile wall, including measures to protect gages and cables, is shown in Figures B-12.

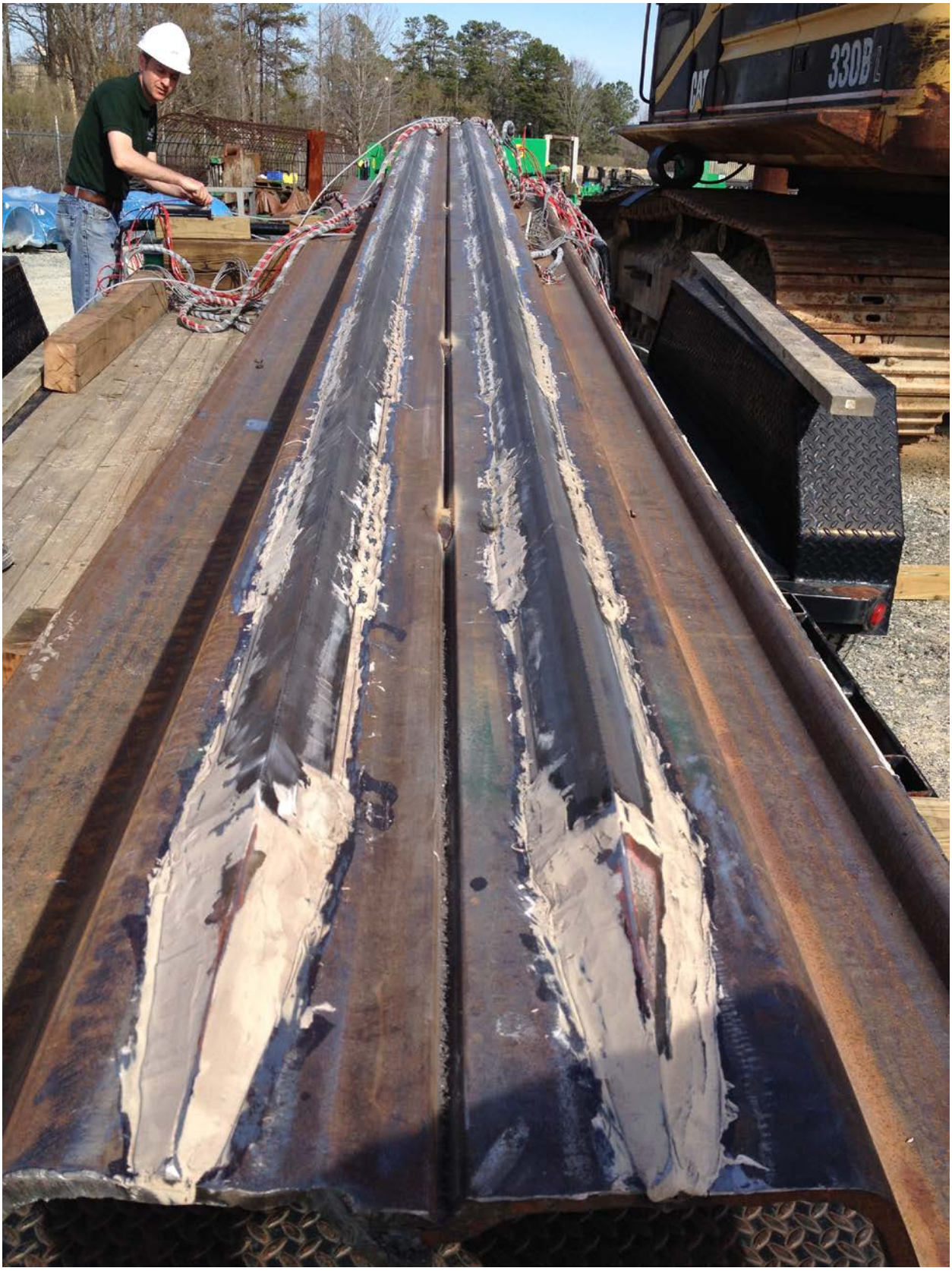

Figure B-12 Photo of instrumented sheet pile wall for field load testing program.

B.5 Test pile installation

Figure B-9: Test piles prior to driving.

(a) ICE 28C vibratory hammer

(b) ICE I-12 impact hammer

Figure B-10: Photos of hammers used to drive piles for ICE field test.

(a) Driving with ICE C28

(b) Placing ICE I-12

(c) Driving with ICE I-12

Figure B-11: Photos of pile driving at ICE field site

Figure B-12: Photo of PDA instrumentation on sheet piles at ICE field site.

Figure B-13: Photo of PDA instrumentation on sheet piles at ICE field site.

B.6 Details of reaction frame system

Additional photos of reaction system are provided in Figure B-14 through Figure B-21.

(a) Piles and beam for reaction frame

(b) Beams for reaction frame

Figure B-14: Photos of reaction frame components and test piles for ICE field test.

Figure B-15: Photo of reaction pile installation guide frame.

.

Figure B-16: Photo of transfer beams bolted to reaction piles.

Figure B-17: Photo of reaction frame with load beam over H-pile.

Figure B-18: Oblique view of installed reaction frame and test piles.

Figure B-19: Side view of installed reaction frame and test piles.

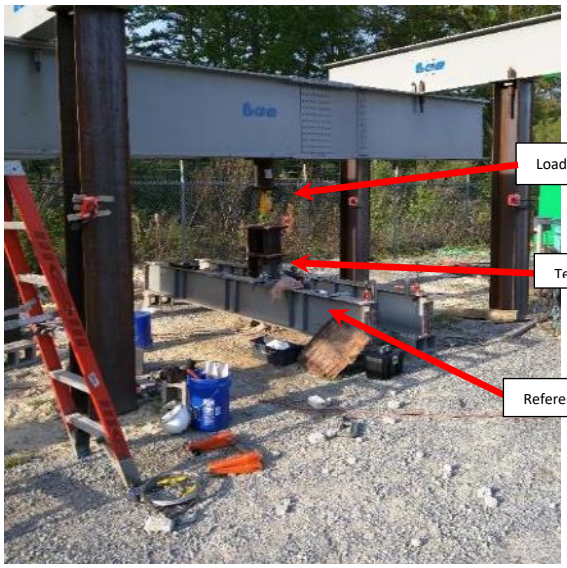

a.) Oblique view of reaction frame over HP 12x53 test pile with reference beams

b.) Side view of reaction frame over HP 12x53 test pile with reference beams

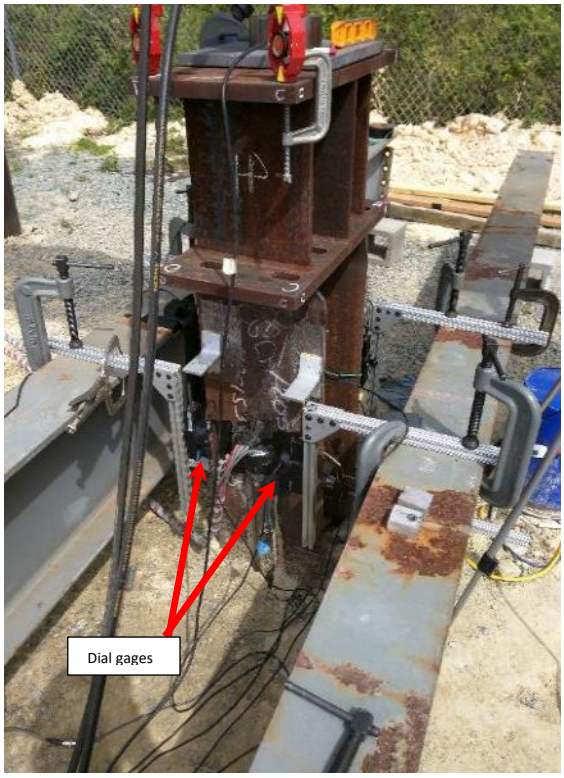

c.) Close up on HP 12x53 test pile showing instrumentation

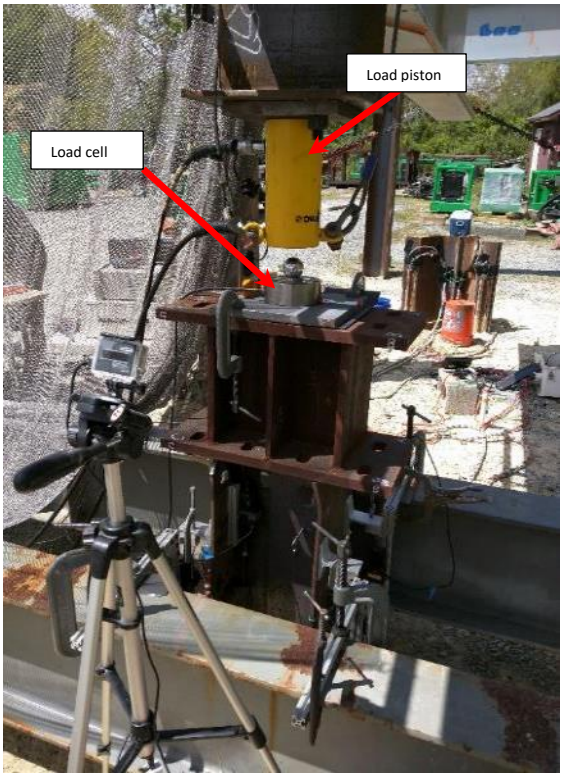

d.) side view of same test pile showing the load piston and load cell.

Figure B-20: Photos of static load test setup for H- pile at ICE field test.

Figure B-21: Photo of static load test setup for sheet pile at ICE field test.

C. Appendix C

Additional Information for parametric study for typical NCDOT short span bridge

C.1 Summary Table used to select the Representative Bridge for Parametric Analyses

Table C-1: Summary of structural details for NC bridges under review.

Bridge ID	No. of Spans	Span, S	Ave. Abutment Width, W	Angle of Skew, θ	Bearing Pile Type	No. of Bearing Piles, N_H	Spacing of Bearing Piles, s_H	Ave. Depth of Bearing Piles, D_H	Sheet Pile Type	No. of Sheet Piles, N_S	Ave. Depth of Sheet Piles, D_S	Spacing b/t Bearing and Sheet Piles, c	Scour Critical Depth	Sheet Pile Shear Anchor Studs	Deadman	ADT	Region
440076	1	64′-0″	43′-2″	0˚	HP 12x53	7	6′-0″	40′-0″	PZ 27	28	27′-0″	22.5″	15′-0″	Yes	No	1785	Mountain
940029	1	96′-0.125″	54′-4″	20˚	HP 12x53	10	5′-8″	20′-0″	PZ 27	34	9′-4″	22.5″	6′′-4″	Yes	Yes	6600	Mountain
210009	2	49′-0″	50′-0.5″	0˚	HP 12x53	7	7′-0″	16′-5″	PZ 27	30	11′-0″	22.5″	N/A	Yes	No	500	Mountain
990031	1	58′-10.125″	45′-1.5″	30˚	HP 12x53	5	9′-6″	11′-11″	PZ 27	29	N/A	22.5″	N/A	Yes	No	665	Mountain
440035	1	61′-9″	37′-4″	15˚	HP 12x53	5	7′-6″	50′-0″	PZ 27	23	16′-6″	22.5″	N/A	Yes	No	408	Mountain
120165	1	58′-0″	36′-0″	15˚	HP 14x73	5	10′-2″	21′-5″	PZ 27	23	14′-3″	25″	8′-6″	No	Yes	4060	Piedmont
590100	1	54′-9″	39′-0″	0˚	HP 14x73	5	9′-0″	40′-0″	PZ 27	26	14′-9″	22.5″	N/A	No	Yes	3605	Piedmont
960718	1	65′-0″	32′-11″	30˚	HP 12x53	5	6′-11″	38′-6″	PZ 27	21	20′-5″	22.5″	6′-5″	No	Yes	143	Piedmont
410024	1	56′-3″	36′-0″	0˚	HP 12x53	6	6′-5″	35′-6″	PZ 27	22	20′-0″	18″	19′-0″	Yes	No	1385	Piedmont
230076	1	66′-9″	39′-0″	0˚	HP 14x73	7	6′-0″	26′-7″	PZ 27	36	14′-7″	24″	N/A	Yes	No	900	Inner Coastal
230078	1	46′-9″	39′-0″	0˚	HP 14x73	5	9′-0″	34′-9″	PZ 27	36	10′-10″	24″	N/A	Yes	No	900	Inner Coastal
390065	1	56′-9″	36′-0″	0˚	HP 12x53	5	7′-6″	18′-10″	PZ 27	22	19′-9.5″	26″	12′-9.5″	Yes	No	877	Inner Coastal
300408	1	66′-9″	36′-0″	0˚	HP 14x73	5	6′-0″	40′-6″	PZ 27	22	16′-6″	20″	18′-6″	Yes	No	365	Inner Coastal
200012	1	59′-8.375″	51′-11″	10˚	HP 14x73	9	6′-1″	57′-6″	PZ 27	34	34′-0″	19″	17′-0″	Yes	No	6280	Outer Coastal
690023	1	62′-9″	39′-0″	0˚	HP 12x53	7	5′-8″	44′-3.5″	PZ 27	24	20′-9″	20″	7′-7″	Yes	No	3150	Outer Coastal
Average and/or Most Common																	
	1	60′-0″	40′-0″	0˚	HP 12x53	6	7′-0″	30′	PZ 27	27	18′-0″	22.5″	12′-0″	Yes	No	2100	Mountain

C.2 Details on Point of Stability Determination

The pile capacity estimates for the parametric study presented in Chapter 5 were based on the effective stress β-method and the suggestions by Yandzio (1998) regarding neglecting shaft resistance from the face of the sheet pile in the active side, specifically for the length of sheet pile above the point of stability. This section provides details regarding the procedure used to compute the location of the point of stability. For the sheet piles, the specified layers were different for the active and passive side of the piles (See Chapter 5). The effective horizontal stresses, using active and passive coefficients, on the piles are as presented in Chapter 5. It is important to note that NCDOT abutment design practice typically involves use of a deadman for lateral support. It is assumed that the deadman provides full lateral support of the sheet pile wall through the abutment cap. Under this assumption, the summation of moments about the abutment cap can be calculated to determine the point at which lateral stability is achieved. Figure C-1 presents the free body diagram, and resultant forces on the sheet pile wall.

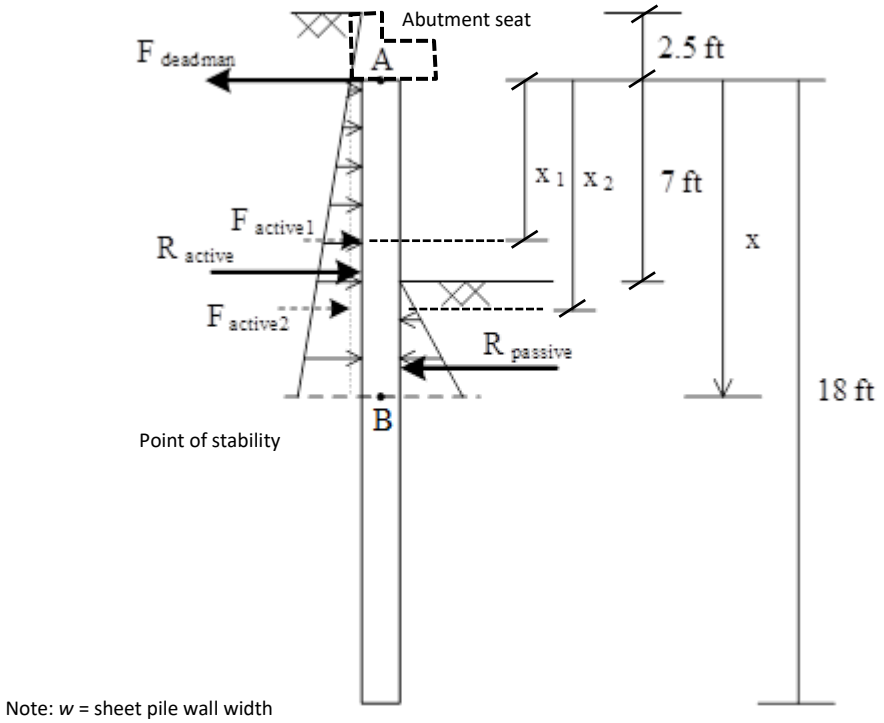

Figure C-1: Force diagram used to define point of stability for parametric study sheet pile wall (Chapter 5).

Figure C-1 shows the resultant forces acting on the active and passive sides of the sheet pile wall. The point of stability (Point B) corresponds to the point of zero bending moment. The bending moment at a depth x below the top of the sheet pile is equal to the sum of all

moments from the resultant forces shown in Figure C-1. The resultant forces and their corresponding depths are as follows:

- Resultant of rectangular distribution of lateral pressure diagram due to surcharge pressure at the top of pile elevation ($F_{active1}$):

$$F_{active_1} = \sigma_{active}(x=0)\cdot w\cdot x \qquad @\, x_1 = \frac{1}{2}x \quad \text{.....Eq. C-1}$$

- Resultant of triangular lateral pressure diagram related to active pressures below pile top that are not related to surcharge pressure ($F_{active2}$):

$$F_{active_2} = \left(\sigma_{active}(x) - \sigma_{active}(x=0)\right)\cdot w\cdot x \qquad @\, x_2 = \frac{2}{3}x \quad \text{.....Eq. C-2}$$

- Therefore the resultant force of $F_{active1}$ and $F_{active2}$ is:

$$R_{active} = F_{active_1} + F_{active_2} \qquad @\, x_{R_{active}} = \frac{F_{active_1}\cdot x_1 + F_{active_2}\cdot x_2}{R_{active}} \quad \text{.....Eq. C-3}$$

In Eq. C-1 through Eq. C-3, w is the width of the sheet pile wall; σ_{active} corresponds to the effective horizontal pressure on the active side at depth, x; and the distances x_1 and x_2 are as defined in Figure C-1.

Similarly, for the passive side of the wall, the resultant force, $R_{passive}$, at a depth x is computed as follows:

$$F_{passive} = \frac{1}{2}\sigma_{passive}\cdot w\cdot\left(x - 7\,ft\right) \qquad @\, x_{passive} = 7\,ft + \frac{2}{3}\left(x - 7\,ft\right) \quad \text{.....Eq. C-4}$$

$$R_{passive} = F_{passive} \qquad @\, x_{R_{passive}} = x_{passive} \quad \text{.....Eq. C-5}$$

where, $\sigma_{passive}$ is the effective horizontal pressure on the passive side.

The moment along the sheet pile wall, at a depth x, can be computed as the sum of the moment contributions from the active and passive resultant forces discussed above.

Considering positive moment as counter-clockwise direction, the resultant moment at a depth x is found as:

$$\sum M_A(x) = R_{active} \cdot x_{R_{active}} \quad \text{for} \quad x \le 7\ ft \quad \textbf{.....Eq. C-6}$$

$$\sum M_A(x) = R_{active} \cdot x_{R_{active}} - R_{passive} \cdot x_{R_{passive}} \quad \text{for} \quad x > 7\ ft \quad \textbf{.....Eq. C-7}$$

To determine the location of the point of stability (B) we equate the moment resultant equal to zero and solve for x.
Using the above procedure, the point of lateral stability (Point B) for the representative bridge conditions described in Chapter 5 was found to be approximately at 11ft below the head of the sheet pile wall (See Chapter 5).